Overbank flow in the river Allier

A flow model

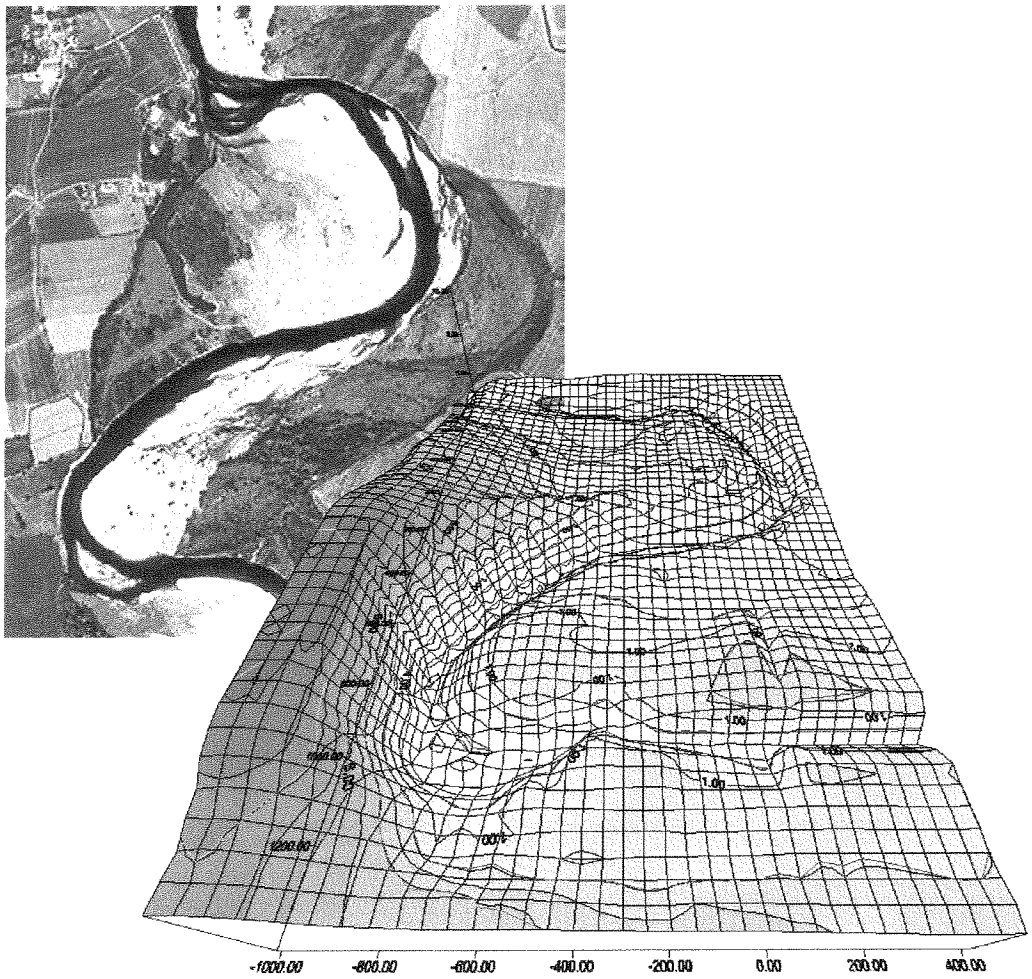

P-J Bart

August 2000

TU Delft

Delft University of Technology

Overbank flow in the river Allier

A flow model

Graduation committee:

Prof. dr. ir. H.J. de Vriend	Delft University of Technology/ University of Twente
Dr. ir. Z.B. Wang	Delft University of Technology/ Delft Hydraulics
Dr. J.H. van den Berg	University of Utrecht
Prof. dr. ir. G.S. Stelling	Delft University of Technology/ DHV

P-J Bart

August 2000

Preface

This graduation thesis is the final part of my study Civil Engineering at the Delft University of Technology.
In this report flow during a flood and its effect on armour layers have been studied using the flow simulation program Delft3D-Flow.

I would like to express my gratitude to my supervision committee, prof. dr. ir. H.J. de Vriend, dr. ir. Z.B. Wang, dr J.H. van den Berg and prof. dr. ir. G.S. Stelling, for their assistance and patience. I thank the University of Utrecht for their support and information on the river Allier. I would especially like to thank drs. Maarten Kleinhans, ir. Fred Havinga and ir. Mathijs van Ledden. Their comments, support and the discussions were very valuable.
Last but not least I would like to thank the students of the field work group, Albert Driesprong, Caroline Neessen, Liesbeth Kruisinga and Jasper van der Bruggen for their contribution to this study. After all, without their work this project would not exist.

Pieter-Jeroen Bart
August 2000
Delft

Index

Summary

For several years the Department of Physical Geography of the University of Utrecht has conducted surveys on the river Allier in France. These surveys always took place during periods of low discharge because at high or even moderate discharges measurements are impossible. As information on the flow during a flood is important to understand the river morphology, a flow model of a part of the Allier was made to simulate the flow during a flood.

During a survey in the summer of 1998 bathymetric data and flow measurements were collected. With this data a flow model was made and calibrated. The discharge during the survey was approximately 20 m^3/s. During the calibration it became clear that the downstream boundary condition (a water level) could not be generated well. This problem was overcome by moving the boundary to a flow measurement section where the water level for a discharge of 20 m^3/s was known. However this left a problem for simulation at higher discharges than 20 m^3/s.
The influence of an error in the downstream boundary condition was estimated both numerically as well as with the Bresse approximation. Both methods showed the backwater effect introduced by an error to extent for about 1000 m upstream of the boundary. The magnitude of a water level error however, was shown to decrease rapidly in the upstream direction.

To simulate flow during a flood several simulations were made, steady- (with a constant discharge) and unsteady state (with a varying discharge). Ten steady state simulations were made, increasing in discharge from 100 to 1000 m^3/s. In the unsteady state run the flood of November 1994 was simulated.
The simulations showed the flow mainly to follow the main channel, leading to an inbank flow pattern. The position of the secondary flow cells – where the bend radius of curvature is smallest—also indicated an inbank flow pattern.
Velocities up to 4 m/s were found in the main channel leading to very large bed shear stresses. At several places the flow was directed onto the point bars. The bed shear stress magnitude here indicated that large grain sizes could be transported onto the point bars.
The differences between the steady state and the unsteady state simulations were small. Although there were some differences the flow pattern and the magnitude of the velocity were the same. This means that for a global impression of the flow pattern at a certain discharge, a steady state simulation is sufficient. This saves a lot of computation time as the unsteady state simulation has a much larger computation time.

Armour layers are layers of coarse grains on top of the bed. They were found at several places in the survey area. During the survey a number of the armour layers were sampled. With the aid of the Oak Creek model by Parker (1990) the threshold of motion of the grain sizes within these armour layers was estimated. By combining the Oak Creek model and the bed shear stresses from the flow model it was shown that the threshold of motion was exceeded for all grain sizes within the sampled armour layers. Also a rough indication of the surface grain size distribution was given based on the Oak Creek model and the bed shear stresses derived from the flow model.

However, the applicability of Oak Creek model to the river Allier was not tested. This requires sediment transport measurements. For the various coefficients in the Oak Creek model the literature values were used.

Symbols

B	:	Bimobility parameter	[-]
c	:	celerity of disturbance in Courant number	[m/s]
C	:	Chézy value	[$m^{1/2}/s$]
D_i	:	grain size of fraction i	[m]
Fr	:	$\frac{U}{\sqrt{gh}}$, Froude number	[-]
g	:	gravitational acceleration	[m/s^2]
h	:	water depth	[m]
h_e	:	$\left(\frac{q^2}{C^2 i_b}\right)^{1/3}$, equilibrium depth	[m]
ki	:	energy loss factor	[m^{-1}]
n	:	Manning coefficient	[$m^{-1/3}s$]
Δt	:	time step	[s]
q	:	discharge per unit width	[$m^3/s/m$]
Q	:	discharge	[m^3/s]
S_j	:	energy gradient	[-]
U	:	depth averaged velocity	[m/s]
σ	:	Courant number	[-]
ρ_w	:	density of water	[kg/m^3]
ρ_s	:	density of sediment	[kg/m^3]
τ_b	:	bed shear stress	[N/m^2]
τ_{rsi}	:	reference bed shear stress for fraction i of the surface layer	[N/m^2]
τ^*_{rsg0}	:	reference Shields stress for the median grain size of the surface layer	[-]
η_i	:	$\frac{h_i}{h_e}$, ratio between water depth and equilibrium depth at distance i from the downstream boundary	[-]
Λ_i	:	$\frac{x_i i_b}{h_e}$, non-dimensional distance from downstream boundary	[-]

Figures

Tables

1 Introduction

1.1 Background

For several years now the Department of Physical Geography of the University of Utrecht has conducted field investigations on the river Allier in France. In their final year, students of the river section of this department have examined various features of the river Allier for their graduation thesis. These investigations always took place during periods of low discharge in summer because at high or even moderate discharges measurements are impossible. Therefore the flow pattern at higher discharges had to be estimated indirectly from flood marks such as disrooted trees, debris deposits on banks etc. One way to partially overcome this lack of information is to make a computational model of a part of the Allier to simulate the flow pattern during higher discharges. Then field observations and model outcome can be combined to make the picture clearer.
One of the reasons why information on the flow pattern during higher discharges is needed is the development of armour layers, a layer of coarse grains on top of the bed material.
To build such a model a field survey was conducted. During this survey the model area, which encompassed two bends, was mapped and flow velocity measurements were conducted. The bathymetric data were used to construct a flow model with the computer package Delft3D-Flow. The flow measurements, executed by students of the Department of Physical Geography, were used to calibrate the model.

1.2 Objectives

The objectives of this thesis are twofold:
1. Make a computational model of a part of the Allier in order to simulate a flood.
2. Use the results of the simulations to try to explain the formation of armour layers in the Allier.

1.3 Outline of report

The outline of the report is as follows:

Chapter 2 is a brief description of the river Allier. It gives some background information on river planform, discharge characteristics and bed material. Also the Life-Loire project is briefly described.

Chapter 3 gives the results of a literature survey on the topics of inbank- and overbank flow. Treated subjects are: secondary flow patterns, influence of overbank flow on discharge capacity and morphology of river bends related to the flow pattern.

Chapter 4 describes the structure, types, development and threshold of movement of armour layers.

Chapter 5 deals with the hydrodynamic model, the data used to build and calibrate the model and the calibration itself.

Chapter 6 discusses the results from the flow model. A link is made with the theory described in chapter 3.

Chapter 7 uses the model results in combination with an emperical relation for the transport of graded sediments to give a rough estimate for the threshold of movement of armour layers in the river Allier.

Chapter 8 gives the overall conclusions.

2 The river Allier

2.1 Introduction

The river Allier is a tributary to the river Loire and has a length of approximately 410 km. Its source lies in the Massif Central at the foot of mount Moure de la Gardille in the department Lozere, at an altitude of 1501m. Its confluence with the river Loire is situated at Bec d'Allier, near Nevers. The main tributaries of the river Allier are the Alagnon, the Couzes, the Dore and the Sioule rivers.

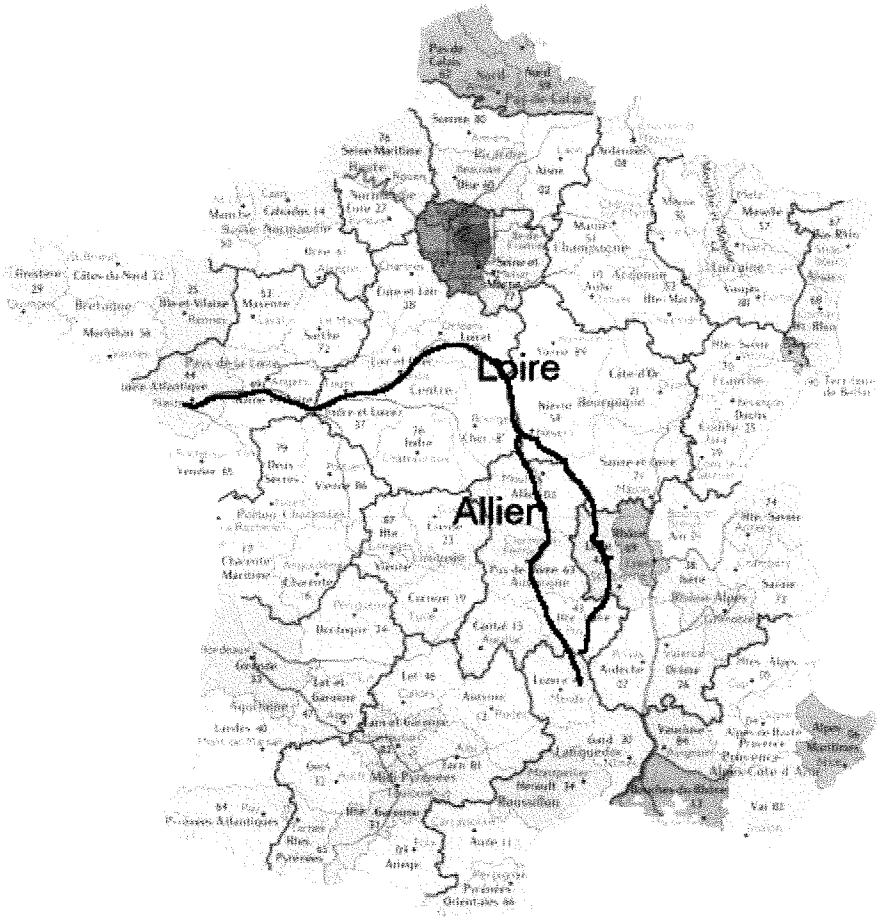

figure 1 : Allier and Loire river

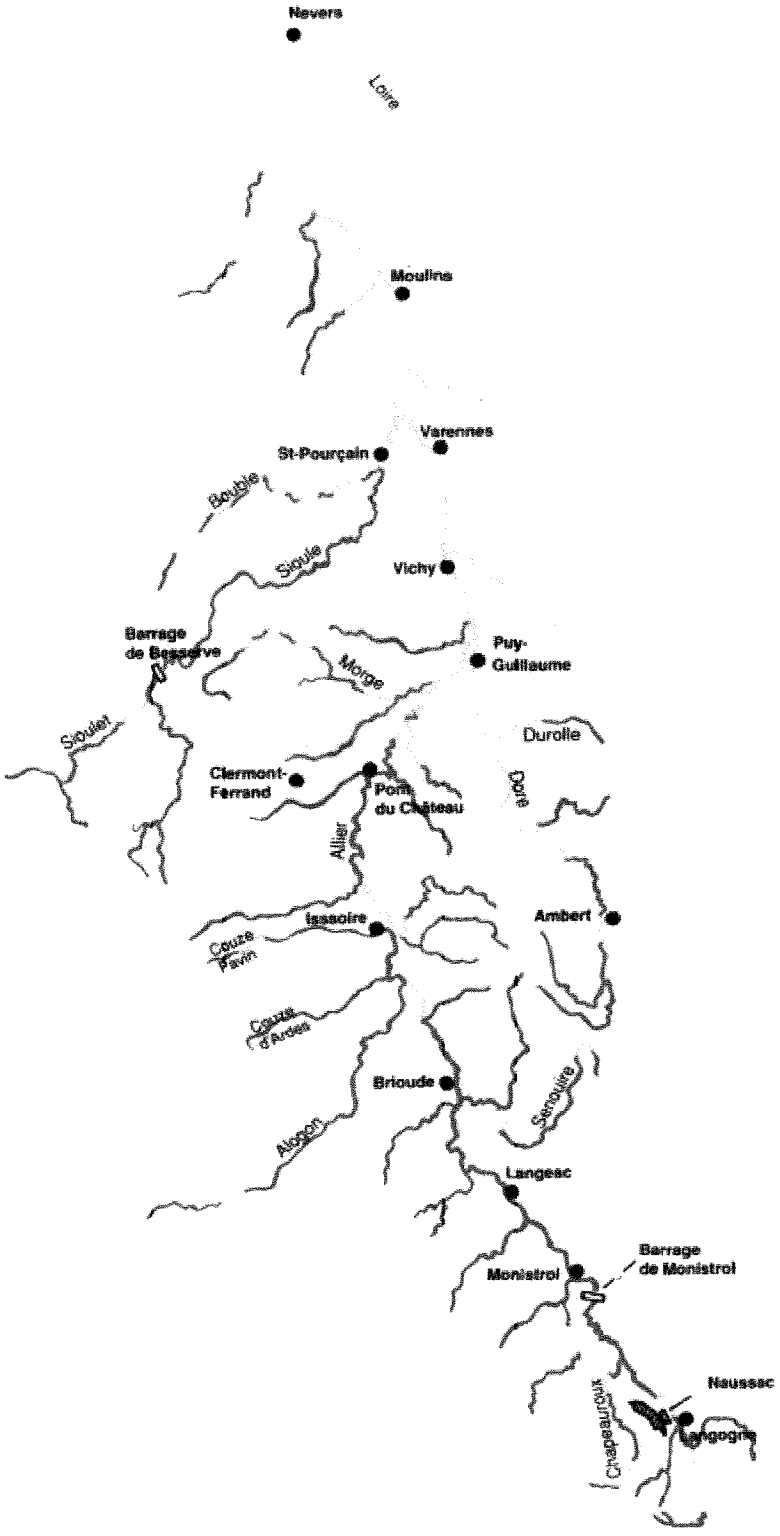

figure 2 : the Allier river basin

2.2 River planform

The Allier is a very natural and dynamic river system with both braiding and meandering reaches, and is continuously changing its planform.
Meandering rivers are characterised by a single channel and alternate bends and usually have a mild slope, whereas braided rivers are characterised by a number of channels separated by islands and bars and a steeper slope. The transition between a meandering river with occasional bars and islands and a braiding river is not very clear. The meandering behaviour of the Allier can be observed in the reach upstream of Moulins, whereas the reach downstream of Moulins has a braided character.
The river flows through an alluvial floodplain which varies in width from several hundreds of metres to over two kilometres. The river cross section can be divided into three areas: the high plain, composed of several terraces and used for agricultural activities, the floodplain, mainly consisting of large point bars, and the main channel, which always conveys water.
The river's longitudinal slope varies from approximately 0.6 m/km up to 0.8 m/km.

2.3 Bed material

The bed material of the Allier ranges in grain size from sand of 0.05 mm to pebbles of more than 10 cm (A.Driesprong, 2000, J v.d. Bruggen, 2000). This wide variety of grain sizes makes the Allier susceptible to a process known as armouring. Armouring of the bed is a phenomenon in which a layer of coarse grains forms on top of the bed material and hence shelters the smaller grains in the river bed from the force of the flow. These armour layers are found on the (point) bars. The main channel consists of a mixture of sand and gravel, a more sandy mixture in the bends and a coarser mixture at the cross over region. Downstream of Moulins the sediment is much finer than upstream. In figure 3 the grain size distribution of the main channel river bed averaged over the area is shown.

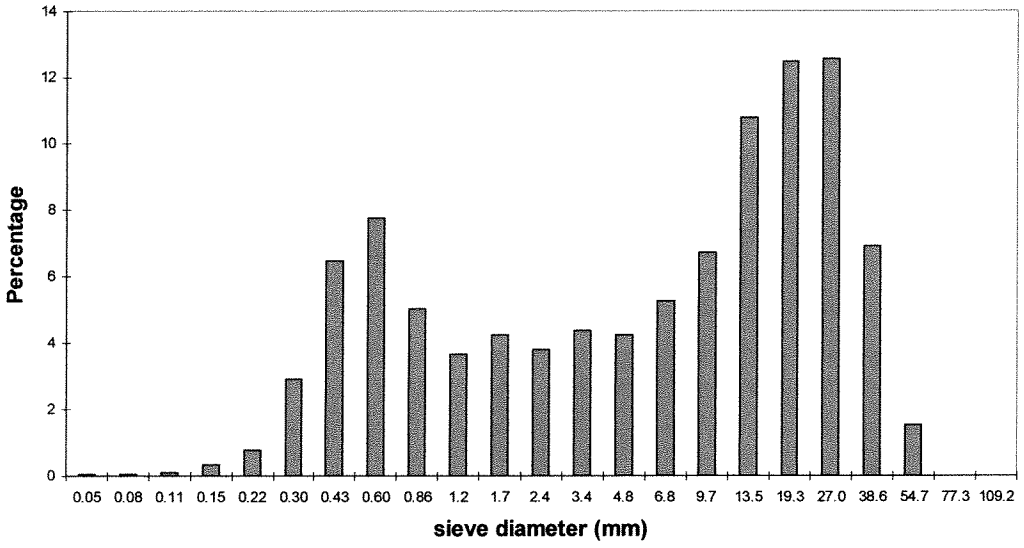

figure 3 : grain size in river bed averaged over the area (A. Driesprong, 2000)

2.4 Discharge

The Allier is a rain-water conveying river, which shows strong discharge variation. After heavy rainfall, the waterlevels increase enormously and the floodplain becomes submerged. The discharge may vary from 25 m^3/s during the summer to 1400 m^3/s during winter or spring. These floods are caused by Atlantic depressions. The situation of waterlevels above bankfull level is called overbank flow. Overbank flow significantly influences the erosion of river banks and hence the rate of meandering. The influence of overbank flow on the overall flow pattern is not yet well understood.

2.5 Examined reach

The reach under examination is situated approximately 6 kilometres upstream of Moulins and consists of the 2 bends directly upstream of Chateau de Lys. The reach is approximately 2 kilometres long and is characterised by a great variation in floodplain width and large point bars. The point bars are partially vegetated.
The aerial photograph shows the contours of the floodplain and several relict channels. These relict channels are found on both sides of the floodplain indicating that the main channel has shifted over the entire floodplain.

figure 4 : surveyed area near Chateau de Lys (aerial photograph 1998)

2.6 Plan Loire Grandeur Nature

The "Plan Loire Grandeur Nature" was issued in 1994 by the French government after strong opposition to the construction of several dams in the Loire river basin.
The project aims at improving the water management, both at high- and low discharges, and at nature restoration for the whole Loire river basin.

figure 5 : dams in the Loire river basin

One of the goals of the project is to restore salmon migration, to this end two dams were decommissioned: the Saint-Etienne-du-Vigan dam on the Upper Allier river and the Maisons rouges dam on the Vienne river.

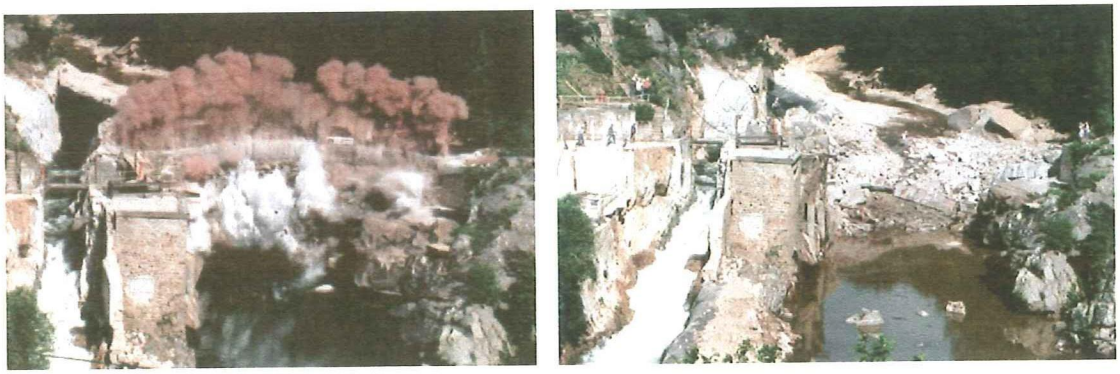

figure 6 : demolition of dam in the upper river Allier

For more information about the river Allier the reader is referred to Blom(1997) , A. Driesprong (2000), C. Neessen (2000), L. Kruisinga (2000), J. v.d. Bruggen (-), De Allier als morfologisch voorbeeld voor de Grensmaas- part I, II & III (2000), Wilbers (1997) and Wilbers (the Allier pages)

3 Bend flow

3.1 Introduction

This chapter deals with some background information on flow in river bends, both below as well as above bankfull discharge. Some knowledge about these phenomena is necessary to evaluate the result of the flow model.
In this chapter inbank- and overbank flow will be treated separately, in order to make a clear distinction between the flow patterns. In a natural river, such as the Allier, there is no sharp transition between the two flow regimes, because flood plain and main channel are not strictly separated, for example by summer dikes, and hence the definition of bankfull discharge becomes a bit blurred.

3.2 Inbank flow.

In a river bend secondary flow develops due to the centripetal force the banks exert on the body of water. The centrifugal force directs the water to the outside of the bend where it causes a set-up of the waterlevel, known as superelevation. Because of the build up of water the hydrostatic pressure is greater at the outer bend than at the inner bend. Averaged over the depth the centripetal- and the hydrostatic pressure force balance each other, but locally these two forces are not in equilibrium. The centrifugal force is proportional to the square of the velocity whereas the resultant hydrostatic force is constant over the water depth. As the flow velocity reaches its maximum at the water surface, the centrifugal force varies from zero at the river bed to its maximum at the water surface. The resultant of the centrifugal and hydrostatic force causes a circular flow pattern with the flow directed outward at the surface and inward at the river bed. Together with the main flow this forms a helical flow pattern, see figure 7.

The secondary flow pattern in a river bend has significant influence on the morphology. The spiral flow is partly responsible for building up the point bar. Near the river bed the flow, and hence the sediment transport, is directed towards the inner bend. The inward directed flow force on a bed particle is balanced by the gravitational force due to the slope of the point bar face. For non-uniform sediments the spiral flow also leads to sorting of the sediment. The outward directed gravitational force is proportional to the cube of the diameter of the grain whereas the inward acting flow force is proportional to the square of the grain diameter. As a consequence the gravitational force is dominant for large grains whereas for small grains the flow force is the dominant force. This implicates that small grains are transported towards the inside of the bend, to the point bar and large grains will be transported to the outside of the bend, to the pool.

Another feature that can be encountered in bend flow is an extra outer bank cell. This cell has a circulation opposite to the main secondary flow cell. This outer bank cell is

not always present. The existence of the outer bank cell in rivers has been confirmed in field studies. The strength of the cell increases with discharge, steepness of the outer bank and the curvature of the bend (Markham and Thorne, 1992).
The outer bank cell has a stabilising effect on the outer bank. The outer bank cell acts as a buffer between the outer bank and the flow. It pushes the core of high velocities away from the bank, see Blanckaert (1999).

In the inner bend another phenomenon is present. There is a net flow over the point bar towards the outer bend. Due to the centrifugal force the water is pushed towards the outer bend. From continuity it then follows that water must be shoaling over the point bar towards the outer bend. This outflow pushes the core of high velocity more rapidly towards the outer bend and the helical flow pattern is confined to the deep part of the main channel. At the point bar face upwelling occurs where the water shoaling over the point bar meets the inward directed flow near the bed in the helix.

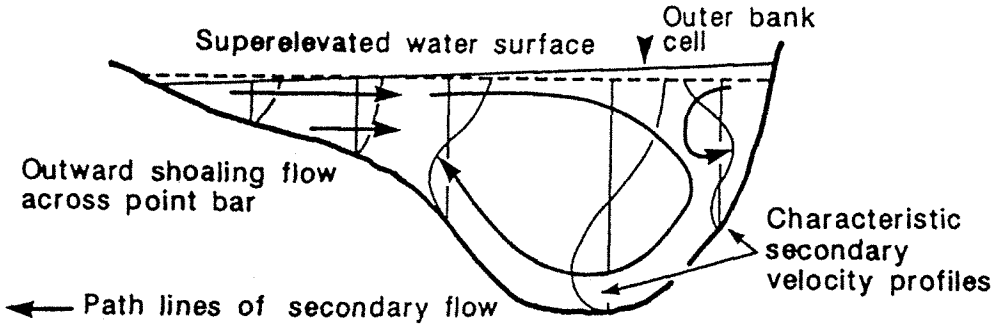

figure 7 : secondary flow pattern in bend for inbank flow (Markham & Thorne, 1992)

Flow separation can occur in rivers at both the out- and inside of the bend. Whether separation takes place is mainly controlled by the ratio of radius of curvature to width, lower values of this ratio promote separation. If the radius of curvature to width ratio approaches 2 the flow can no longer follow the inside bank and separates. Usually just after the bend apex. At the outer bank the superelevation reduces the downstream surface slope and causes a stagnant zone and separation near the outer bank just before the bend apex.
Separation zones usually contribute to deposition of sediment, due to a lower velocity. In the stagnant zone created by the separation, fine sediment can be deposited.
At the inner bend flow separation pushes the flow away from the point bar and hence restricts the flow width, leading to a increased flow velocity near the outer bend. At the outer bank separation has a similar effect, it protects the outer bank from erosion. However if a strong reverse flow develops, a separation zone at the outer bank can occasionally lead to scouring.
For more information on this topic the reader is referred to Markham and Thorne (1992).

3.3 Overbank flow

Overbank flow, especially around bends, is a poorly understood phenomenon.
In recent years however, more research has been done to gain insight into overbank flow. Most of this research has been concentrated on the decreased conveyance capacity – water-transport capacity of a river -- in meandering channels due to nonbed energy losses.
These nonbed energy losses are all energy losses that are not related to bottom friction. The increased energy losses during periods of overbank flow can be explained by dividing the river flow into two flow fields; the flow in the main channel, lower layer flow, and the flow over the floodplain, upper layer flow. As the flow over the floodplain has to cross the main channel at bends, additional turbulence is introduced due to the interaction of the two bodies of water which have different velocities. This turbulence causes the increased energy losses.
Because of the interaction between the upper- and lower layer flow the flow pattern changes. Measurements at the " Flood Channel Facility" at Hydraulic Research Wallingford (Ervine et all, 1993) showed the following flow pattern:
As the floodplain flow approaches the main channel at a bend it dives into the channel and becomes partly entrained in it. In doing so, it drives a large vortex which grows along the crossover length. At the next bend the rotation of this vortex is opposite to that of secondary cells at bends for inbank flow only. After the bend this vortex cell decays rapidly and water from the main channel flows onto the floodplain.

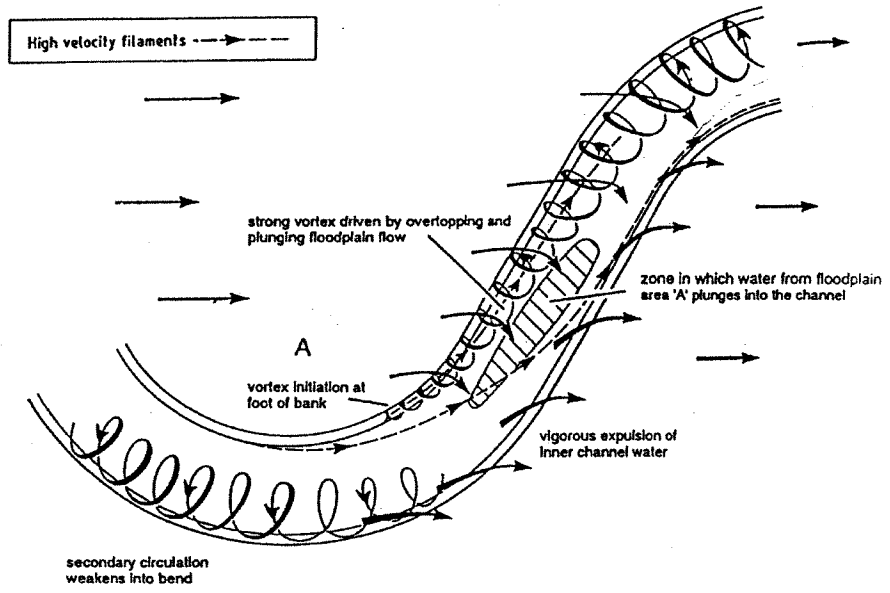

figure 8 : overbank flow pattern (Ervine et all, 1993)

This overbank flow pattern clearly has implications for the sediment transport. Ishigaki, Muto and Sawai (1998) conducted experiments to investigate the influence of overbank flow on river morphology. These experiments showed a different erosion pattern for inbank- and overbank flow. At the cross over region the upper layer flow dives into the main channel and, depending on the aspect ratio (width to depth ratio), can reach the riverbed. For most practical situations this will be the case. As the upper

flow plunges onto the bed sediment is picked up transported downstream. The secondary flow cell driven by the upper layer flow is opposite to the secondary flow for the inbank case, this means that in the bend the flow near the bed is directed towards the outer bend. Sediment is therefore transported from the point bar at the inside of the bend to the outside of the bend. In the second half of the bend the flow is partly directed onto the floodplain and hence sediment can be transported onto the floodplain.

3.3.1 Parameters influencing overbank flow pattern

The effect of the interaction between the upper- and lower layer flow on the overall flow pattern depends on the geometry of both the floodplain and the main channel, and the rougness of the floodplain.
This flow pattern is influenced by the following parameters:

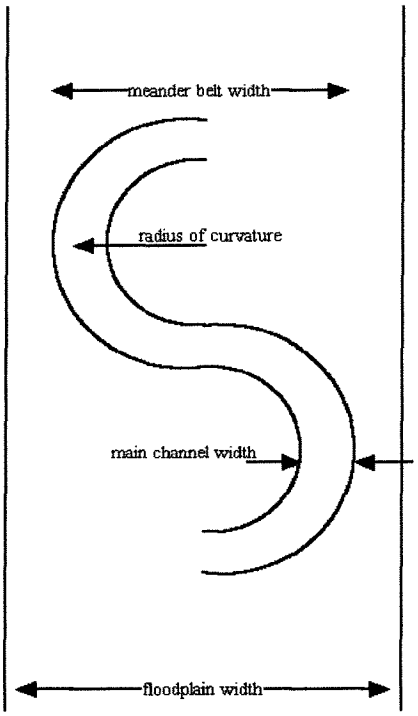

figure 9 : definition of terms

3.3.1.1 Sinuosity of the main channel

The sinuosity of the main channel is the curved meander length of the channel divided by the straight floodplain length. A high value of the sinuosity indicates a very curved channel, if the sinuosity is equal to one the channel is straight. It is a measure for the resistance to the conveyance capacity of a river as the curvature of a channel increases

the floodplain flow has to cross a greater area of the channel. Up to a value of about 1.5 an increase in the sinuosity has a great influence on the flow pattern, above a value of 1.5 an increase in sinuosity has a far lesser impact.
The sinuosity of the river Allier in the survey area is approximately 1.6, so the influence of the sinuosity on the flow pattern can be expected to be significant during overbank flow.

3.3.1.2 Floodplain roughness

The floodplain usually has a greater hydraulic roughness than the main channel because of the vegetation present on the floodplain. This increased roughness influences the flow exchange between main channel and floodplain, a higher value of the floodplain roughness leads to less flow exchange.
Floodplains in Allier are partly vegetated. Most vegetation is found on the upper parts of the point bars which very rarely are flooded. Of the regularly flooded areas only the right side bank just after the upstream bend is vegetated.

3.3.1.3 Aspect ratio of the main channel

The aspect ratio is the width of a channel divided by the depth. This parameter influences the way in which the floodplain flow crosses the main channel, for high values of the aspect ratio (wide channels) the floodplain flow plunges into the main channel and drives two vortex cells, causing shearing and recirculation. Whereas for low values of the aspect ratio the floodplain flow merely " glides" over the main channel and only drives one vortex cell.
For the surveyed stretch the aspect ratio is presumed to be large at the cross over region, in the order of magnitude of 100.

3.3.1.4 Relative depth

The relative depth is the depth above the floodplain divided by the depth in the main channel. It is a measure for the significance of the floodplain flow compared to the main channel flow. At low values of the relative depth the main channel flow is dominant while at increasing relative depth the influence of the floodplain flow becomes more significant and in the extreme case a negligible influence of the main channel. At low- and intermediate values of the relative depth the interaction between the upper- and lower layer flow has the greatest influence on the overall flow pattern. Because the influence of the bottom roughness on the flow pattern depends on the water depth, the relative depth is also a measure for the influence of the bottom roughness on the floodplain on the overall flow pattern.

3.3.1.5 Meander belt width

The Meander belt width is the width of the floodplain occupied by the curved main channel and is more or less like the sinuosity a measure for the resistance to conveyance. In the surveyed area the floodplain more or less follows the contours of the main channel. It is therefor the question whether the above described flow pattern for an idealised situation, straight floodplain of constant width and a meander belt width which is smaller than the floodplain width, will actually occur in the surveyed area.

3.3.1.6 Variation in the width of the floodplain

A variation in width or in the orientation of the floodplain causes the floodplain flow to accelerate or decelerate. If the floodplain boundaries are not parallel to the main channel the flow over the floodplain is directed across the main channel, this is called skewed flow. This skewed flow causes additional nonbed losses.

3.3.2 Methods to estimate energy loss during overbank flow

There are two ways to describe the influence of the nonbed energy losses; the first is to estimate energy dissipation due to each source, e.g. bedfriction, planform-bend losses ect. , the second is to express the losses in a correction coefficient by comparing the real discharge with the theoretical one(estimated with bed friction only).

As an example of the first method the approach of Muto, Imamoto and Ishigaki (Muto, Imamoto and Ishigaki, 1998) is described. They based their work on previous research by Ervine and Ellis. The channel is divided into three zones and for each zone the energy losses are determined.

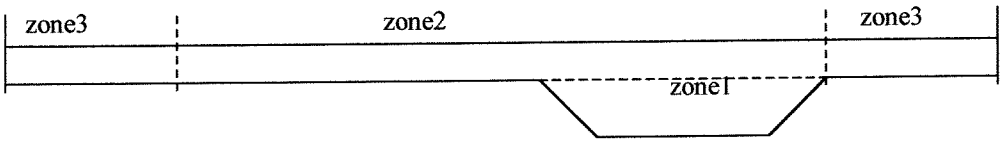

The three zones are:

- zone 1 The main channel upto bankfull level
- zone 2 Floodplain meander belt width
- zone 3 Floodplain outside the meander belt width

The different energy losses are expressed as a change in the energy head, S, defined by:

$$S_j = \sum_{k_i} k_i \frac{u^2}{2g} \qquad (3.1)$$

Where S_j is the energy gradient for zone j (j = 1,2 or 3), u is the velocity, g is the gravitational acceleration and k_i is a energy loss factor expressing the energy loss due to source i.
As energy loss sources are identified: boundary friction, secondary flow, turbulent shear stress, flow expansion and contraction.

An example of the second the method is the one adopted by Ervine, Willets and Sellin (Ervine, Willets and Sellin, 1993).
They used a non dimensional function F* for the ratio of the actual measured discharge in a compound channel to the theoretical discharge estimated with skin friction only. The theoretical discharge is computed by dividing the cross section into the same three zones as in the approach of Muto, Imamoto and Ishigaki.

3.4 conclusion

Inbank flow shows a different flow pattern than over bank flow. Inbank flow is characterised by one or more secondary flow cells in the bend. These secondary flow cells develop under influence of the centripetal force. The secondary flow leads to a sorting of the grain sizes in a bend, large grains are transported towards the outer bend, whereas fine grains are transported inwards. The outer bank cell has a stabilizing effect on the outer bank. For bends with a small radius of curvature the flow can separate. These separation zones usually lead to deposition of sediment.
Overbank flow is dominated by the interaction between the flow over the floodplain and the flow in the main channel. Due to this interaction a secondary flow cell develops which has an opposite flow direction compared with the one for inbank flow. Overbank flow can lead to a strong exchange of water and sediment between main channel and floodplain. At the cross over region the floodplain flow reaches the river bed and high bed shear stresses can occur. Just after the bend apex water and sediment flow from the main channel onto the floodplain.

4 Armour layers

4.1 Introduction

In gravel-bed rivers the wide gradation of the sediment can lead to the formation of a coarse surface layer that protects the underlying sediment from erosion. Such a surface layer is called an armour layer.
An armour layer consists of clusters of large grains in which the largest grains act as an anchor. Large grains embed themselves by sliding into a scour hole, which evolves around their front perimeter, and hence decrease their protrusion.
Due to this decreased protrusion they can act as a stable support for other large grains while the smaller grains can be deposited in the shelter of the larger grains or in the pores between them. In this way clusters are formed in which all grains support one another. The formation of clusters explains why all grain sizes can be present in an armour layer. During the formation clusters trap grains transported in the flow direction. As a consequence the shape of the clusters indicates the flow direction during the formation process Raudkivi (1990).
Failure of clusters can be triggered by erosion of the bed around it. The anchor stones then move downstream to a new stable position and the cluster formation starts again.

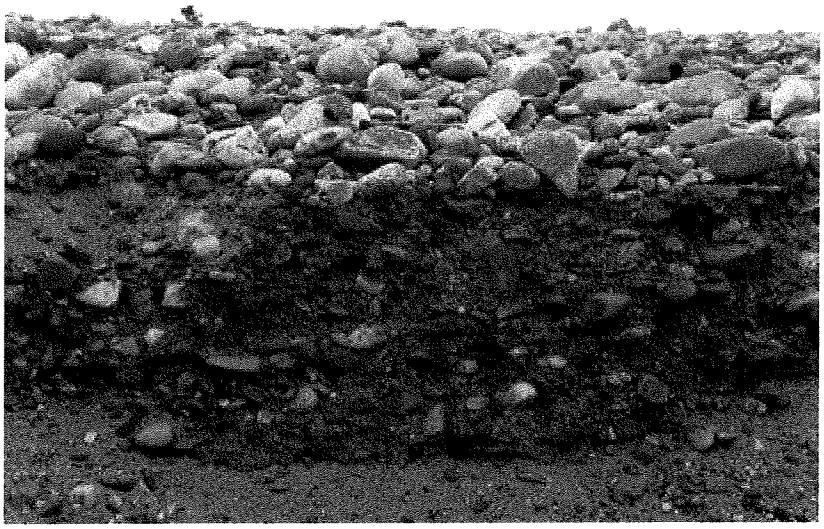

figure 10 : side view armour layer

There are two types of armour layers, static- and mobile armour. The subdivision between the two types is based on the frequency of bed particle motion. A static armour is a stable layer of coarse grains which develops by clear-water scour, only a discharge higher than the previous largest will be able to remove sediment from the layer and hence coarsen it. They are typically found behind outlet structures such as reservoir dams and have a low frequency of movement.

Mobile armour layers have a greater frequency of movement and develop under non-zero bedload conditions (live bed scour). The sediment supply prevents the armour layer from becoming static. Particles which pass over the bed as bed load can get trapped in the pores of the armour layer. On the other hand, particles which have settled not too deep in the pores can be extracted from the armour layer and added to the bed load.
The armour layers in the river Allier are thought to be mobile armour layers because of the sediment supply from upstream.

However, if the flow velocity, and hence the sediment supply decreases, there will be less sediment to fill the pores and the flow will only be able to extract sediment from a smaller depth in the pores, and hence the armour layer can become static.

4.2 Threshold of motion

For a bed of an uniform non-cohesive sediment the flow resisting force is the weight of the particles. However in a bed consisting of a graded sediment the resisting force is not only caused by the weight of a particle but also on the variation in stability caused by the difference in the surrounding particle sizes. The threshold of motion becomes dependent on the grading of the sediment. Smaller particles tend to be shielded whereas the larger particles tend to be more exposed to the flow. This is known as the hiding/exposure effect. Studies by Fenton and Abbot showed that coarse sediments with large protrusions can exhibit threshold values of one sixth of the Shields value. Similar work by Church showed the same trend, but when imbrication, a roof-tile like stacking of the grains, occurred coarse particles showed threshold conditions up to a quarter greater than the Shields value White and Day (1982).

The two types of armour layers have different threshold conditions. For a static armour layer there is no sediment transport upto a certain threshold condition and when, during a flood, this threshold condition is exceeded all bed particles are entrained and the armour layer is destroyed. For a mobile armour layer there is no clear threshold condition, with increasing bed shear stress the maximum transportable grain size will increase and the armour layer will coarsen. This will continue until all grain sizes in the armour layer are in transport and the armour layer will cease to exist. However, even if all grain sizes are in transport, the moving coarse particles in the bed-transport layer can still protect the bed.

4.3 Hiding factors

Due to the grading of a sediment the threshold of motion can no longer be described by one grain size and the Shields criterion is no longer valid.
To incorporate the effects of hiding and exposure in the formulations for the threshold of motion, the concept of a hiding factor was introduced. The hiding factor corrects the critical shear stress of a mixture for the individual grain sizes. The concept of a hiding factor assumes that in every mixture, there is a grain size which has the same critical shear stress as it would have in a uniform sediment, denoted as D_A. Usually the D_{50} is taken for this grain size, but Day and White (Day and White, 1982) showed this grain

size to vary with the grading of the mixture. For narrowly graded sediments D_A was found to be a little greater than the D_{50} and for widely graded sediments a little smaller.

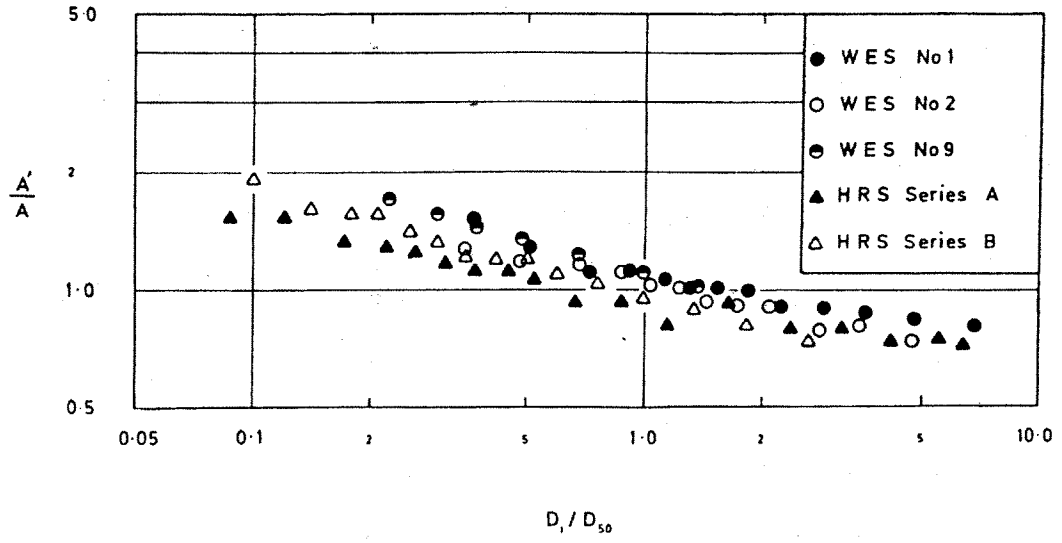

figure 11 : variation D_A with grading (White & Day, 1982)

The symbol A is the critical value for the threshold of motion of the mobilty parameter in the Ackers and White formula (Ackers and White, 1973). It is in fact a modified Shields parameter. A' is the critical value for a graded sediment.
In figure 11 A'/A is plotted versus D_i/D_{50} for a number of mixtures with different grading. It is shown that the ratio A'/A = 1 for a certain range of values of the ratio D_i/D_{50}. Outside that range A/A' deviates from 1, which implies that D_A varies with grading.

Most hiding factors have the form of:

$$\frac{\tau_{*i}}{\tau_{*50}} = \left(\frac{D_i}{D_{50}}\right)^{-n} \qquad (4.1)$$

in which: τ_{*i} is the dimensionless shear stress of fraction i, τ_{*50} is the dimensionless shear stress of D_{50}, D_i is the grain size of fraction I, D_{50} is the D_{50} of the mixture.

If the coefficient n = 1, then every grain size fraction has the same critical shear stress. This means that all size fractions will simultaneously get into transport and that the bedload size distribution equals the bed substrate. This is called equal mobility and was introduced by Parker and Klingeman (1982).

$$\tau_{c*i} = \frac{\tau_{ci}}{(\rho_s - \rho_w)gD_i} \qquad (4.2)$$

If we assume ρ_s, ρ_w and g to be constants then,

$$\frac{\tau_{c*i}}{\tau_{c*50}} = \frac{\tau_{ci}/D_i}{\tau_{c50}/D_{50}} = \left(\frac{D_i}{D_{50}}\right)^{-n} \qquad (4.3)$$

so,

$$\tau_{ci} = D_i\left(D_i^{-n}D_{50}^{n}\right)D_{50}^{-1}\tau_{c50} = D_i^{1-n}D_{50}^{n-1}\tau_{c50} \qquad (4.4)$$

if n = 1 then,

$$\tau_{ci} = \tau_{c50} \qquad (4.5)$$

if n < 1 then,

$$\tau_{ci} = \left(\frac{D_i}{D_{50}}\right)^{1-n}\tau_{c50} \qquad (4.6)$$

$$\text{if } \frac{D_i}{D_{50}} \le 1 \quad \text{then} \quad \tau_{ci} \le \tau_{c50} \qquad (4.7)$$

$$\text{if } \frac{D_i}{D_{50}} \ge 1 \quad \text{then} \quad \tau_{ci} \ge \tau_{c50} \qquad (4.8)$$

A physical explanation for equal mobility can be given on the basis of the hiding/exposure effect and the greater availability of coarse grains on the surface of the bed. Due to the hiding/exposure effect smaller grains are shielded from the flow whereas larger grains are more exposed to the flow, thus increasing and decreasing respectively the critical shear stress for fine and coarse grains. This explains the reduction of part of the difference between the critical shear stress of fine and large grains, the rest of the difference is compensated for by the greater availability of coarse grains on the bed surface.

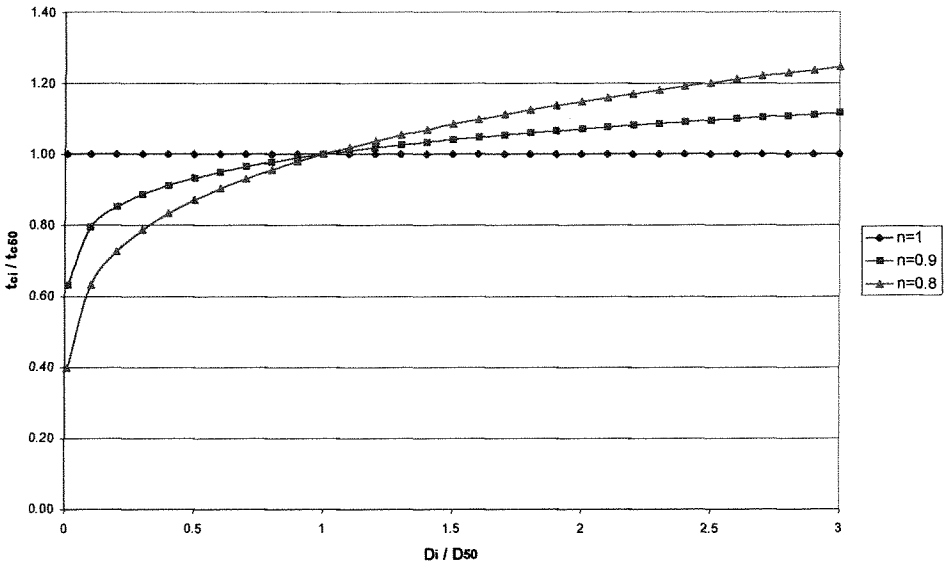

figure 12 : influence coefficient n on critical shear stress

Parker found in the Oak creek data (Milhous 1976) evidence for near equal mobility. However Oak Creek is a gravel bed stream and has little or no sand throughput. Wilcock (Wilcock 1993) found that the threshold of motion depends on the sediment size distribution. The approximation of equal mobility seemed to hold for most size distributions except for bimodal distributions. A bimodal distribution is characterised by two size fractions, called modes, which contain most of the sediment in the sample. In a plot of the grain size versus the amount of sediment of that grain size in a sample this shows as a " double peak " distribution, in contrast to a unimodal distribution which is characterised by a single peak.

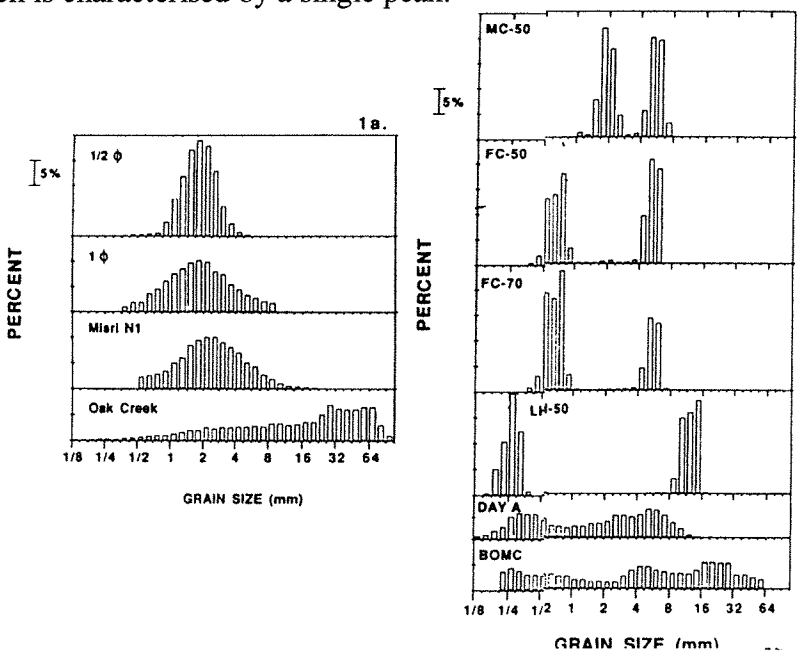

figure 13 : example of unimodal (left) and bimodal (right) mixtures (Wilcock, 1993)

For strongly bimodal mixtures it is found that finer fractions have a smaller critical shear stress than the coarser fractions and hence equal mobility is not satisfied.

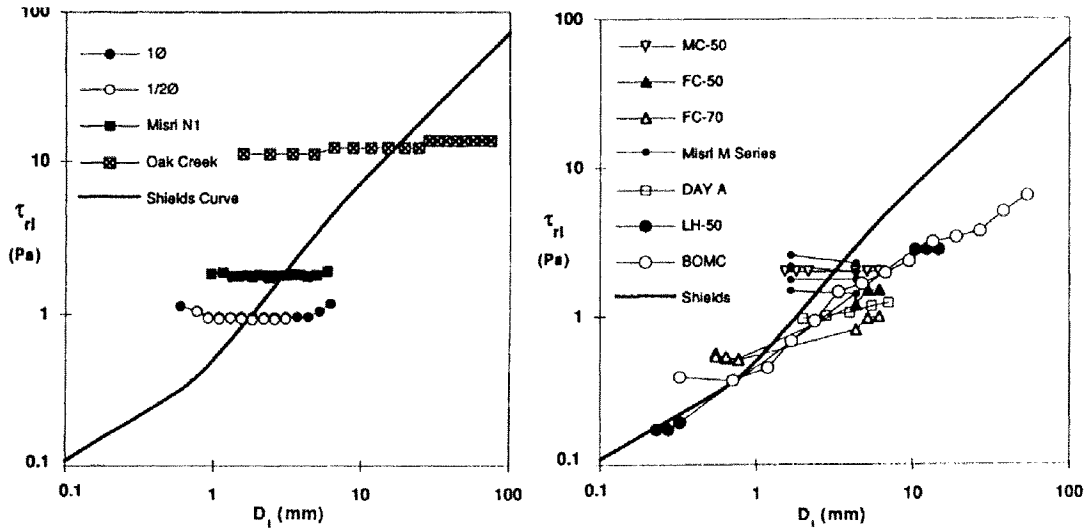

figure 14 : D_i versus t_c for unimodal (left) and bimodal (right) mixtures (Wilcock, 1993)

This can be explained as follows: as two size fractions are dominant in the mixture and these modes contain most of the sediment, there is little material to create a gradual transition from coarse to fine grains and hence to create a well-mixed layer.
It can be compared to a bottom protection. If only big rocks are dumped on top of a sand bed the flow will still be able to extract sand from under the rock layer, however if the protection is build with several layers --increasing in median grain size from bottom to top-- between the sand bed and the top rock layer, no sediment can be transported through the protection.
From the above example it becomes clear that the difference in grain size between and the proportion of sediment in the two modes determines the difference in critical shear stress for the two size fractions. It is therefore important to define a degree of bimodality, based on the above mentioned parameters, in order to describe the critical shear stress of a mixture as a function of bimodality.

Wilcock defined a bimodality parameter:

$$B = \sqrt{\left(\frac{D_c}{D_f}\right)} \times \Sigma P_m \qquad (4.6)$$

in which: D_c is the grain size of the coarse mode, D_f is the grain size of the fine mode, ΣP_m is the proportion of the mixture contained in the fine- and the coarse modes. It has a maximum value of one for a purely bimodal mixture. The width of a mode is defined as the four $^1/_4$ ϕ units surrounding the maximum diameter within the mode. So a mode has a width of one ϕ unit.

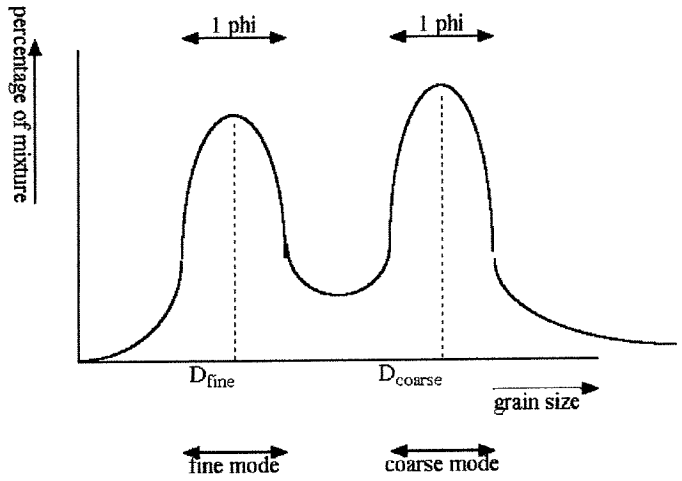

figure 15 : definition of parameters

It was found that for a value of the bimodality parameter, B, of less than 1.7 all size fractions in a mixture had more or less the same critical shear stress, which means near equal mobility. However, if B becomes greater than 1.7 smaller grain sizes begin moving at lower shear stresses than coarser grain sizes.
From figure 3 the bimodality of the Allier sediment can be calculated.

With D_c = 22.4 mm, D_f = 0.5 mm and ΣP_m = 0.51, the bimodality parameter, B, becomes 3.4. So according to Wilcock equal mobility is not satisfied for the survey area. This means that large particles have a higher critical shear stress than smaller particles, so $n < 1$ in equation (4.1). Unfortunately the value of the coefficient n for the survey area is not known. This requires bed load measurements.
For more information on transport of graded sediments the reader is referred to the work of A. Blom (2000).

4.4 Conclusion

In rivers with graded sediments a layer of coarse particles can form on top of the bed material. Such a layer is called an armour layer.
In graded sediments the threshold of movement for a particle is no longer governed by the weight of the particle alone. Due to the difference in particle sizes some particles are more exposed to the flow whereas others are protected from it by larger particles, the hiding-exposure effect. As a consequence the Shields criterion for the threshold of motion is no longer valid. To account for the hiding-exposure effect a hiding factor was introduced. With this hiding factor the critical shear stress for the D_{50} is corrected for the individual particle sizes. Calculations by Parker on the Oak Creek data showed that, although the sediment was graded, all particle sizes began to move at nearly the same critical shear stress. This was called equal mobility. Wilcock, however, showed that near-equal mobility only occurred for unimodal sediments. For bimodal sediments different particle sizes showed different critical shear stresses.

5 A hydrodynamic model for the study area

A computational model of a part of the river Allier is made in order to simulate the river flow during a flood. In this way, observations made during periods of low discharge and model output can be combined to enhance the understanding of river flow and morphology in combined sand-gravel bed rivers.
This chapter describes some basic features of the program Delft 3D-Flow, the construction of the model, the most important input parameters and the calibration of the model.

5.1 The program DELFT 3D-FLOW

Delft 3D-FLOW is the flow module of the Delft 3D package, an integrated modelling environment consisting of a set of modules developed by Delft Hydraulics. The hydrodynamic flow module DELFT 3D-FLOW is the core of the modelling environment and can be combined with other modules such as:
Wave module (WAVE)
Morphodynamic module (MOR)
Ecological module (ECO)
Water quality module (WAQ)
Particle tracking module (PART)
Sediment transport module (SED)

The FLOW module is a 2 -and 3-dimensional hydrodynamic simulation program that calculates non-steady flow and transport phenomena on a curvilinear boundary fitted grid. It can simulate flow phenomena with horizontal length scales that are significantly larger than the vertical length scales --shallow water flow -- an assumption which is generally correct for river flow. The non-steady shallow water equations can be solved in 2 (depth averaged) or 3 dimensions. In 3 dimensions it is possible to specify the number of depth layers and to express the distance between the layers in percentages of the total depth. This allows for a decreasing size thickness of the layers towards the bed in order to accurately calculate the velocities near the bed.

The most important assumption made in the FLOW module is that the vertical accelerations are assumed to be small compared to the gravitational acceleration and are neglected. The vertical momentum equation is therefore reduced to the hydrostatic pressure relation.

5.2 Data

The data necessary to build the model were obtained during a field survey by students of the Department of Physical Geography of the University of Utrecht near the city of Moulins in the summer of 1998. The retrieved data consists of bathymetry measurements, flow velocity measurements and sediment samples. For the set up and the calibration of the model the bathymetry measurements and the flow measurements are of importance.

The examined reach is situated approximately 6 km south of the city of Moulins and encompasses the 2 bends just upstream of Chateau de Lys. This reach is about 2 km long and is characterised by a high sinuosity [curved meander length/straight floodplain length, approximately equal to 1.6] and large point bars -- sediment deposits at the inside of the bend – which are partly vegetated.
To map the area first a framework of bathymetry measurements was laid over the area. This framework consisted of 17 cross sections, containing some 800 points. On each point bar the cross sections sprang radially from a base point while each cross section was rotated approximately 40 degrees with reference to the previous one. The base point on the upstream point bar was linked to the one on the downstream point bar. In this way all bathymetry measurements could be described in the same co-ordinate system with its origin on the downstream point bar. The positive x- and y axes directed south- and eastwards, respectively. The base point on the downstream point bar was chosen as the origin of the co-ordinate system as it proved to be the most stable point in the area, being located at the foot of a electricity pylon. This framework of bathymetry measurements is marked by the red dots in figure 16.

figure 16 : position of bathymetry measurements

In each cross section several measured points were marked by a small pile of stones and numbered with a fluorescent green colour in order to provide easily retraceable points from which further measurements could be made. These points are further called fixed points.
To obtain an indication of the maximum deviation of the bathymetry measurements a fixed point at the upstream boundary was linked with one at the downstream boundary, during the measurement of the water line. The position of the downstream fixed point was then known both by its co-ordinates as well as relative to the upstream fixed point. The difference between the two measurements of the position of the downstream fixed point was used as an indication of the maximum deviation.
The distance along the waterline between the upstream- and the downstream point was approximately 2500 m. The deviation in the horizontal plane was 20 m. In the vertical plane the deviation was 0.2 m. The total difference in height between the upstream point and the downstream point was 1.61 m. Locally the deviation was much smaller, both in the horizontal- as well as in the vertical plane.
Next, the flow measurements were carried out, they are marked by the yellow dots in figure 16. Starting from the upstream boundary the flow velocity was measured in 31 sections. Each section consists of several verticals in which at a number of fixed heights above the bed the flow velocity was measured with the aid of an EMF -- an electro magnetical flow meter--, a device that can measure flow velocities in two directions. From bottom to water surface at 5,10,15, 20, 30 , 40 , 60 , 80 and 100 cm, the velocity was measured in 2 directions, u_x and u_y, in order to detect secondary flow patterns. These velocities were later converted to one velocity and a flow direction. The sections were aligned perpendicular to the main channel and distances between the sections were approximately 100 m.
For each vertical the bed- and water level and its position in the horizontal plane were measured and linked to a fixed point. This provided an additional 200 bathymetry measurements for the model bathymetry.

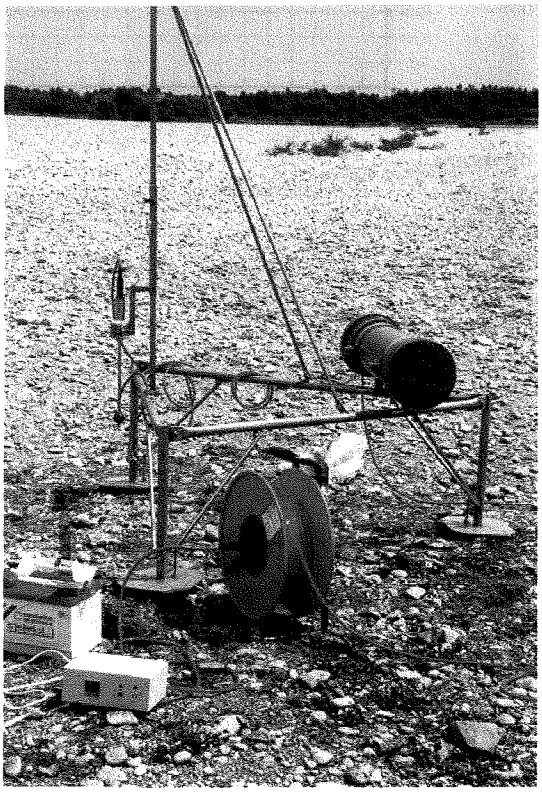

figure 17 : frame for velocity measurements

During the period of measurements at one point along the river the water level was recorded daily to account for differences in discharge.

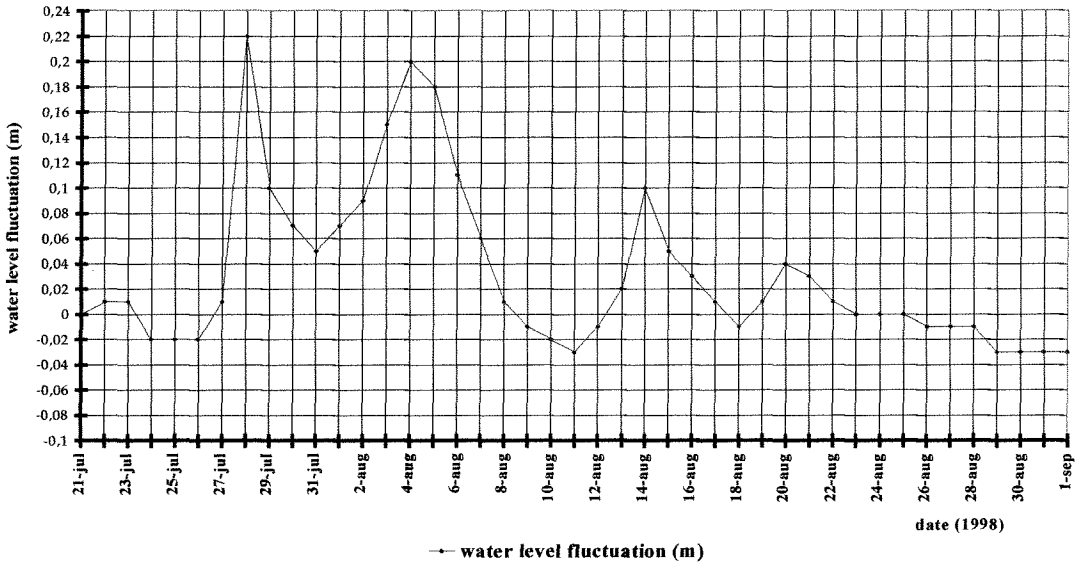

figure 18 : water level fluctuation during measurements (Neesssen, 2000)

For more information on the survey see appendix A

5.3 Computational grid and bathymetry

The core of every flow model consist of the grid and depth file, the grid being the spatial discretization of the area and the depth file the implementation of the bathymetry. To construct the grid- and depth file the bathymetry measurements were used.

First the bathymetry measurements were transformed from radial co-ordinates to a cartesian co-ordinate system (x,y,z) with its origin on the downstream point bar. This point was used as the basis from which all points were measured, all distances and heights are relative to this point. Then the x,y co-ordinates were used to define the land boundaries for the surveyed area and for the main channel. A land boundary is a line which follows the contours of a part of the area which has to be modelled, for example the main channel, and thereby allows for an easier and more precise implementation of the area shape onto the grid. These land boundaries were then loaded into the grid generator program RGFGRID (Delft Hydraulics) which was used to construct the grid.
This program can construct curvilinear grids, which can follow the boundaries of the area of interest smoothly and hence avoid the introduction of numerical diffusion caused by the jagged boundaries of rectangular grids. Another advantage of this

program is the possibility of applying high grid resolutions in areas of interest and low resolutions in other areas in order to minimise the computational effort.
The grid has to fulfil 2 important restrictions of numerical nature:

- Orthogonality , the perpendicular intersection of the grid lines.
- Smoothness in the variation of the grid spacing.

Both restrictions have to be met in order to minimise inaccuracy errors in the finite difference operators.

After the grid had been generated the bed level was assigned to the grid points by means of the program QUICKIN (Delft Hydraulics), a program to create and modify the model bathymetry. To generate a depth file the bathymetry measurements (x,y,z co-ordinates) were loaded into Quickin and then the bathemetry was interpolated to the grid points. Although the field data were rather comprehensive there were still some "gaps" left, so the interpolation was both based on the field data and on personal observations made during the survey.

5.4 Input parameters

This paragraph deals with the most important input parameters, such as: time step, boundary & initial conditions, roughness coefficient and eddy viscosity.

5.4.1 Number of layers

The difference between a 2D- and a 3D calculation is the number of layers in which the flow quantities are calculated. For a 3D calculation the water depth is divided into a number of layers, whereas for a 2D calculation only one layer is used. It is necessary to specify the number of layers in the input file. The more layers are specified, the better the internal flow structure is calculated.
For all the simulations the water depth was divided into 6 layers. As the maximum water depth for the highest discharge is estimated at 6 or 7 m, this gives a fair representation of the internal flow structure. Also the distance between the layers was decreased towards the river bed in order to improve the accuracy of the calculated velocities near the bed. The distance between two adjacent layers is given by a percentage of the water depth. From surface to bed the distance between the layers is 30, 20, 20, 15, 10 and 5 % from the local depth, respectively.

5.4.2 Time step

Delft 3D uses an implicit, unconditionally stable scheme, hence for stability the time step is not limited. For accuracy reasons however, the Courant number, σ, still has to be small. To obtain accurate results the value of the Courant number should not exceed 20, preferably the Courant number should be smaller.
The Courant number reads:

$$\sigma = c\frac{\Delta t}{\Delta x}$$

In which c is the celerity of a disturbance, in case of flow simulations c equals $\sqrt{gh}$, Δt is the time step, Δx is the distance between the grid points, g is the gravitational acceleration and h is the water depth.

The model was calibrated for a discharge of 20 m^3/s. For the calculations a time step of 3 seconds is used. In figure 19 the Courant numbers for this discharge are shown. The values of the Courant number are sufficiently small for accurate simulation results.

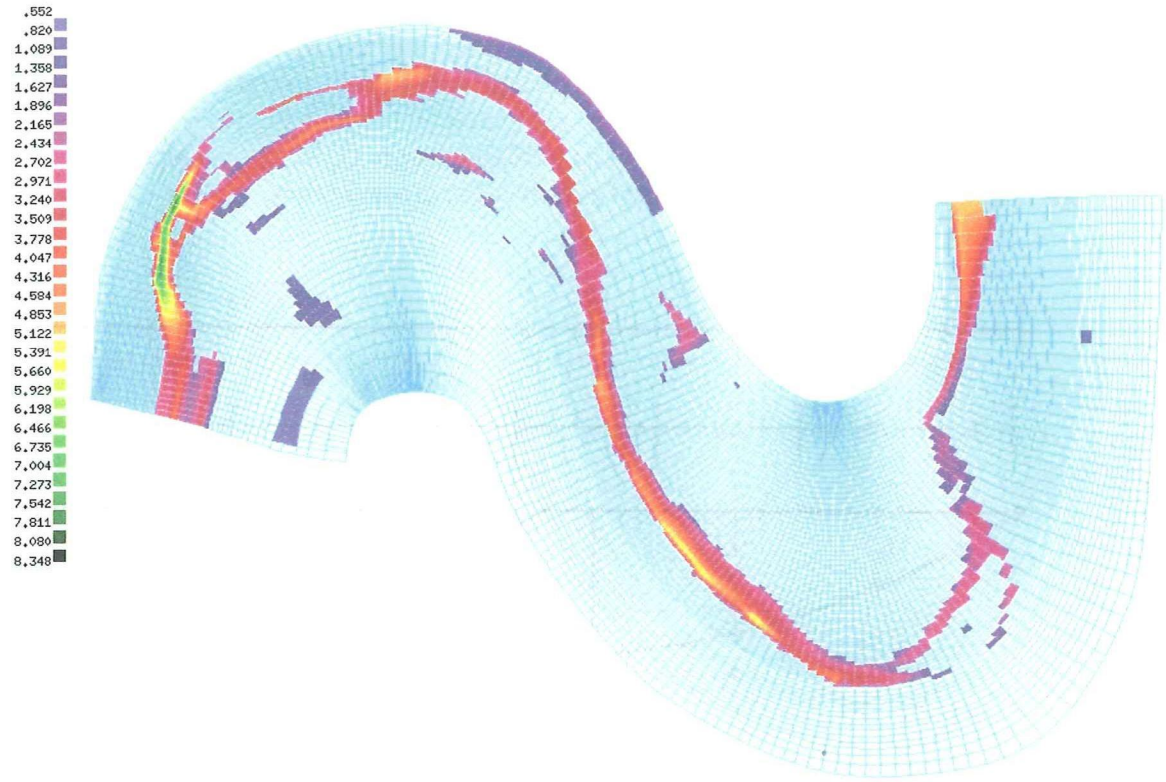

figure 19 : courant numbers for a discharge of 20 m^3/s

5.4.3 Boundary conditions

As only a small part of the river is modelled, the boundaries of the model will have to be situated far enough away from the area of interest to prevent small errors in the boundary conditions to influence the model results during the simulation. At the upstream boundary a discharge is prescribed and at the downstream boundary a water level.
As discharge data is only available for the cities of Moulins and Chatel de Neuvre there is no stage – discharge relation available for the model area. Therefore a stage - discharge relation has been estimated for the model area, with the aid of the Manning equation.

$$U = \frac{1}{n}\sqrt[3]{R^2}\sqrt{i} \qquad (5.1)$$

In which U is the mean flow velocity, R the hydraulic radius, i the energy slope of the flow and n the Manning parameter.
Because the energy slope is not known, the discharge is estimated based on the main channel slope. Also the water depth is used instead of the hydraulic radius, a simplification which is possible due to the large width to depth ratio.
At the upstream boundary the required discharge has to be divided over the grid cells.

To achieve this, first the velocity per grid cell, U_i, is calculated on the basis of the bed level, z_{bi}, the water level, z_{wl}, and the bed slope, i. For the Manning coefficient a value has to be assumed. This value can change during the calibration of the model. Second the discharge per grid cell,q_i, is calculated by multiplying the velocity with the width and the depth of the grid cell. The total discharge, Q, is then obtained by summation of the discharges per grid cell over the cross section.

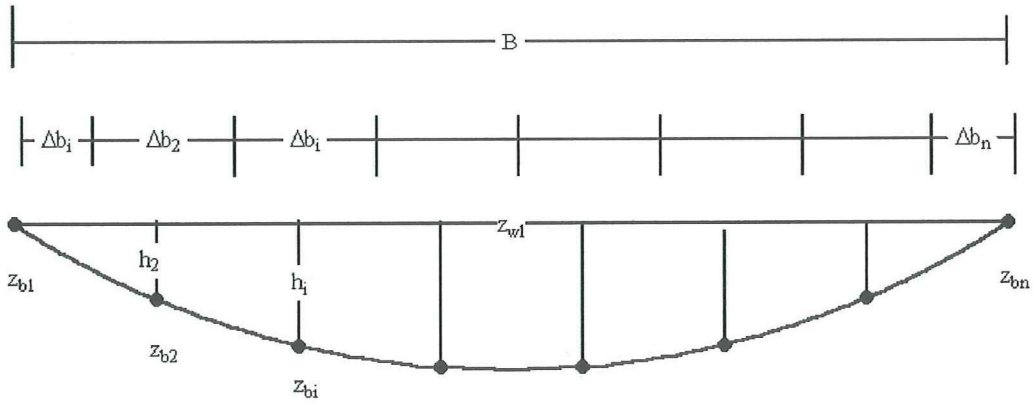

figure 20 : schematisation upstream boundary

$$h_i = z_{wl} - z_{bi} \qquad (5.2)$$

$$U_i = \frac{1}{n}\sqrt[3]{h_i^2}\sqrt{i} \qquad (5.3)$$

$$q_i = \Delta b_i \frac{1}{n}\sqrt[3]{h_i^2}\sqrt{i} \qquad (5.4)$$

$$Q = \sum_B \Delta b_i \frac{1}{n}\sqrt[3]{h_i^2}\sqrt{i} \qquad (5.5)$$

By using the water- and bed level to calculate the depth the only unknown variable over the cross section is the water level, as bed slope and bed level are known from the model bathtymetry.

At the downstream boundary the water level which matches the required discharge is prescribed. This water level is calculated with the same procedure as for the upstream boundary.

The value of the Manning coefficient influences the velocity and the water level and hence the discharge distribution over the grid cells. If the value of the Manning coefficient used for the estimation of the discharge does not correspond with the one used in the model, discrepancies between the boundary conditions and the simulation

results can occur. For discharge boundary conditions small errors in the discharge distribution are not much of a problem as the model can correct itself and will reach the correct distribution a few grid cells downstream of the boundary. For water level boundary conditions however, a much larger distance is needed for the error to correct itself (at the scale of the backwater curve).
Therefore the upstream discharge distribution and the downstream water level have to be recalculated several times during the calibration of the model with an adapted Manning coefficient.

As an initial condition the water level at the upstream boundary, corresponding with the calculated discharge is prescribed.

5.4.3.1 Influence downstream boundary condition

At the downstream boundary a water level is prescribed. Water level boundaries are sensitive to errors. An error in the prescribed water level causes a backwater effect, which forces the water depth to differ from the equilibrium depth. This backwater effect can influence the flow for a considerable distance upstream of the boundary. The influence of an error in the water level boundary condition can be estimated with the Bresse approximation:

$$\eta_i = 1 + \left(\frac{1}{2}\right)^{\frac{\Lambda_a}{\Lambda_0}} (\eta_0 - 1) \qquad (5.6)$$

with,

$\eta_i = \frac{h_i}{h_e}$, ratio between water depth and equilibrium depth at distance i from the downstream boundary

$\Lambda_i = \frac{x_i i_b}{h_e}$, non-dimensional distance from downstream boundary

$h_e = \left(\frac{q^2}{C^2 i_b}\right)^{1/3}$, equilibrium depth

$\Lambda_{1/2} = 0.24\eta_0^{4/3}$, value of Λ where the difference between h and h_e is halved

The Bresse formula is in fact a simplification of the Belanger formula, which is derived for steady, one dimensional flow. The simplification of the Belanger formula to the Bresse approximation is only allowed when the actual water depth is much larger than the critical water depth. For more information the reader is referred to De Vriend (1997).
To estimate the influence of an error in the downstream boundary condition for the model area, the examined reach is schematised to a 3000 m long channel with a width of 63.5 m and a slope of 0.0005 (0.5 m per km). For the width the averaged width of all velocity cross sections was taken. For the bed slope the elevation of the deepest point in each cross section was plotted against the distance along the thalweg and a line was fitted through these points.

As the variation of width with discharge is not known for the model area, the value of the discharge per unit width, q, cannot be calculated and hence the values of the equilibrium depth, h_e, and η cannot be determined for discharges other than the one for which the measurements were carried out. Therefore the estimation of the influence of the boundary condition error is restricted to discharges in the range of 20 - 40 m^3/s, which occurred during the survey. Even in this range the width of the channel changes significantly due to the gently sloping banks. However, it is not likely that the shallow near bank zone contributes substantially to the discharge increase within this range. It is therefore assumed that the width of the channel is constant for these discharges.
In figure 21 the results of the Bresse approximation for a discharge of 20 m^3/s are shown.

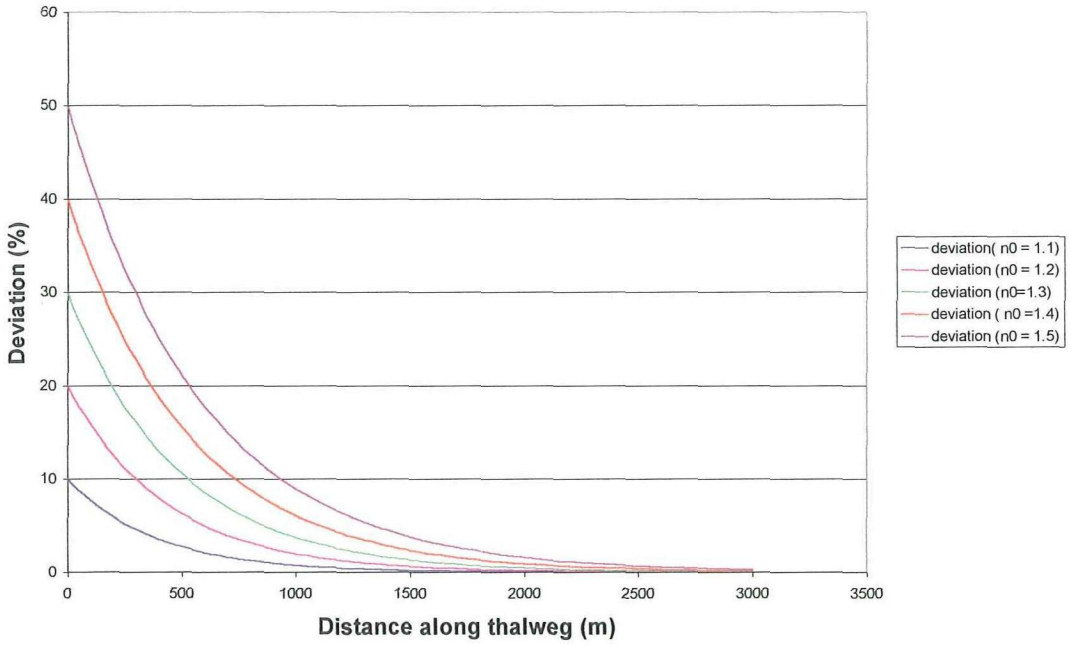

figure 21 : Deviation with reference to equilibrium depth

To obtain a numerical estimate of the influence of the downstream boundary condition, in the program DELFT3D-Flow the downstream water level was purposely changed with reference to a previous calculation. By raising the downstream water level with 10% and 20 %, respectively, with reference to the thalweg, the introduced backwater effect can be plotted against the distance along the thalweg and the analytical- and numerical results can be compared.
In figure 22 the results for the numerical estimation of the influence of the downstream boundary condition are shown.

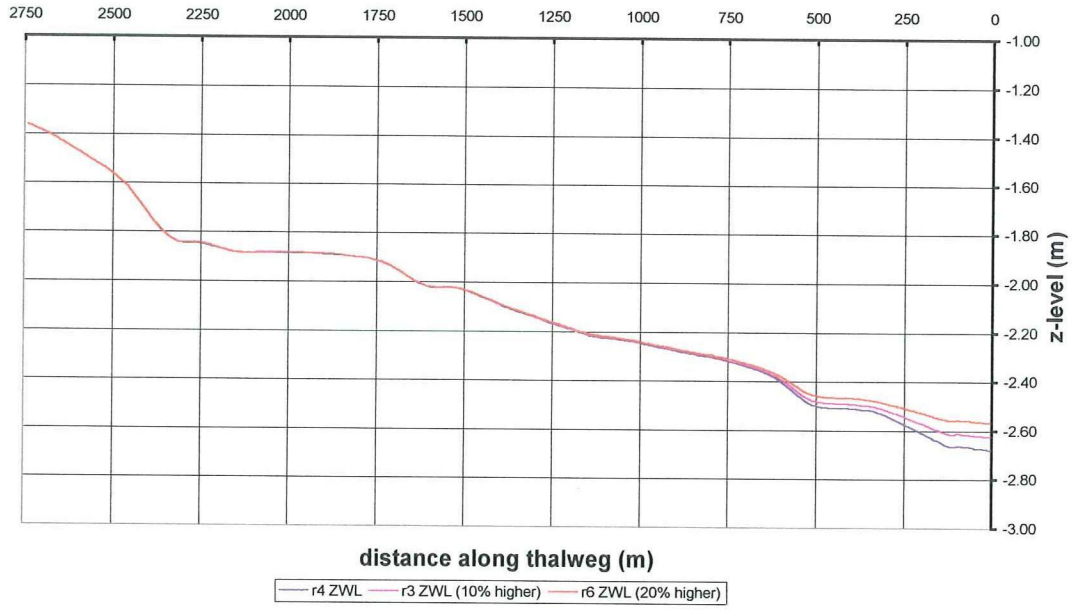

figure 22 : Numerical back water effect

The Bresse approximation gives a back water effect for $^{+}$/- 1000 m. upstream of the downstream boundary while the numerical estimation gives a back water effect for approximately 750 m. upstream. Despite the strong simplification of the geometry in the Bresse approximation, it still gives a fair estimate of the influence of the downstream boundary condition.
For the model it follows that the area downstream of cross section 3 is influenced by an error in the downstream boundary condition. It must be noted however that 250 m upstream of the boundary the error is already halved, see figure 22.

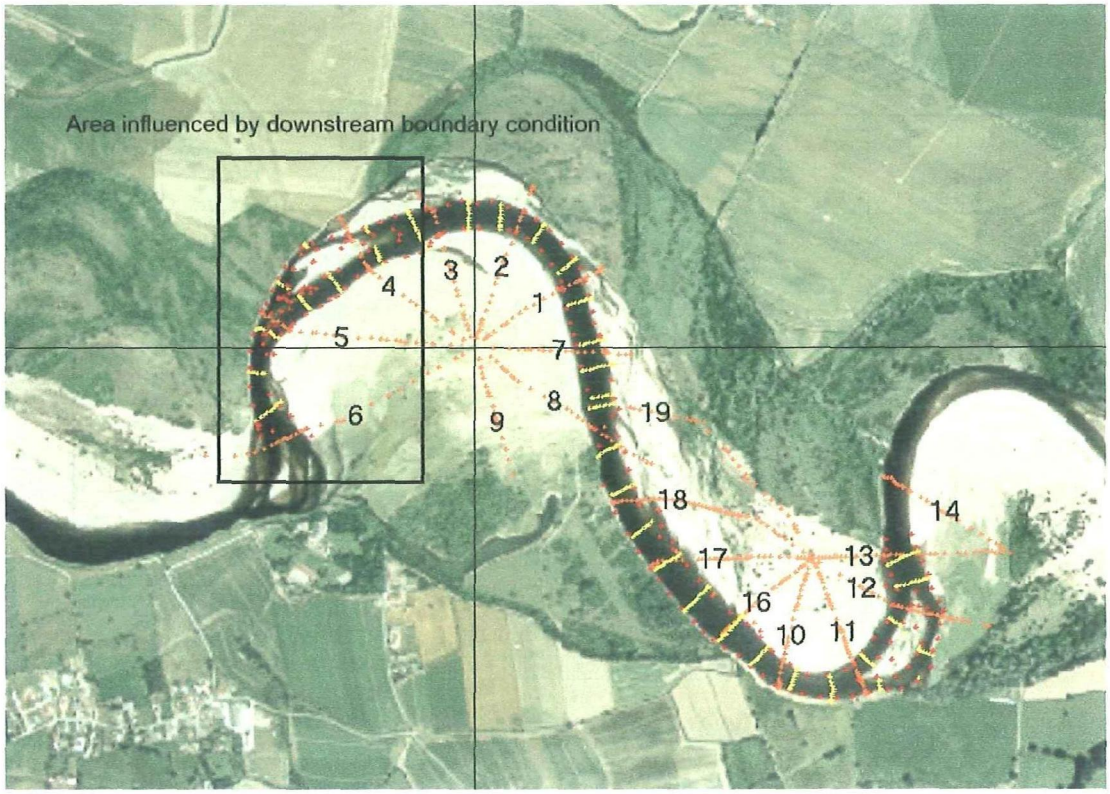

figure 23 : area influenced by downstream boundary condition

5.4.4 Bed stress formulation, Roughness coefficient

To account for the hydraulic roughness a bed stress coefficient has to be specified. For this model the Manning coefficient is chosen. The Manning formula is preferred over the Chezy formula as the numerical implementation of the Manning formula incorporates the influence of the water depth on the hydraulic roughness.

For a 2D computation the bed shear stress is determined according to:

$$\tau_b = \rho \frac{g}{C_{2D}^2} \left|\overline{U}\right|^2 \qquad (5.7)$$

In which: τ_b is the bed shear stress, ρ the mass density of the water, g the gravitational acceleration, C_{2D} the bed roughness coefficient and U the depth averaged velocity.

And the roughness coefficient, according to the Manning formula, is calculated by:

$$C_{2D} = \frac{\sqrt[6]{h}}{n} \qquad (5.8)$$

In which h is the water depth, and n is the Manning coefficient.

For a 3D-computation the bed stress is determined in a similar way, only the velocity in the first layer above the bed, u_b, instead of the depth averaged velocity, is used:

$$\tau_b = \rho \frac{g}{C_{3D}^2} |u_b|^2 \qquad (5.9)$$

And the roughness coefficient is defined as:

$$C_{3D} = \frac{\sqrt{g}}{\kappa} \ln\left(1 + \frac{0.5\Delta z_b}{z_0}\right) \qquad (5.10)$$

In which: Δz_b is the thickness of the computational layer at the bed and z_0 the roughness height determined by:

$$z_0 = h \bullet e^{-\left(1 + \frac{\kappa}{\sqrt{g}} C_{2D}\right)} \qquad (5.11)$$

By substituting (5.11) in (5.10) the relationship between the 2D and the 3D-roughness coefficient becomes approximately:

$$C_{3D} = C_{2D} + \frac{\sqrt{g}}{\kappa}\left(1 + \ln\left(\frac{\frac{1}{2}\Delta z_b}{h}\right)\right) \qquad (5.12)$$

To estimate the influence of the Manning parameter the flow velocities in section 17 are compared for two simulations with different roughness coefficients. In the first simulation the roughness coefficient, n, around section 17 is 0.024, in the second n = 0.028, an increase of approximately 17%.

section	Utot (r7) (m/s)	Utot (rl%) (m/s)	difference (m/s)	difference (%)
	n = 0.024	n = 0.028		
17.1	0.48	0.43	-0.05	9.90
17.2	0.63	0.59	-0.04	6.89
17.3	0.69	0.63	-0.05	7.67
17.4	0.66	0.61	-0.05	7.63
17.5	0.57	0.53	-0.04	6.88
17.6	0.26	0.27	0.00	1.43
17.7	0.26	0.27	0.00	1.43
17.8	0.09	0.10	0.01	9.37
mean difference over cross section:				6.40

table 1 : influence Manning coefficient on flow velocity

As shown in
table 1, a change in the Manning coefficient does influence the flow velocity noticeably, although the magnitude of the change in velocity is limited. As a tool to calibrate the model the Manning coefficient is therefore more a fine tuning instrument.

The final values of the Manning coefficient, after calibration of the model, vary from 0.022 at the downstream end of the model to 0.026 at the upstream end.

5.4.5 Eddy viscosity

In Delft 3D the transport of turbulent momentum within the flow is accounted for by the Reynold stresses. These stresses are associated with the way turbulence is modelled. As turbulence cannot be modelled on a micro scale, necessary to simulate the highly irregular character of the turbulence, the description is usually limited to the "averaged " properties of the turbulence. The most common way to describe turbulence is to split the velocity into a mean part and a fluctuating part. This splitted velocity then can be substituted into the momentum equations and averaged over a period T, large enough to smooth the irregularities but small enough to discern the averaged values of the turbulence. During this averaging process, due to the non-lineair advection terms, residual terms are introduced, the so-called Reynolds stresses, which are the mean products of pairs of the fluctuating part of the velocity components. By introducing these extra terms the number of variables exceeds the number of equations and the equations can no longer be solved. This is called the turbulence closure problem. The extra equations needed are provided by the so-called turbulence closure model.
In Delft 3D four different turbulence models are implemented, one model is simply a constant value that can be specified and three models based on the eddy viscosity concept of Kolmogorov- Prandtl. In this concept the Reynolds stresses are expressed as a function of the velocity difference between adjacent layers in the flow, as an analogy to viscous shear. The proportionality between the Reynolds stresses and the velocity difference is accounted for by the eddy viscosity. In Delft 3D the eddy viscosity is composed of a (constant) 2D part and a part that is calculated by the turbulence model:

$$\nu = \nu_{2D} + \nu_v \qquad (5.13)$$

$$\nu_v = c_\mu L\sqrt{k} \qquad (5.14)$$

in which ν_v is the vertical eddy viscosity, L is the mixing length, k is the turbulent kinetic energy and c_μ is a constant ($\approx$0.5774).
The 2D-eddy viscosity has to be specified by the user and therefore can be used as a calibration parameter.
For more information the reader is referred to Delft3D-Flow user manual, release 2.48 (1996) .

To examine the sensitivity of the model to the eddy viscosity, two simulations were made: one with a ν_{2D} coefficient of 0.1 m^2/s and a second with a ν_{2D} coefficient of 0.2 m^2/s.
The differences for section 17 are given in the table 2.

section	Utot (r10)	Utot (r11)	difference	difference (%)
	ν_{2D}=0.1 m^2/s	ν_{2D}=0.2 m^2/s		
17.1	0.63	0.63	0.00	0.61
17.2	0.76	0.76	0.00	0.36
17.3	0.93	0.91	-0.01	1.57
17.4	0.95	0.93	-0.02	2.16
17.5	0.93	0.91	-0.02	2.27
17.6	0.84	0.83	-0.01	1.66
17.7	0.54	0.55	0.01	1.71
17.8	0.40	0.41	0.01	2.89
mean difference over cross section:				1.65

table 2 : influence eddy viscosity on flow velocity

As can be seen in table 2 the influence of the 2D eddy viscosity is very small. It can hardly be used as a calibration tool.

5.5 Calibration of the model

Purpose of the calibration is to tune the model to correctly predict the river flow as measured during the survey. The model was calibrated with the aid of velocity measurements obtained during the field survey. During the calibration two goals had to be achieved, the first was to correctly simulate the flow pattern, the second to correctly predict the water levels and flow velocities.
There are three parameters in the model to influence the flow. In order of importance: the bathymetry, the hydraulic roughness and the eddy viscosity.

As there were less bathymetry measurements than grid points, inter- and extrapolation was necessary to generate a bathymetry file and hence errors were introduced. These errors in the bathymetry have a large influence on the flow. After errors in the bathymetry are corrected the model can be "fine tuned" by adjusting the hydraulic roughness and the eddy viscosity.
The calibration procedure is as follows: Starting with the initial depth file the Manning coefficient was calibrated against the measured velocities and water levels. If one of the coefficients had to be chosen out of its normal range in order to approximate the measured velocities or water level, the depth file was modified, of course within the possibilities allowed by the bathymetry measurements.
The procedure is schematised in figure 24.

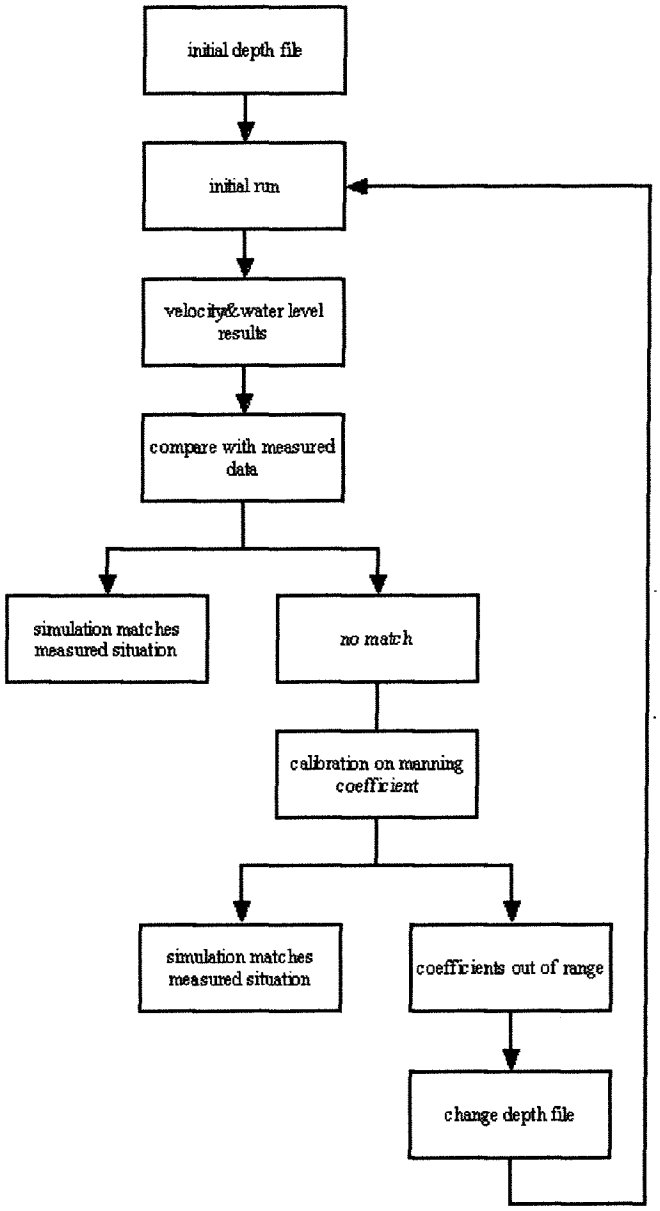

figure 24 : calibration procedure

Four out of the 31 velocity sections were selected to calibrate the model on. All four sections were measured at a discharge of approximately 20 m3/s. Section 4, near the upstream island, section 17, at the cross over region, and sections 25 & 26 near the downstream island. The sections are evenly distributed over the area, see figure 25, only near the downstream island two sections were used due to the complex flow pattern around the island. Between section 4 and section 17 a number of velocity sections are incomplete. Due to a deep pool in the outer bend it was only possible to obtain velocity measurements over a part of the cross section. For each cross section the measured values of the water level and the depth-averaged velocity were compared with the water level and depth-averaged velocity obtained from the model. As a calibration criterion a 15 % deviation for both the water depth and the depth averaged velocity was used.

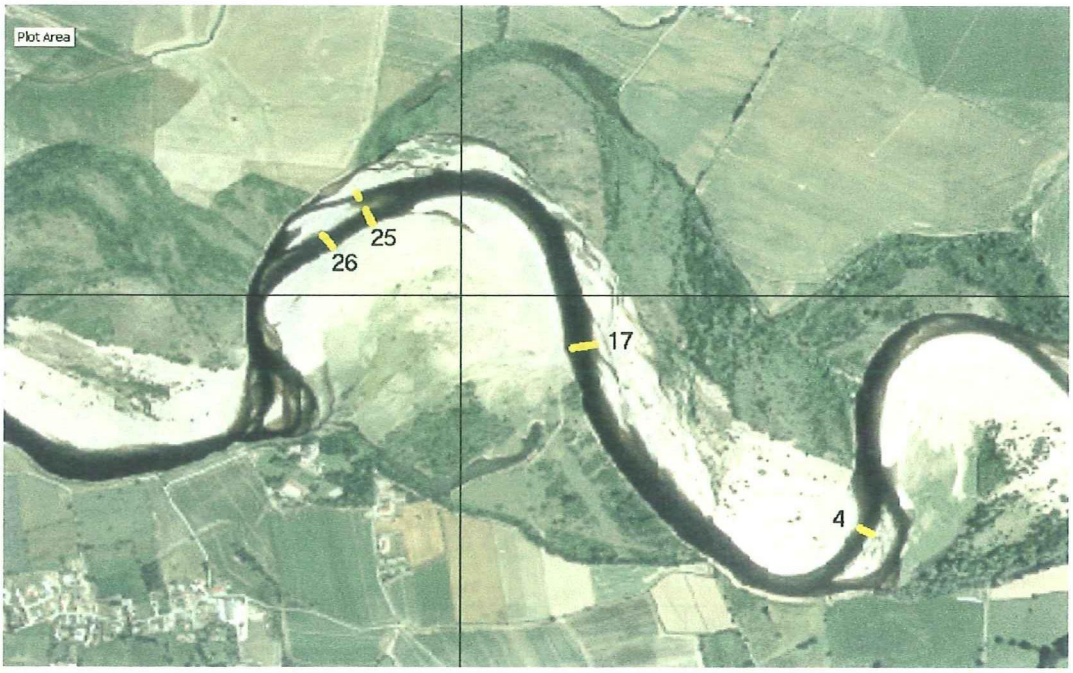

figure 25 : position of cross sections used for the calibration

5.5.1 Results of the calibration

This section describes the calibration results for a discharge of 20 m^3/s.
The vector plots clearly show the flow pattern and the discharge distribution around the 2 islands. The detailed vector plot of the flow around the downstream island (figure 26) shows the flow crossing the channel twice, once upstream of the island and once downstream of the island. It also shows an increase in the flow velocity at the beginning of the island due to the fact that the channel at the inner bend conveys most of the discharge.
This downstream bend consists of two curved stretches connected by a more or less straight stretch, this is called a double headed bend.
The plots of the depth averaged current magnitude (dacm) show a strongly varying velocity distribution over the area. At the upstream island (figure 27) the velocities in the channel at the inner bend vary between 0.8 and 1.2 m/s, in the secondary channel the velocities range from 0.2 and 0.6 m/s. At the end of the upstream bend the velocities decrease due to an increased depth (pool-riffle system). Near the island at the downstream bend the velocities first decrease due to a back water effect caused by the riffle and then accelerates to a maximum of about 1.6 m/s after which it slows down to about 0.8 m/s. At the end of the bend the velocities again increase to a value of 1.2 m/s due to a narrowing of the channel.

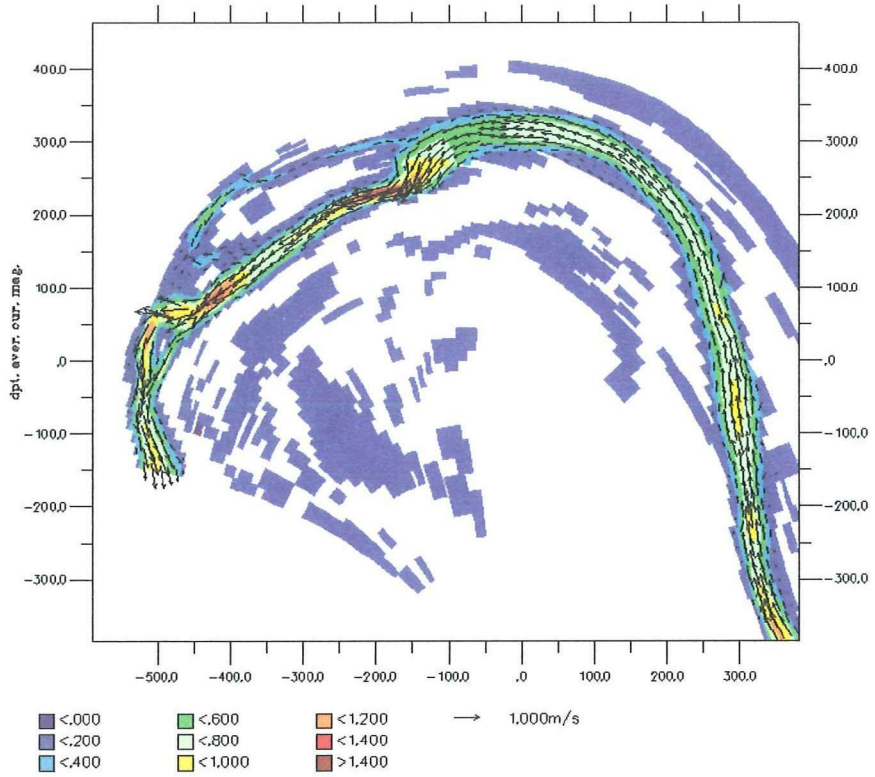

figure 26 : flow velocity for a discharge of 20 m^3/s , downstream bend

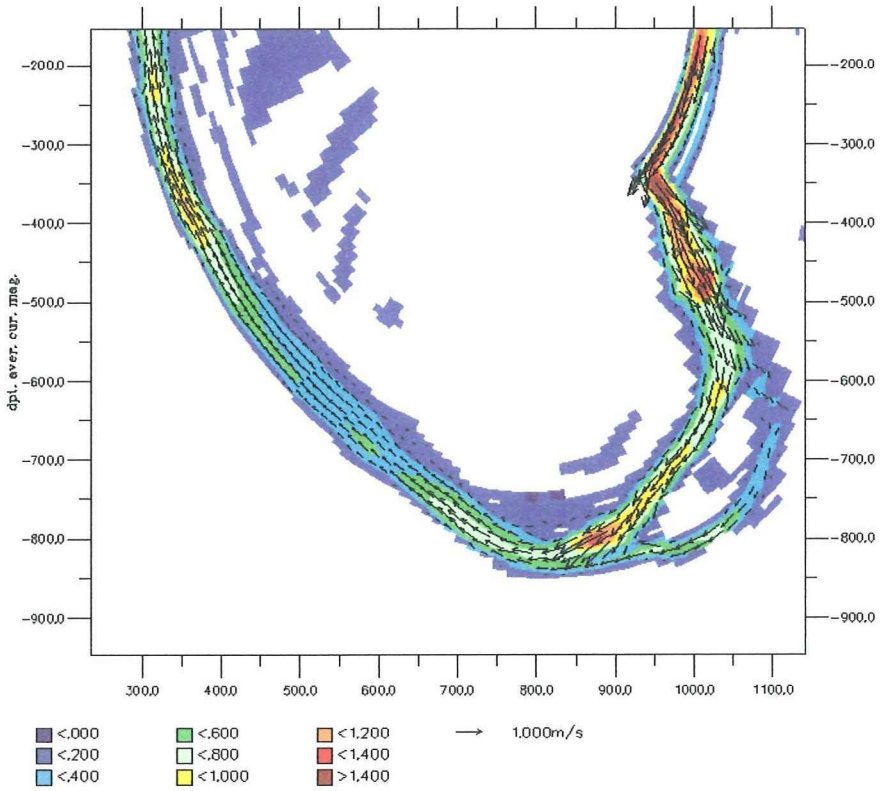

figure 27 : flow velocity for a discharge of 20 m^3/s , upstream bend

In the following table the deviation of the simulated depth averaged velocity and the water depth from the measurements, averaged over the cross section, is given for run r4.

section	velocity deviation (%)	water depth deviation (%)
4	4.97	5.74
17	21.86	4.47
25	7.22	14.69
26	22.06	21.10

table 3 : velocity- and waterdepth deviation between measured and simulated situation

The results show a good agreement for the upstream section, 4, but a poor one for the downstream sections, 17, 25 and 26. The latter three sections show higher water levels in the simulations than during the measurements, which indicates a back water effect. Section 17, however shows only a significant deviation for the velocity. If section 17 is investigated more carefully, see table 4, it is found that the deviation in the velocity is mainly caused by one velocity point near the bank. Due to the low velocity in that point a small difference between measured and calculated velocity will give a very large relative deviation. If this point is removed section 17 fulfils the 15 % deviation criterion. Therefore no further attention is paid to section 17.

	Usimulation	U measured	difference	diff. (%)
17.1	0.48	0.41	0.07	16.48
17.2	0.57	0.59	-0.02	3.21
17.3	0.69	0.69	0.00	0.07
20 min.	0.70	0.70	0.00	0.07
17.4	0.66	0.77	-0.10	13.61
17.5	0.57	0.62	-0.05	8.81
17.6	0.26	0.44	-0.18	39.79
17.7	0.09	0.26	-0.17	63.96
cross sectional averaged deviation:				18.25

table 4 : detailed velocity deviation for section 17

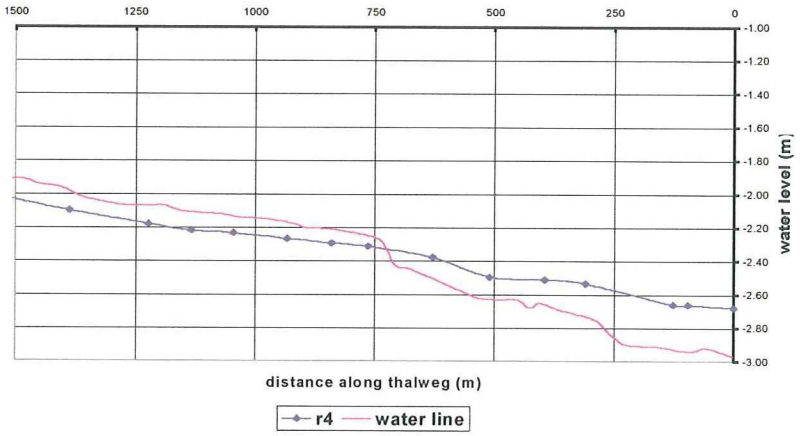

figure 28 : back water curve for first 1500 m from section 31

In figure 28 the water level, both measured and simulated, along the thalweg is plotted for the first 1500 m upstream from the last measured velocity section, section 31. The downstream boundary is situated further away. The water level is plotted from section 31 because that is the most downstream point where the water level was measured. From figure 28 it is immediately clear that the downstream boundary condition is not well calculated, the calculated value, approximately –2.7 m, is considerably smaller than the measured one, -2.97 m. The difference is too large to be explained from a wrong hydraulic roughness coefficient. Also if the calculation of the water level is inverted to calculate the gradient, that is if the measured water level is prescribed and the roughness is kept constant, the necessary gradient is approximately 2.5 *10-3, much higher than the measured value. A possible explanation is the contraction of the main channel in the last part of the downstream bend. Here the flow accelerates and decelerates after the contraction, as a consequence the flow can probably not be considered uniform and therefore the Manning equation is not valid.
As there is no information about the stage-discharge relation at the downstream boundary this problem cannot be fixed. It is therefore important to estimate the influence of this error on the flow pattern.

If the downstream boundary is positioned on section 31 and for the downstream boundary condition the measured value of –2.9 m is chosen instead of the calculated one, the results of the model should show a better similarity with the measured water level (run r2). In figure 29 it is shown that although the similarity is improved in the last 250 m before the boundary, further upstream the deviation between the measured and calculated water level is the same as during the previous simulation. Apparently a second error is present in the model.

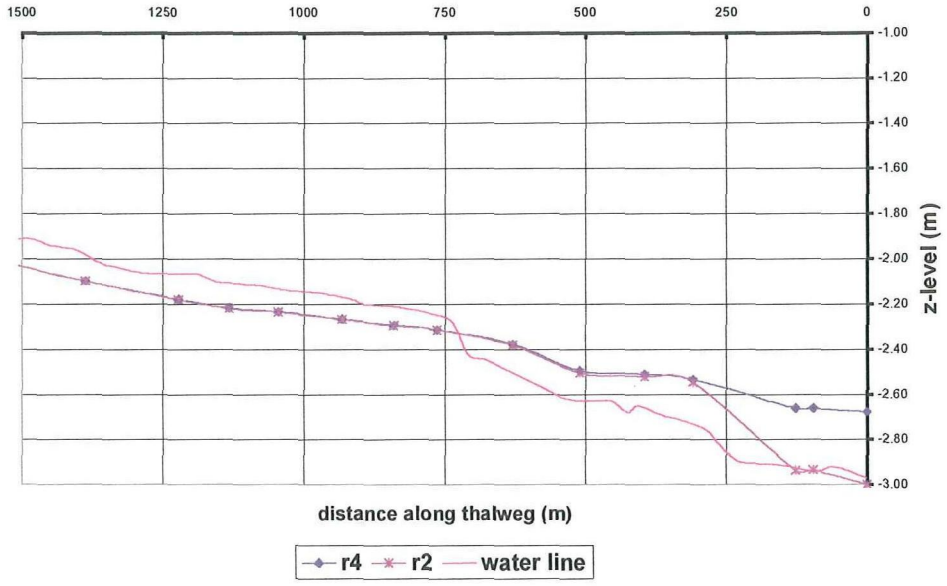

figure 29 : Back water effect for run r2

Between 750 and 250 m before the downstream boundary a back water effect occurs. It can be concluded that around 250 m before the boundary the flow encounters an obstacle in the model. This area is situated just downstream of the island in the downstream bend and consists of several bars, which divide the main channel more or less into an inner- and an outer channel. Here the thalweg jumps from the inner bend to

the outer bend. The flow is directed over a bar from the inner bend towards the outer bend. Further comparison between the flow pattern and the depth file reveals that although in this area the flow crosses the main channel, there is no clear connecting channel between the inside and the outside of the bend. This forces the flow over a bar and hence causing extra resistance. This area is not well modelled due to the lack of bathymetry measurements in this area.
If a connecting channel is included in the depth file the similarity is improved significantly (run r7) as shown in figure 30.

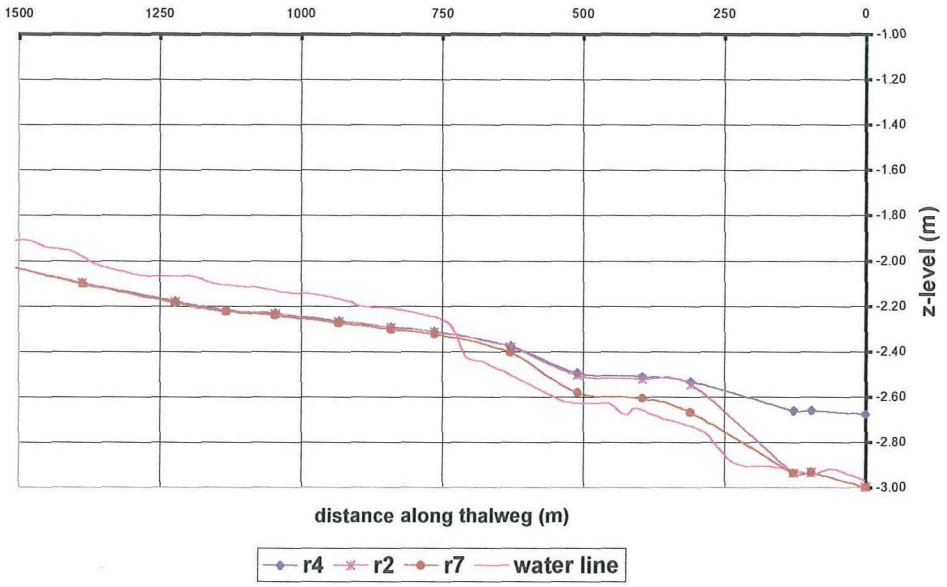

figure 30 : Back water effect for run r7

5.5.2 Conclusion

All cross sections now fulfil the 15 % deviation criterion for both the depth averaged velocity and the water depth, except for section 17. This is, as stated before, due to one velocity point near the bank.
As can be seen in figure 30 there are still some differences between the measured water level and the calculated one, but these differences are small enough to fulfil the 15 % deviation criterion.
In table 5 the final results of the calibration are shown.

velocity profile	measured velocity (m/s)	calculated velocity (m/s)	deviation (%)	measured water level (m)	calculated water level (m)	Water depth deviation (%)
4.1	0.17	0.18	2.98	-1.52	-1.48	6.06
4.2	0.47	0.41	12.78	-1.51	-1.48	3.40
4.3	0.59	0.58	2.03	-1.55	-1.48	9.00
4.4	0.73	0.72	2.24	-1.52	-1.49	4.68
cross sectional averaged deviation:			5.01			5.73
17.1	0.41	0.48	16.48	-2.11	-2.10	2.57
17.2	0.59	0.57	3.21	-2.11	-2.10	0.32
17.3	0.69	0.69	0.07	-2.12	-2.10	2.05
17.4	0.70	0.70	0.07	-2.12	-2.10	1.95
17.5	0.77	0.66	13.61	-2.11	-2.10	0.78
17.6	0.62	0.57	8.81	-2.11	-2.10	0.81
17.7	0.44	0.26	39.79	-2.10	-2.10	-1.10
17.8	0.26	0.09	63.96	-2.11	-2.10	5.31
cross sectional averaged deviation:			18.25			1.59
25.1	0.50	0.53	-6.04	-2.61	-2.58	6.32
25.2	0.79	0.90	-15.02	-2.59	-2.58	1.29
25.3	1.01	1.07	-5.92	-2.63	-2.58	6.94
25.4	1.00	0.85	14.32	-2.61	-2.59	7.61
cross sectional averaged deviation:			10.32			5.54
26.1	0.58	0.52	10.77	-2.65	-2.61	5.89
26.2	0.77	0.67	13.87	-2.66	-2.61	5.93
26.3	0.80	0.73	8.47	-2.67	-2.61	8.87
26.4	0.49	0.57	16.90	-2.67	-2.61	7.34
cross sectional averaged deviation:			12.51			7.01

table 5 : results of the calibration

6 Simulation results

6.1 Introduction

The flow model is used for two types of simulations: steady state and unsteady state. The steady state simulations have a constant discharge and a simulation period of two hours, and therefore a short computation time. Because of the short computation time they were used to give an overview of the flow pattern over a wide range of discharges. A discharge range of 100-1000m^3/s was chosen because of the limitations of the flow model.
The maximum recorded discharge for the Allier over the period 1968-1995 was about 1400 m^3/s. At this discharge however, a larger area is flooded than the model area. The farmlands on the right side of the main channel, in downstream direction, are flooded at a discharge of approximately 1000 m^3/s. These farmlands were not included in the survey and therefore not incorporated in the flow model.
For the unsteady simulation the flood of November 1994 was chosen. To shorten the simulation time, only a part of the flood is simulated. The simulation starts with a discharge of about 350 m3/s and ends when the discharge has again decreased to approximately 500 m^3/s. This is possible because the main interest of the research is in the flooding of the point bars and the bed stress for the higher discharge ranges. This gives a simulation time of 5 days, from the 5th until 10th of November, and a computation time of several days. To schematise the flood, in the input file every 12 hours the discharge is prescribed. Within these twelve hour intervals Delft 3D interpolates the discharge for every time step to obtain a smooth wave.

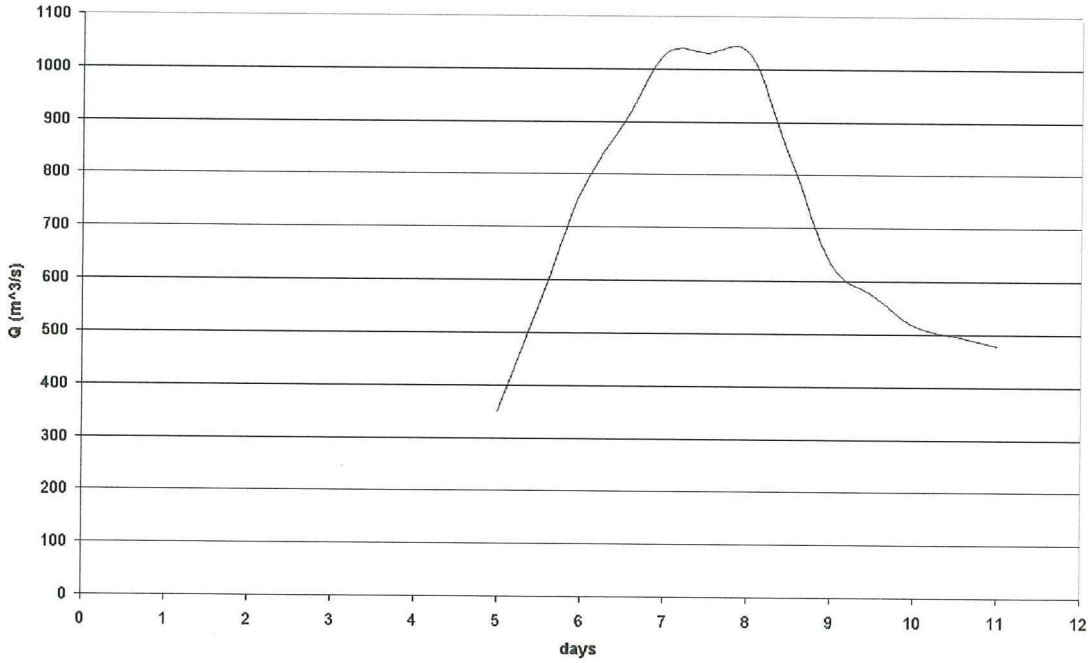

figure 31 : flood november 1994

Run id		Discharge (m^3/s)	Time step (s)	Number of layers	Manning coefficient
S61	Steady state	100	3	6	0.022-0.026
S62	Steady state	200	3	6	0.022-0.026
S63	Steady state	300	3	6	0.022-0.026
S64	Steady state	400	3	6	0.022-0.026
S65	Steady state	500	3	6	0.022-0.026
S66	Steady state	600	3	6	0.022-0.026
S67	Steady state	700	3	6	0.022-0.026
S68	Steady state	800	3	6	0.022-0.026
S69	Steady state	900	3	6	0.022-0.026
S60	Steady state	1000	3	6	0.022-0.026
N94	Unsteady state	500-1000	3	6	0.022-0.026

table 6 : overview runs

In the following chapter the results of both steady- and unsteady state simulations will be described. To minimise the overlap between the steady state simulations and the unsteady state simulation the description of the steady state is limited to the flow in the discharge range of 100 - 500 m^3/s. The unsteady state simulation will describe the flow in the range of 500 - 1000 m^3/s. At the end of the chapter the steady state simulations in the range of 500 - 1000 m^3/s will be compared with the results of the unsteady state simulation

In all runs the main channel and floodplain have the same roughness. The roughness file is included in appendix (C).

6.2 Influence downstream boundary condition

As stated in chapter 5, the downstream boundary condition could not be generated well. To study the effect of an error in the downstream boundary condition the steady state run with discharges of 500 m^3/s was repeated with a different downstream boundary condition. For this run, run %65, the downstream water depth was chosen 10 % deeper, relative to the thalweg, than for run S65. The difference in water level between the steady state run, s65, and run %65, is plotted in figure 32.

Run id	Discharge (m^3/s)	Zwl (m)at downstream boundary	Depth (m)
S65	500	-1.6	2.09
%65	500	-1.42	2.27

Within 500 m the difference becomes less than 0.02 m, so a difference in downstream boundary condition seems to dampen quite fast. Of coarse there is no data on the real water level for the higher discharge ranges, this analysis only shows the influence of a change in downstream boundary condition on the flow. It is not a measure for the difference between the real water level, as it would occur in nature, and the calculated one, which is used as the boundary condition.

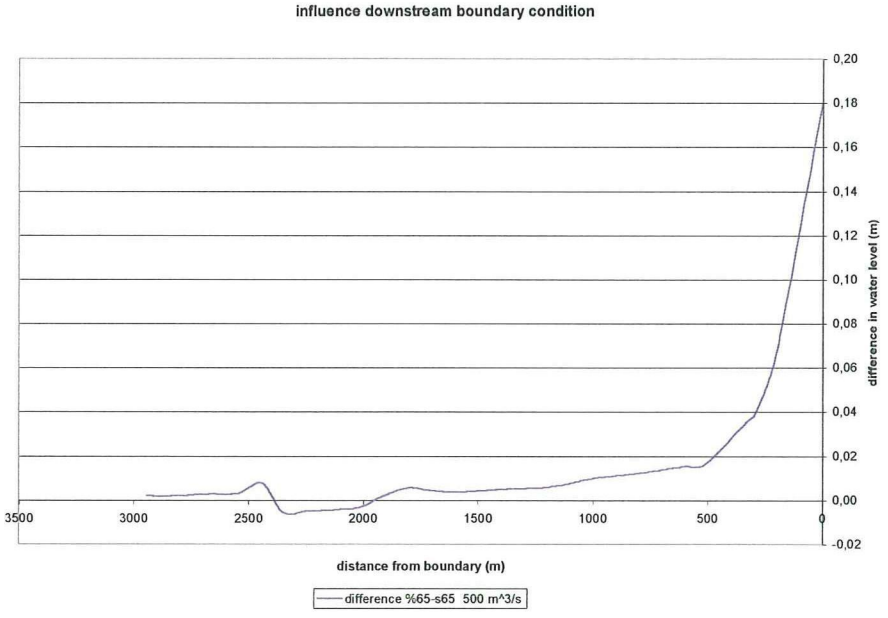

figure 32 : influence downstream boundary condition

6.3 Courant numbers

Although Delft 3D uses an unconditionally stable scheme the Courant number still has to be small to limit the numeric errors.
The next figure shows the courant numbers for a discharge of approximately 1000 m^3/s and a time step of 3 seconds. The Courant number nowhere exceeds 12, which is sufficiently small.

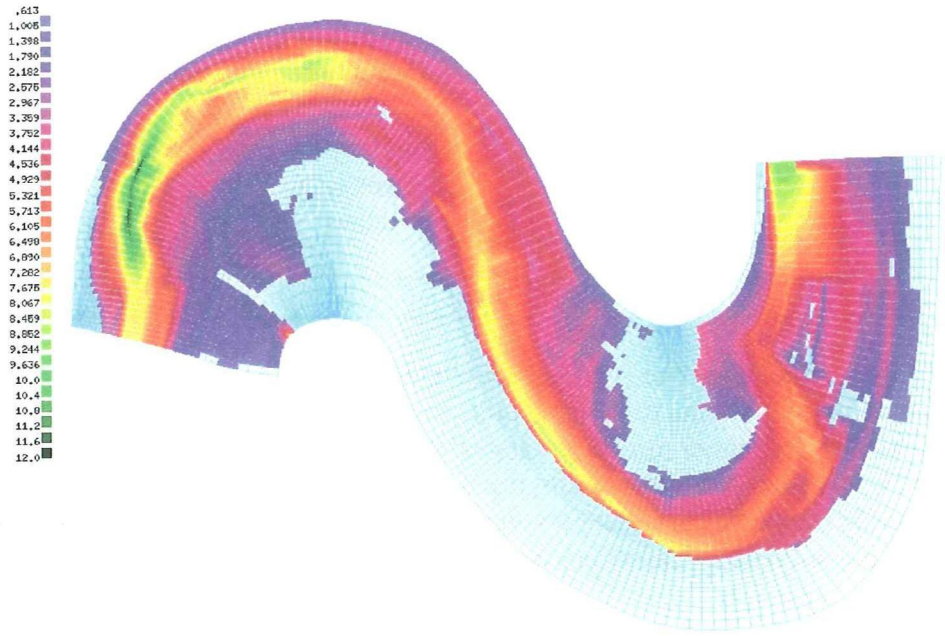

figure 33 : courant numbers for a discharge of 1000 m^3/s

6.4 Secondary flow

The secondary flow can be visualised by plotting the difference in the flow direction between the layer1, near the surface, and layer 6, near the bed.
In figure 34 The difference in flow direction between the surface- and the bed layer,and hence the secondary flow pattern, is shown for a discharge of 100 m^3/s. The difference in flow direction is mainly concentrated at the two bends, the greatest difference in flow direction between the upper- and lower layer is situated where the bend radius of curvature is shortest.
This is more clearly illustrated in figure 35. In the downstream bend two clear secondary flow cells can be distinguished. This bend is more or less composed of two sharply curved stretches connected by a straight channel, the largest difference in flow direction between the two layers, marked by the orange-red cells in figure 35, is found at these curved stretches. In the upstream bend also two secondary flow cells can be seen, the blue cells. The purple band of secondary flow cells at the beginning of the upstream bend is probably caused by the fact that the grid lines here do not follow the main channel smoothly. In the model the edges of the main channel here have a

staircase form, with on the one side the main channel and on the other the (high) banks. In this jagged pattern eddies are formed.

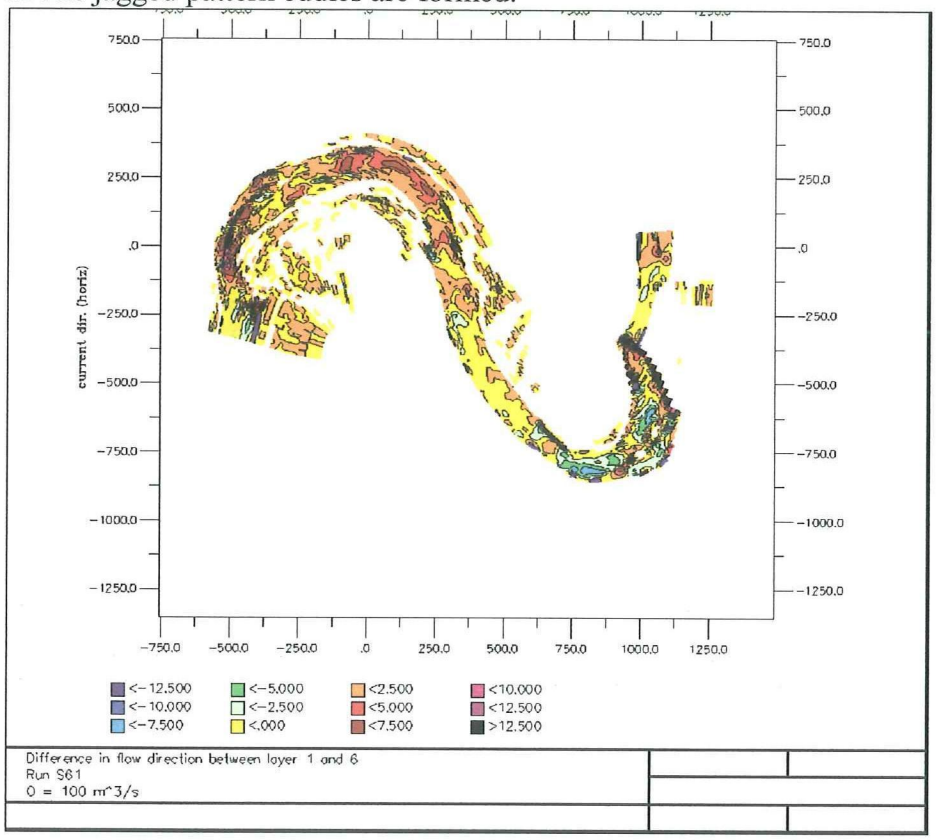

figure 34 : difference in flow direction between surface- and bed layer for a discharge of 100 m^3/s

In figure 36 the difference in flow direction for a discharge of approximately 1000 m3/s is shown. The cells where the secondary flow is strongest have become somewhat larger and at the upstream bend they have developed into one big secondary flow cell but the pattern is the same as in figure 35. No large secondary flow cell has yet developed at the crossover region as there is no difference in direction between the upper- and lower layer of the flow. It can therefore be concluded that the flow in the range from 500 - 1000 m^3/s follows an inbank flow pattern. Because the point bars are still not fully flooded the flow in both the upper- and lower layer are more or less in main channel direction. The characteristic overbank flow pattern, as described in chapter 3, will only develop at those discharges which do flood a significant part of the point bars.

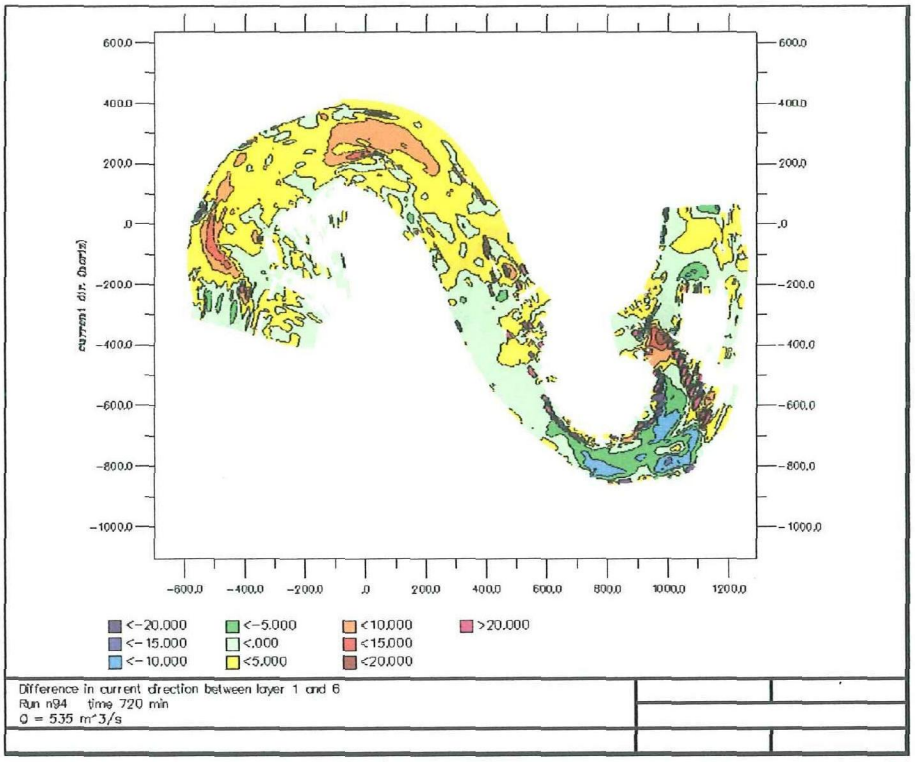

figure 35 : difference in flow direction between surface- and bed layer for a discharge of 500 m^3/s

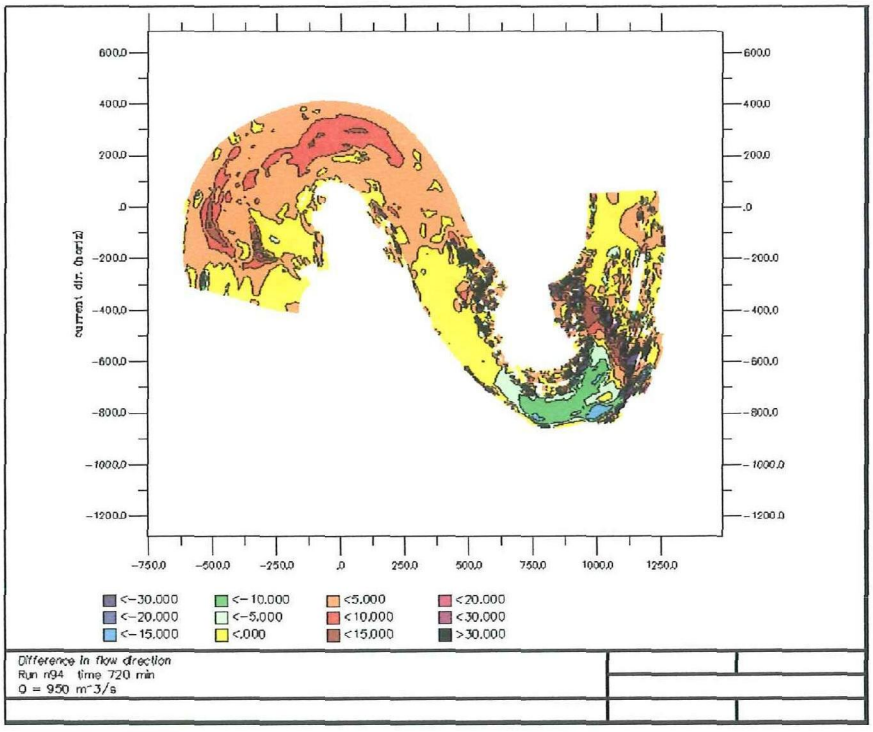

figure 36 : difference in flow direction between surface- and bed layer for a discharge of 1000 m^3/s

6.5 Flow velocity

The following sections describe the results of the steady state simulations for the flow velocity in the surface layer (layer 1).

6.5.1 Downstream bend

6.5.1.1 Steady simulations

In figure 37 till figure 39 the variation of the flow velocity at the water surface (layer 1) is shown over a discharge range of 100 - 500 m^3/s for the downstream point bar. Over this discharge range the flow velocities in the main channel increase from between 1.5- 1.75 m/s to 2- 2.5 m/s.

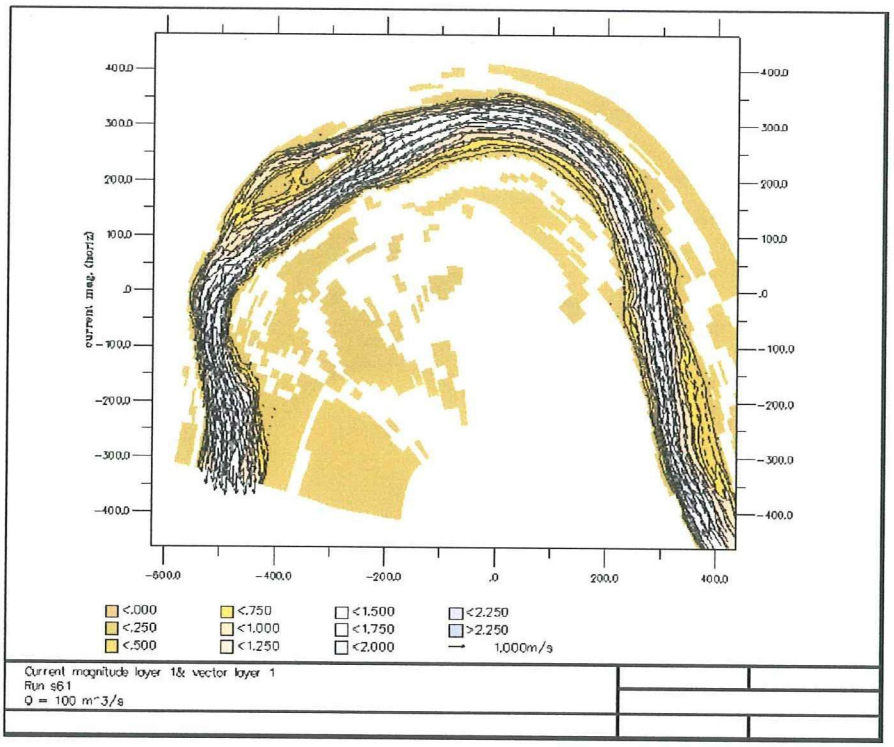

figure 37 : Flow velocity surface layer downstream point bar for a discharge of 100 m^3/s

The point bar is gradually flooded. As can be seen in figure 38 and figure 39 first the downstream part of the point bar is flooded and then the upstream part. Flow velocities on the point bar increase from 0.25- 0.75 m/s for a discharge of 300 m^3/s to 0.25- 1.0 m/s for a discharge of 500 m^3/s.
Between 300- and 500 m^3/s the upstream part of the point bar is flooded. Here the flow is directed onto the point bar, so bed material from the main channel could be transported onto the point bar.

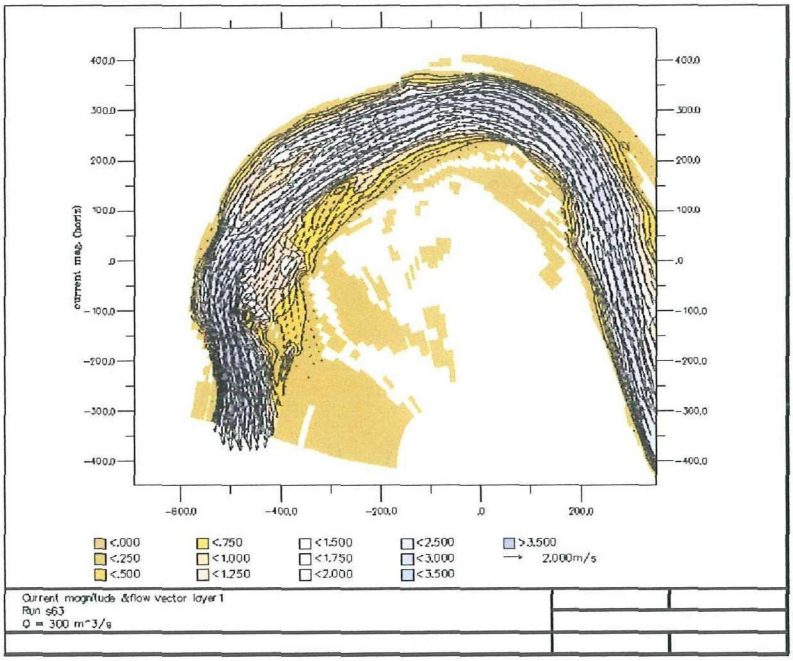

figure 38 : flow velocity surface layer downstream point bar for a discharge of 300 m^3/s

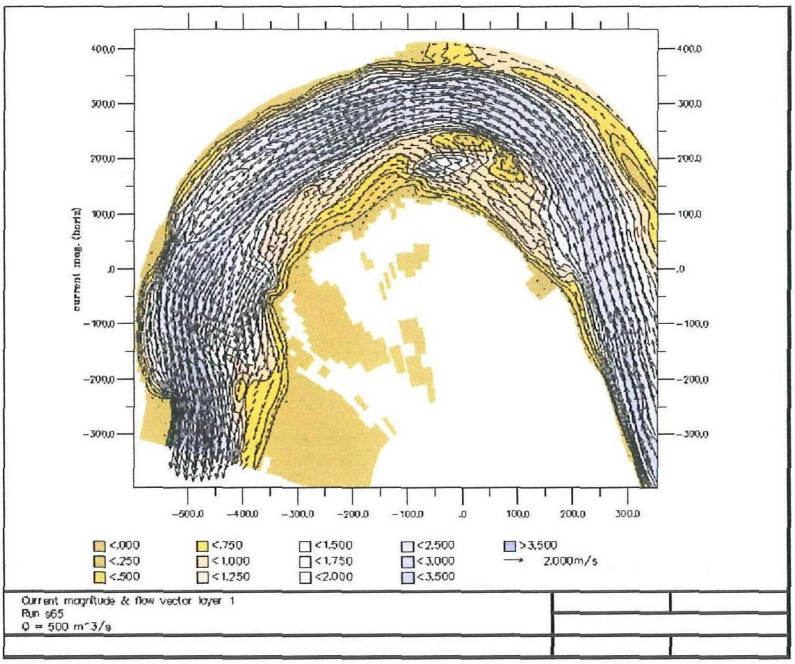

figure 39 : flow velocity surface layer downstream point bar for a discharge of 500 m^3/s

6.5.1.2 Unsteady state

In figure 40 the flow velocity for a discharge of 1000 m^3/s is shown. For this discharge the flow velocity in the main channel increases to approximately 3 m/s. As the

discharge increases the second half of the downstream point bar is gradually flooded. At the beginning of the bend velocities on the point bar increase from 1-1.25 m/s at a discharge of 500 m3/s to 1.75-2.0 m/s at a discharge of 1000 m^3/s. In the second half of the bend the velocities increase from 0.5- 1.0 m/s at a discharge of 500 m3/s to 0.5-1.75 m/s at a discharge of 1000 m^3/s. Also, for a discharge of 1000 m^3/s, a much larger part of the point bar is flooded and the velocity in the second part of the bend has turned onto the point bar.

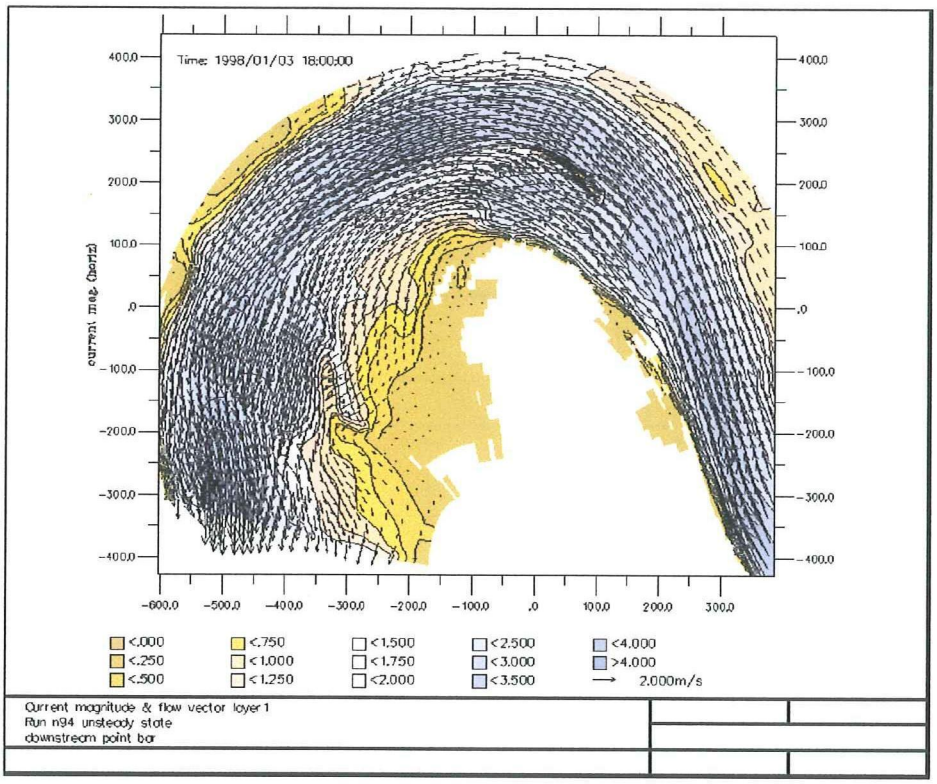

figure 40 : flow velocity surface layer for a discharge of 1000 m^3/s

The Froude numbers are quite large. The depth in the main channel at a discharge of 1000 m3/s varies between 2.5 m and 3.5 m. With a maximum velocity of 4 m/s this leads to Froude numbers in the range of 0.65 –0.8.

6.5.1.3 Flow pattern

If one looks at the cross sections the pattern of flooding can be explained. In cross sections 7, 1 and 2 a secondary channel is present around 150 m from the electricity pylon. This is the area at the beginning of the bend that is flooded between 300- and 500 m^3/s, as shown in figure 38 & figure 39.

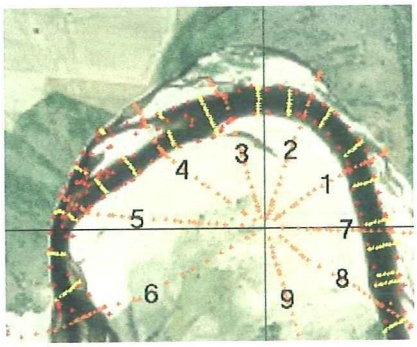

figure 41 : position cross sections downstream point bar

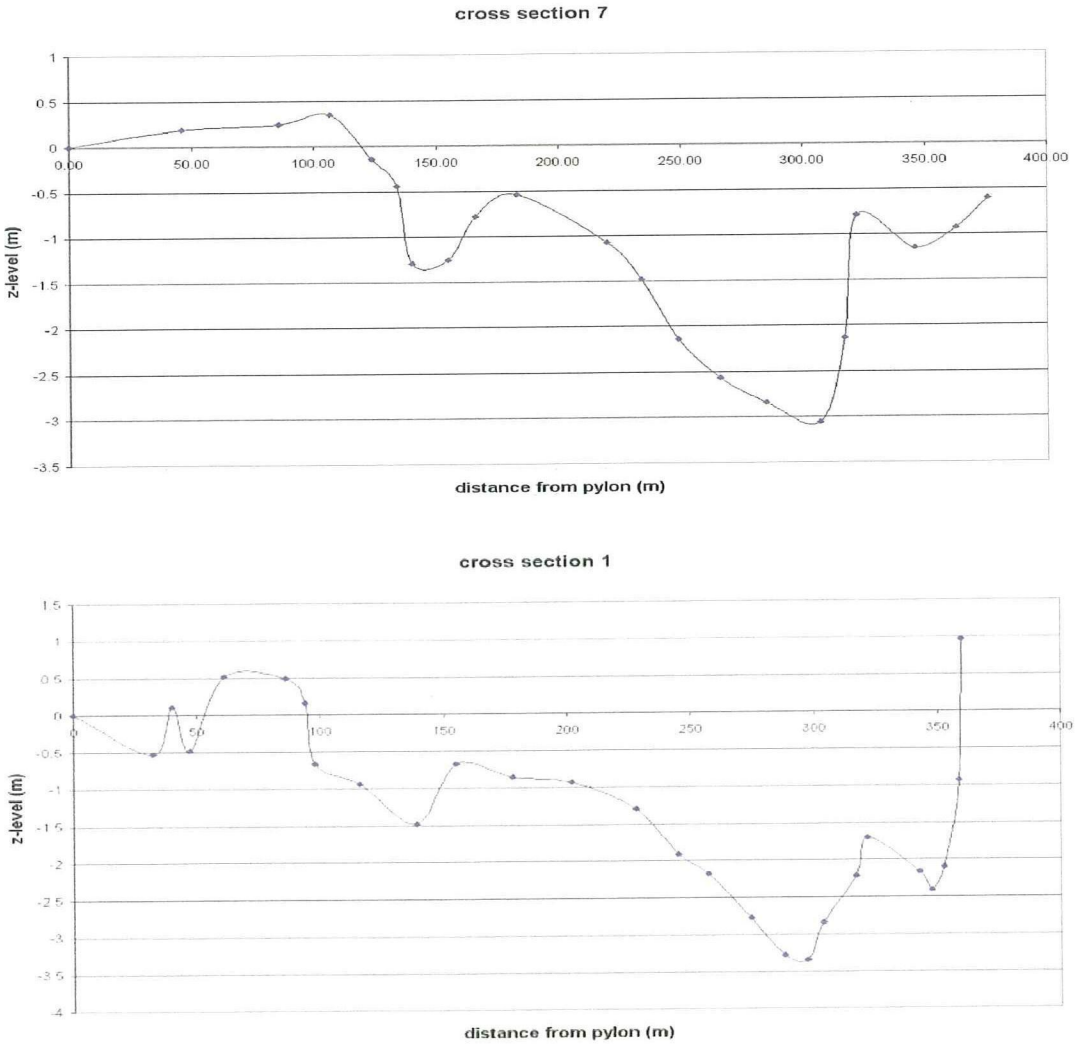

figure 42 : cross sections 1 &7

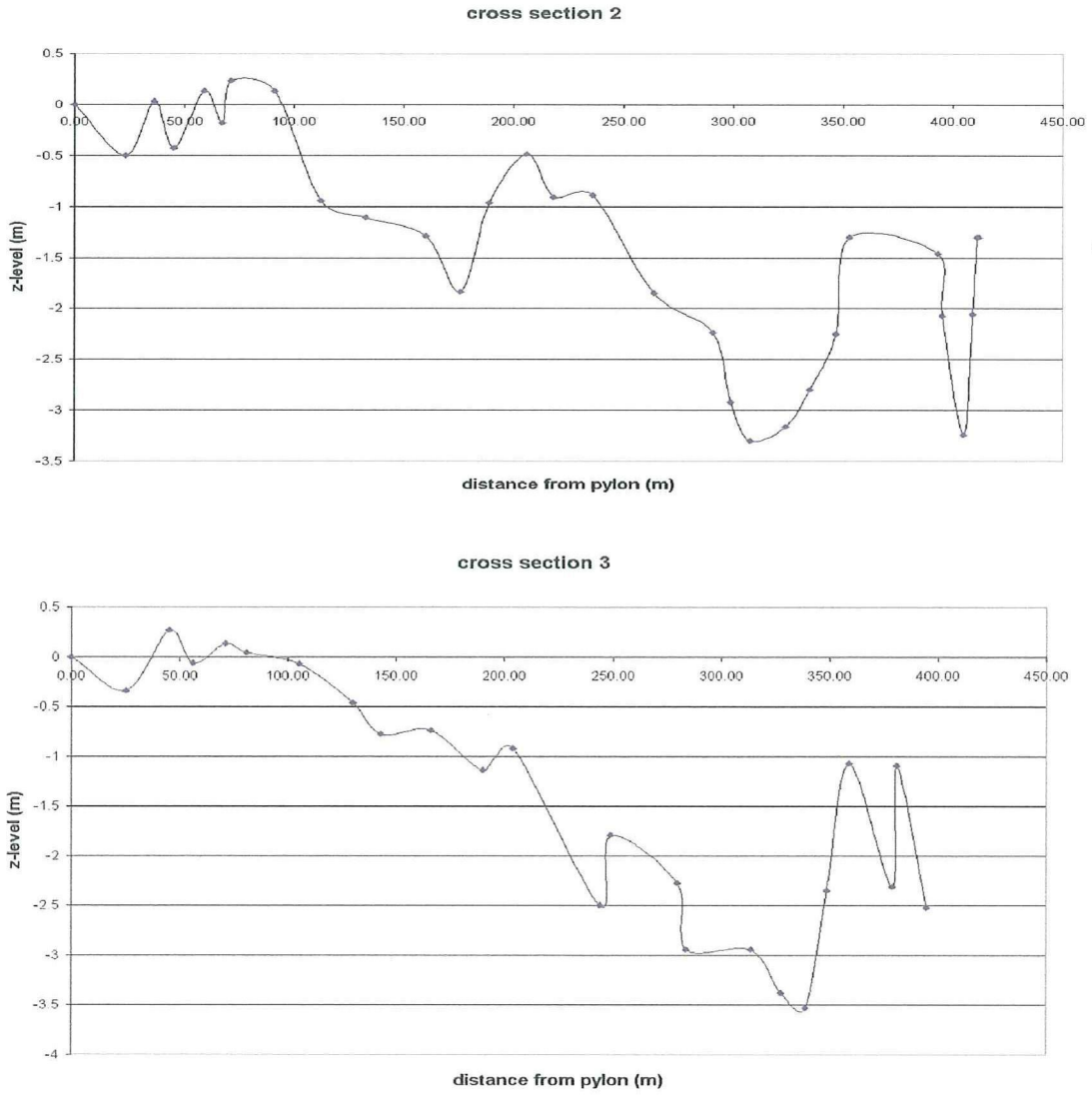

figure 43 cross sections 2 & 3

Cross sections 4 to 6 show the downstream part of the point bar to be lower than the upstream part. This lower part of the point bar is flooded first, see figure 38. The flow curves around the highest part of the point bar, see figure 40. Cross section 3 forms a transition between cross section 2 and 4.

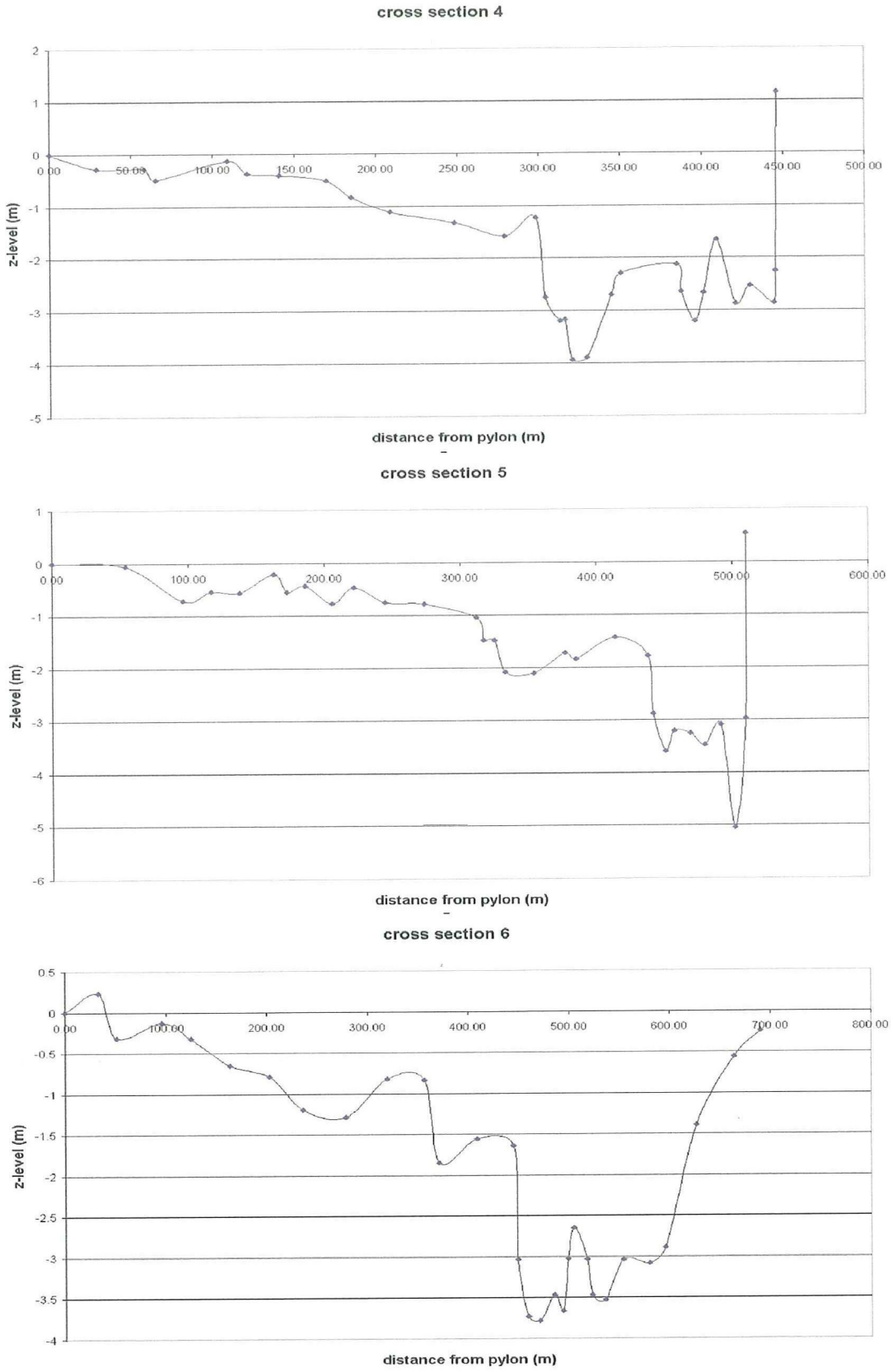

figure 44 : cross sections 4 & 5 and 6

6.5.2 Upstream bend

6.5.2.1 Steady state

In the following figures the flow velocity for the surface layer for the upstream bend is shown. It must be noted however, that the most upstream part of this bend is also the end of the surveyed area and near the upstream boundary of the model. The density of bathymetry measurements in this area is not high and the results for this part of the bend should be considered with caution.

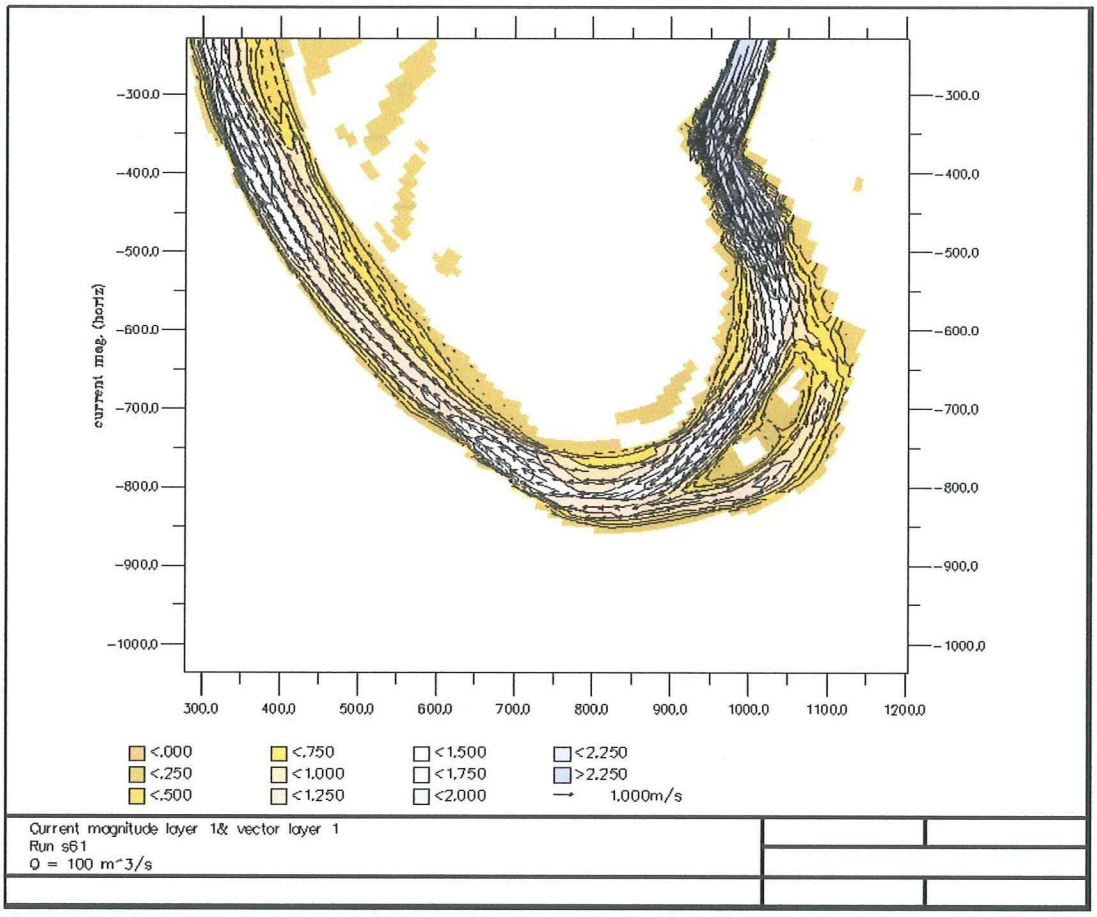

figure 45 : flow velocity upstream point bar surface layer for a discharge of 100 m^3/s

In figure 45 to figure 47 the flow velocity for discharges of 100-, 300- and 500 m^3/s are plotted. It can be seen that in the first half of the upstream bend the flow follows the main channel but in the second half of the bend the flow is directed onto the point bar at increasing discharges. The flow velocity in the main channel increases over this discharge range from 1.25-1.5 m/s to well over 2.0 m/s. The velocity on the point bar in the second half of the bend varies from 0.25 to 1.25 m/s.

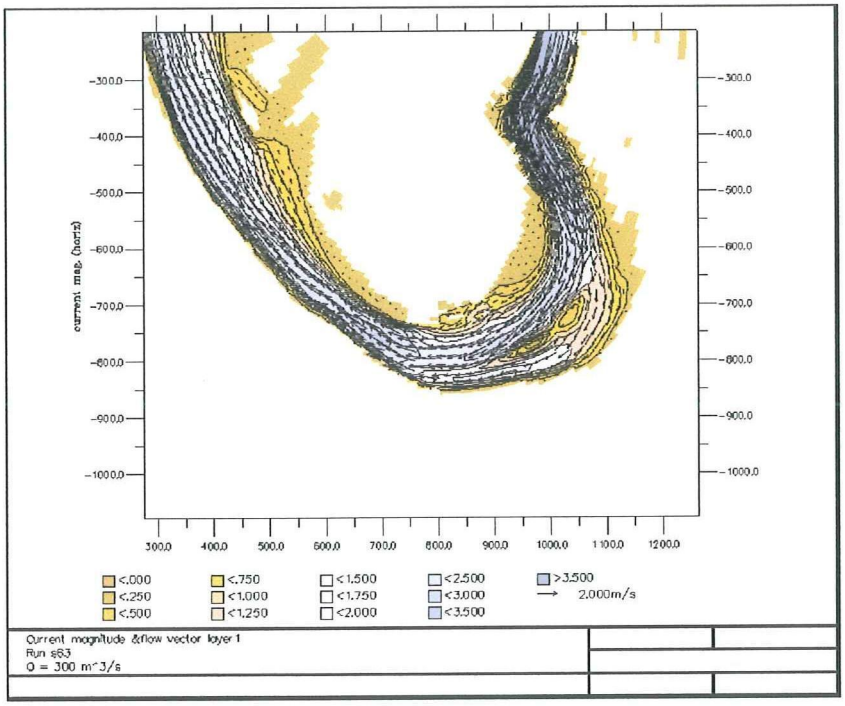

figure 46 : flow velocity surface layer upstream point bar for a discharge of 300 m^3/s

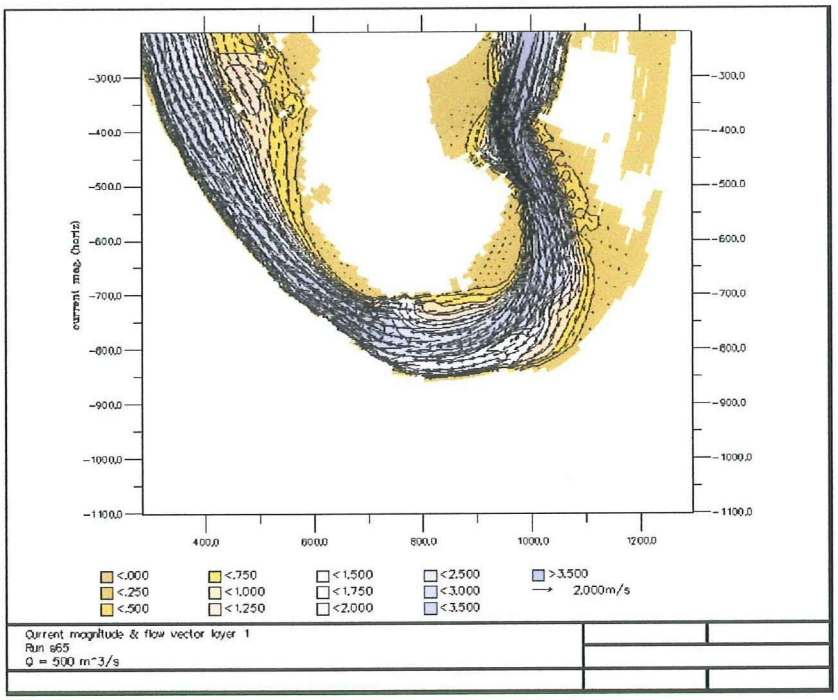

figure 47 : flow velocity surface layer upstream point bar for a discharge of 500 m^3/s

6.5.2.2 Unsteady state

In figure 48 the velocities at a discharge of 1000 m^3/s are shown. The flooded area in the second half of the point bar has become somewhat larger, velocities here range now from 0.5 to 1.75 m/s. Now also the first part of the point bar is starting to flood, velocities here vary between 0.25- and 0.75 m/s. At the upstream part the flow is very distorted due to a lack of bathymetry measurements. This part should be considered with extreme caution.

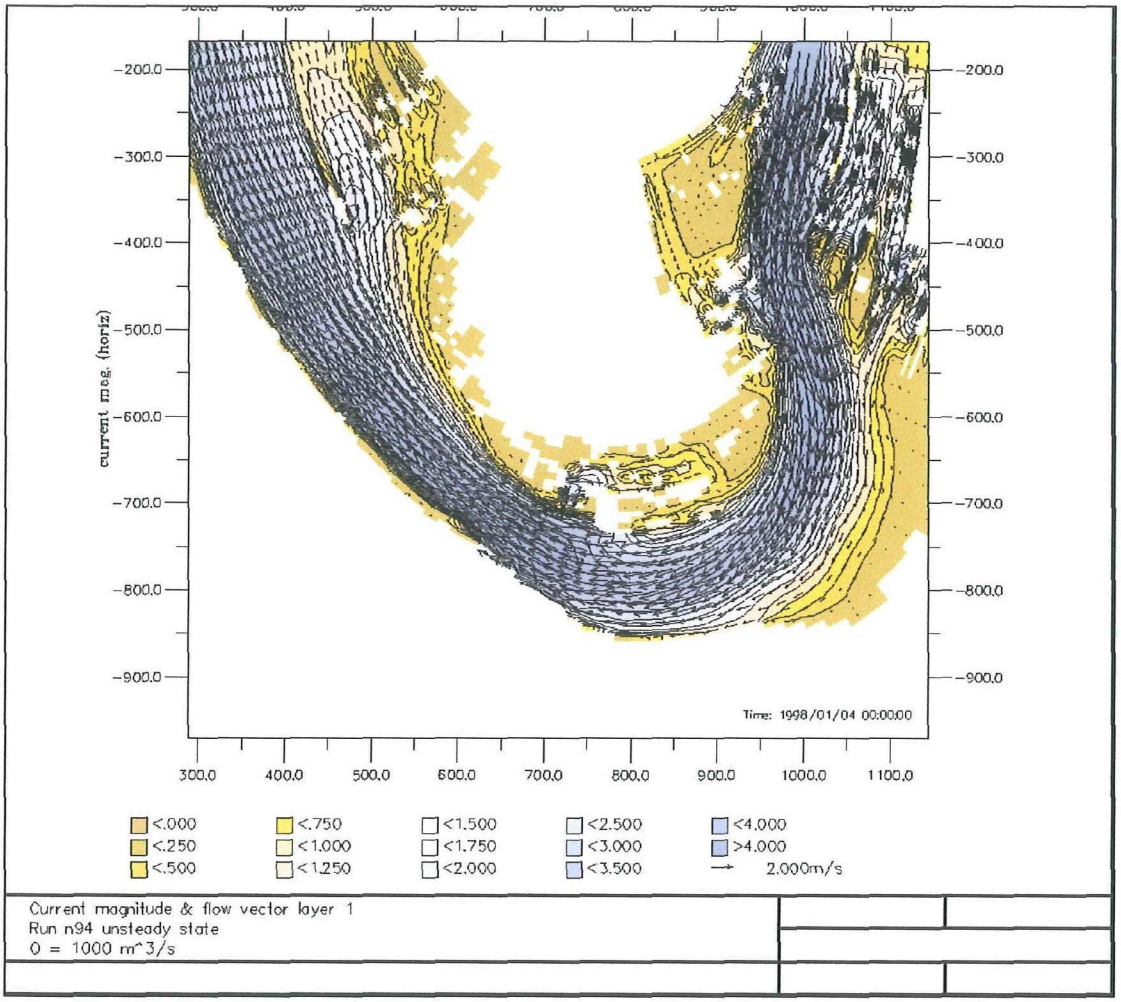

figure 48 : flow velocity for a discharge of 1000 m^3/s

The water depth in the upstream bend at a discharge of 1000 m^3/s is larger than 3 m. With a maximum velocity of about 4 m/s the maximum Froude number is 0.74.

6.5.2.3 Flow pattern

As can be seen in the cross sections 10 to 18 the steep point bar face of section 16 gives way to a more gradual slope in sections 17 and 18. Due to the more gentle slope around cross sections 17 &18, this part of the point bar is flooded first.
The upper platform of the upstream point bar is not flooded at discharges up to 1000 m^3/s. Therefore the flow is concentrated in the main channel, and upper- and lower layer flow near the cross-over region have the same flow direction.

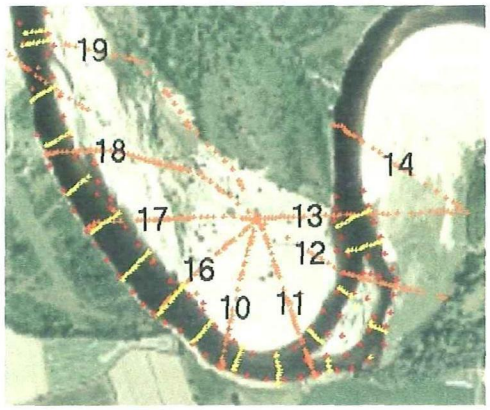

figure 49 : cross sections upstream point bar

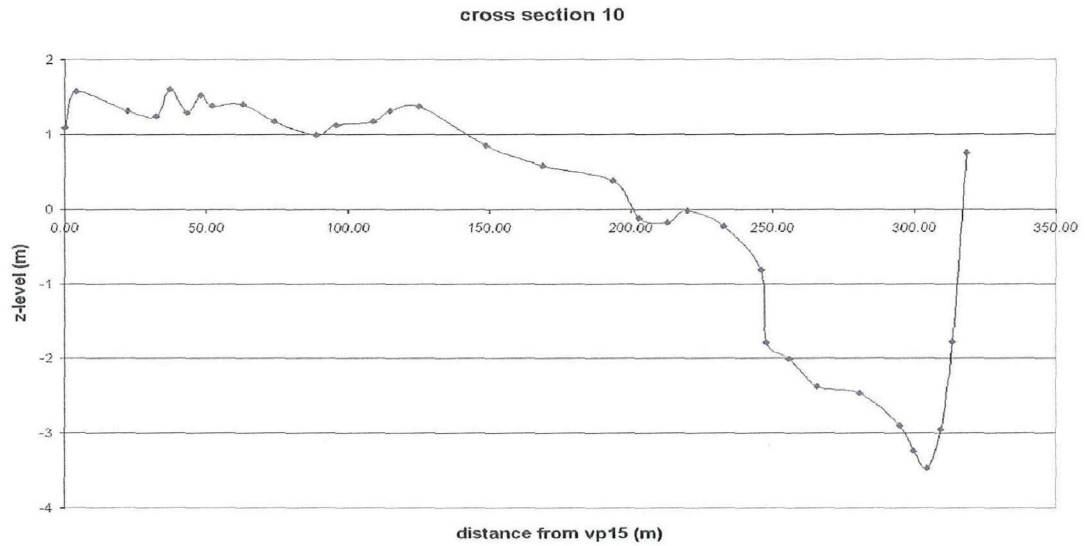

figure 50 : cross section 10

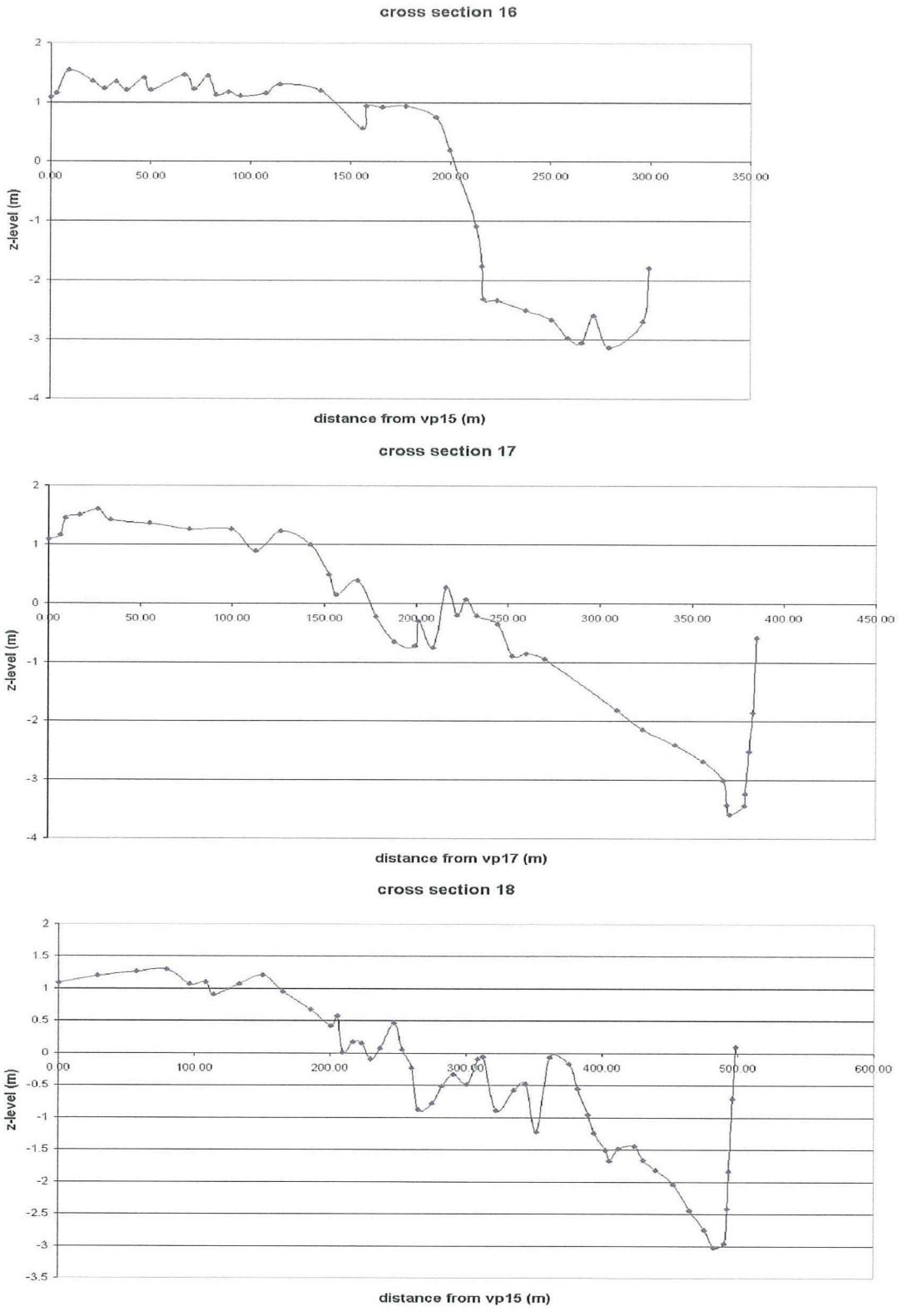

figure 51 : cross sections 16,17&18

6.5.3 Bed shear stress

The next paragraph describes the variation of the bed shear stress and the flow vector in the layer near the bed (layer6). To link the bed shear stress to a transported grain size the Shields-vRijn criterion is used. (van Rijn, 1993) For several grain diameters the critical shear stress was calculated and plotted below.

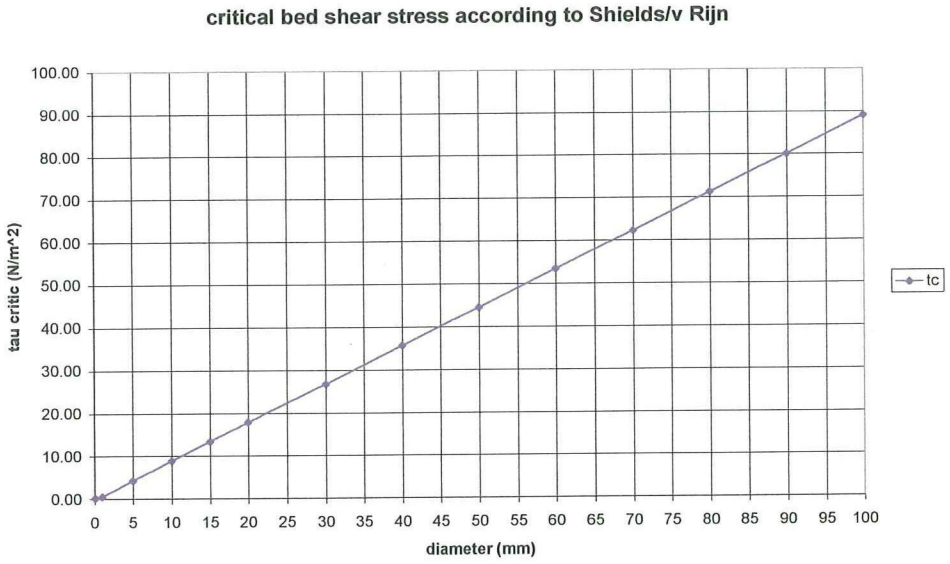

figure 52 : critical bed shear stress per grain size according to Shields-vRijn

6.5.4 Downstream bend

6.5.4.1 Steady state

At a discharge of 100 m3/s the bed shear stress at the downstream bend varies from 5 - 15 N/m^2. According to the Shields-vRijn criterion the maximum transported diameter is about 15 mm. There is no transport on the point bars yet.
For a discharge of 300 m^3/s, sediment transport is initiated on the second half of the downstream point bar. The bed shear stress reaches values of 5 N/m^2 and particles with a maximum diameter of about 5 mm can be transported. In the main channel the bed shear stress mainly varies from 10 - 20 N/m^2, with a maximum of about 40 N/m^2 at the end of the downstream bend, leading to a maximum transported diameter of about 23 mm for the shear stress range of 10 - 20 N/m^2 and about 45 mm at the shear stress peak of 40 N/m^2 near the end of the downstream bend.
The flow direction near the bed (layer 6) is still more or less in main channel direction.

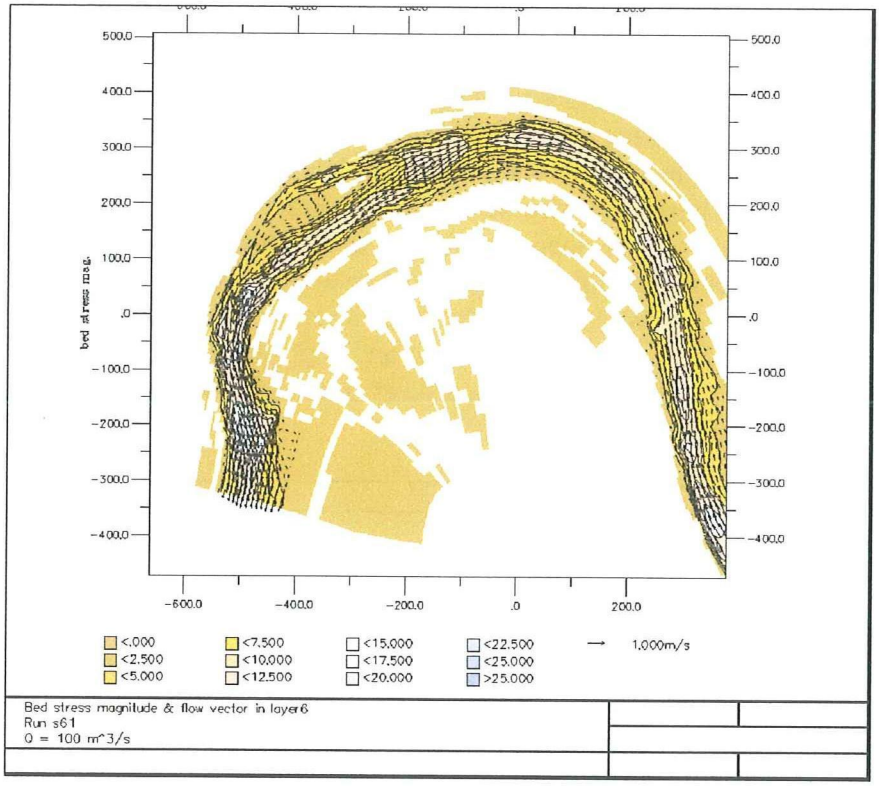

figure 53 : bed shear stress downstream point bar for a discharge of 100 m^3/s

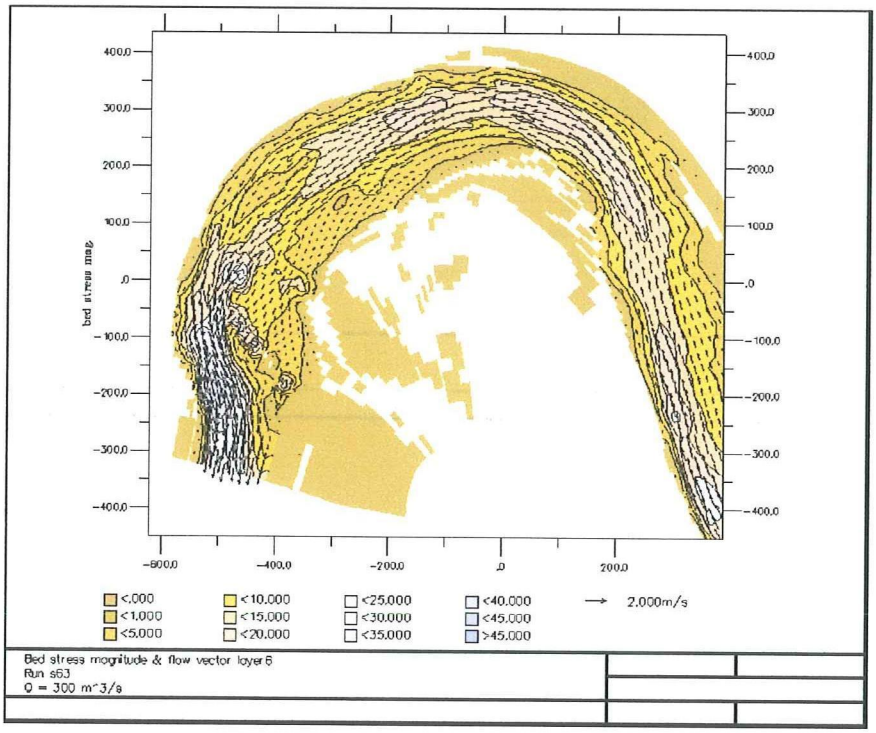

figure 54 : bed shear stress downstream point bar for a discharge of 300 m^3/s

In figure 55 The bed shear stress at a discharge of 500 m^3/s is shown. In the beginning of the downstream bend the bed shear stress is approximately 10 N/m^2, and hence bed material with a maximum grain size of about 10 mm can be transported onto the point bar. However, a little further downstream the bed shear stress drops from 5- 10 N/m^2 to below 5 N/m^2 and the coarser fractions of the bed load will be deposited. Just after this deposition area high shear stresses are found, indicating erosion. Again the coarser fractions eroded here will be deposited further downstream. This isolated area of high bed shear stresses could lead the formation of an armour layer. At the end of a flood this part of the point bar will show higher bed shear stresses than the surrounding area. Here larger particles can still be transported and deposited on top of smaller grains further downstream. Also the higher bed shear stress here will prevent sand from settling on top of the coarse particles.

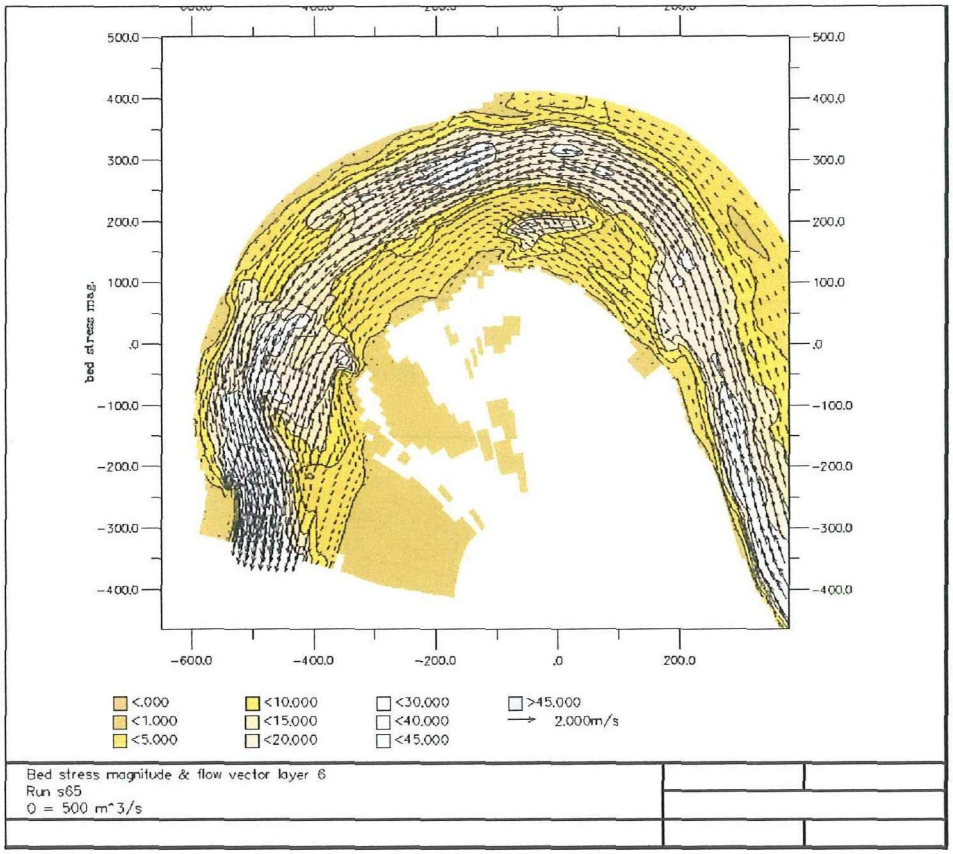

figure 55 : bed shear stress downstream point bar for a discharge of 500 m^3/s

6.5.4.2 Unsteady state

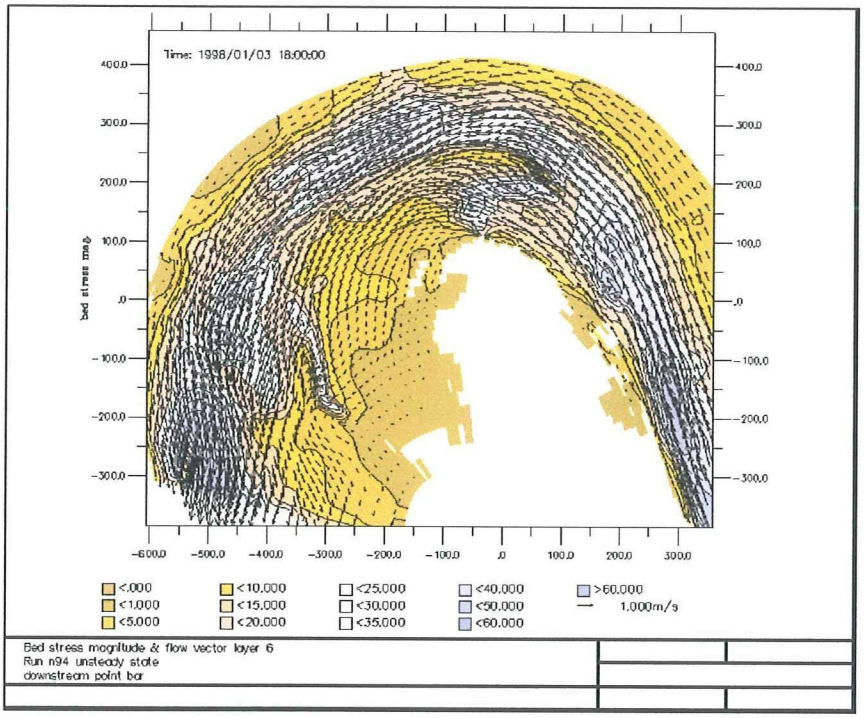

figure 56 : bed shear stress and flow vector near the bed for a discharge of 1000 m^3/s

In figure 56 the bed shear stress for a discharge of approximately 1000 m^3/s is plotted, it reaches values of over 40 N/m^2 at the deepest points in the river bed. The bed shear stress at the upstream part of the point bar shows the same pattern as for 500 m3/s, only the magnitude of the shear stress has increased. It now varies from 15 - 20 N/m^2 at the beginning of the bend to 30 N/m^2 further downstream. According to the Shields-vRijn criterion the maximum grain size which can be transported from the main channel onto the point bar is about 15-20 mm, coarser fractions in the bed load directed onto the point bar will be deposited here. Further downstream on the point bar the bed shear stress decreases to a maximum of 10 N/m^2 and the maximum transportable grain size becomes approximately 10 mm. This means that the coarsest fractions of the sediment transported onto the point bar will be deposited in the transition zone between the two bed shear stress areas. In the second half of the downstream bend the flow is again directed onto the point bar, but now with a maximum bed shear stress of about 10 N/m^2. This means that, again according to the Shield/vRijn criterion, a grain size of approximately 10 mm can be transported onto the point bar.

6.5.5 Upstream bend

6.5.5.1 Steady state

In figure 57 and figure 58 the bed shear stress at the upstream bend is shown. In the main channel the bed shear stress varies between 5- and 15 N/m^2 for a discharge of 100 m^3/s and it increases to 30 – 40 N/m^2 for a discharge of 500 m^3/s. With increasing discharge the flow in the second half of the bend is directed onto the point bar and the bed shear stress here varies from 1- to 15 N/m^2. The maximum grain size that can be transported onto the point bar is about 13 mm.

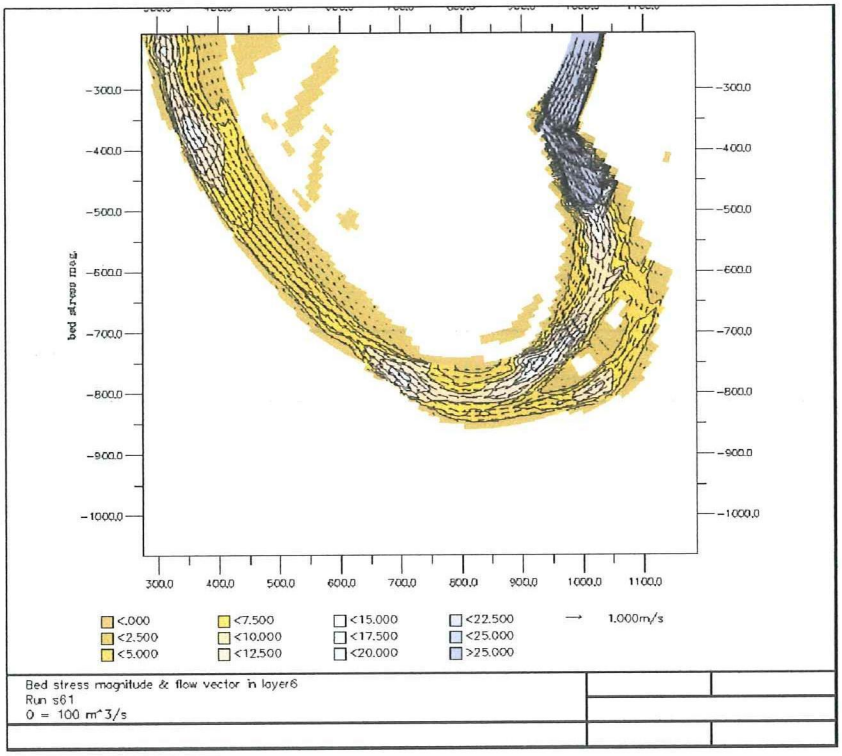

figure 57 : bed shear stress upstream point bar for a discharge of 100 m^3/s

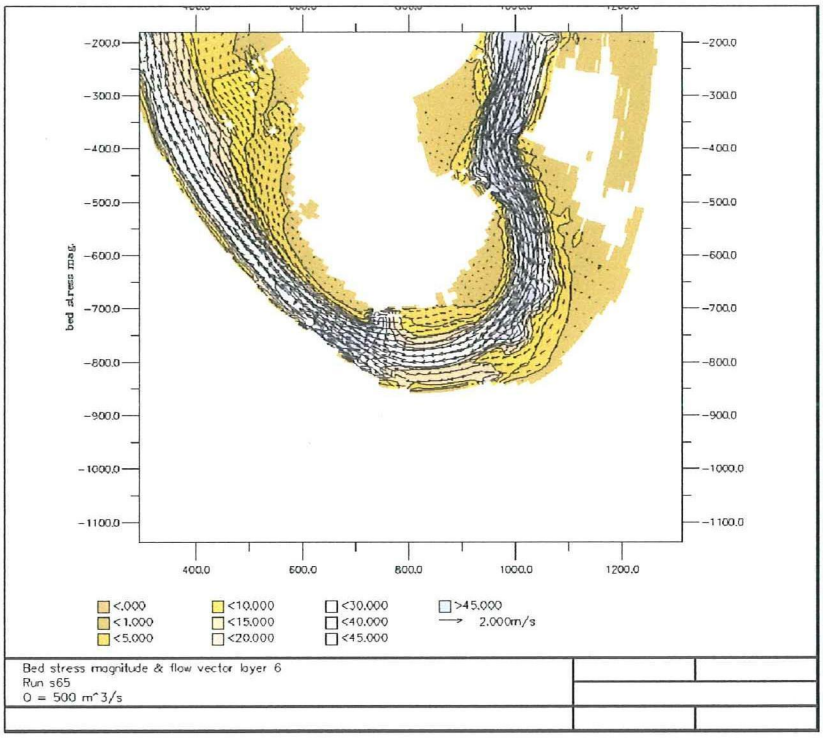

figure 58 : bed shear stress upstream point bar for a discharge of 500 m^3/s

6.5.5.2 Unsteady state

As can be seen in figure 59 in the second half of the bend the flow is directed onto the point bar. The flooded area does not increase much above the 500 m^3/s but the bed shear stress increases from a maximum of 10 N/m^2 to a maximum of 20 N/m^2 leading to an increase of the maximum transportable grain size from 10 mm to about 18 mm.

In figure 52 the areas of the maximum grain size (mm) which can be transported are plotted for a discharge of about 1000 m^3/s.

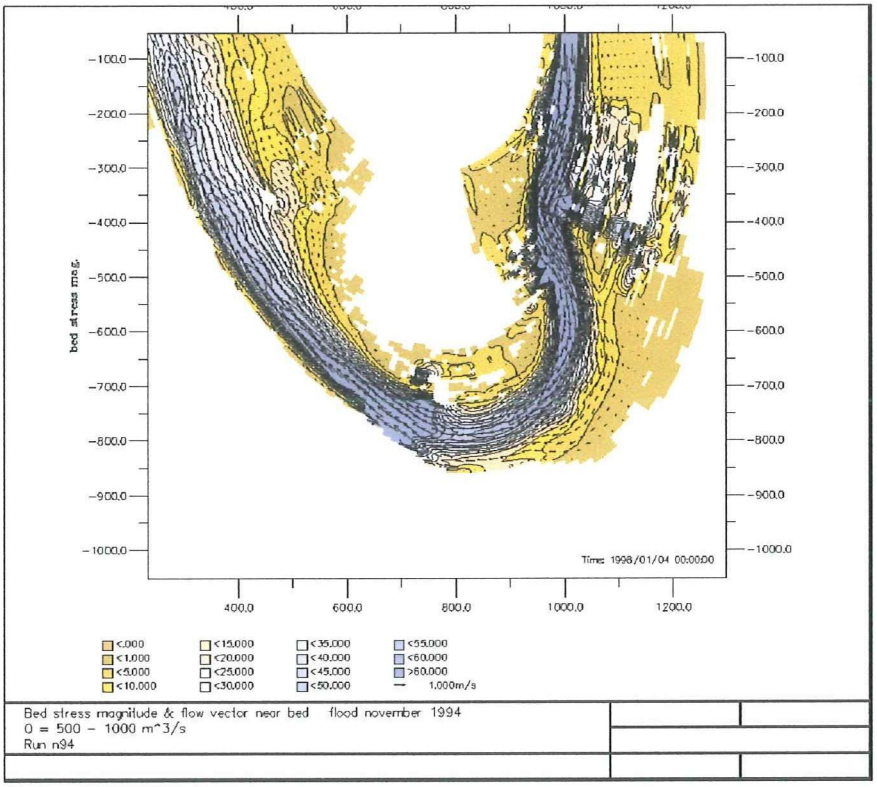

figure 59 : Bed stress magnitude upstream point bar for a discharge of 1000 m^3/s

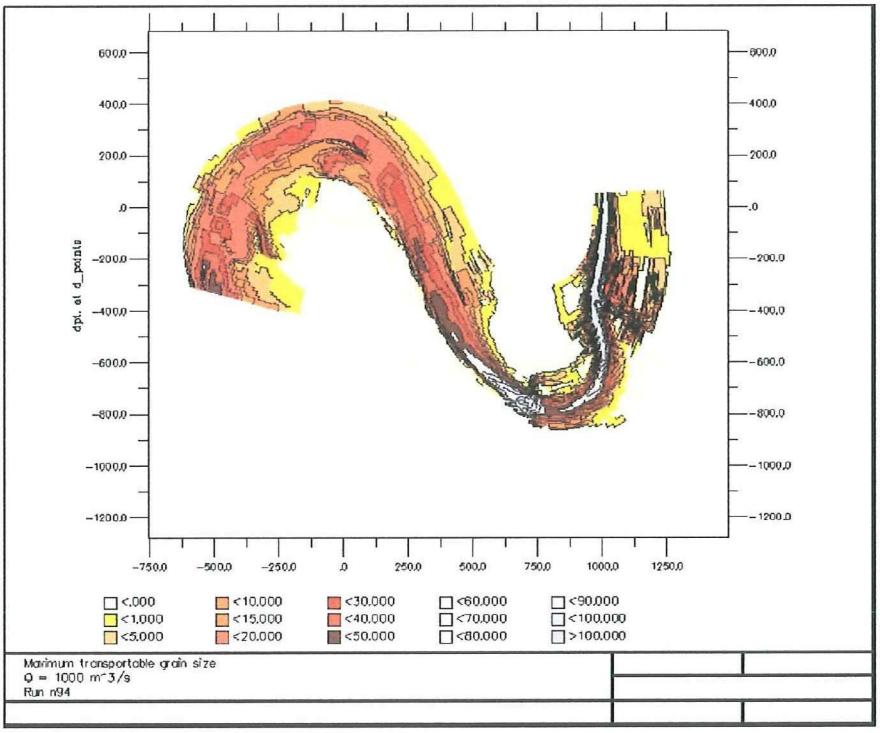

figure 60 : maximum transportable grain size for a discharge of 1000 m^3/s

6.6 Differences between steady- and unsteady state

To analyse possible differences between the steady- and unsteady state simulations, plots of the current magnitude for discharges of 500 - and 1000 m^3/s are compared.

As can be seen in figure 61 till figure 64 the differences in the flow velocities between the steady and unsteady state simulations are small. Although the magnitude of the velocity can differ locally the flow pattern is nearly identical except for the upstream bend. For a discharge of 1000 m^3/s the flow pattern near the upstream bend is not the same for the steady- and unsteady state simulations

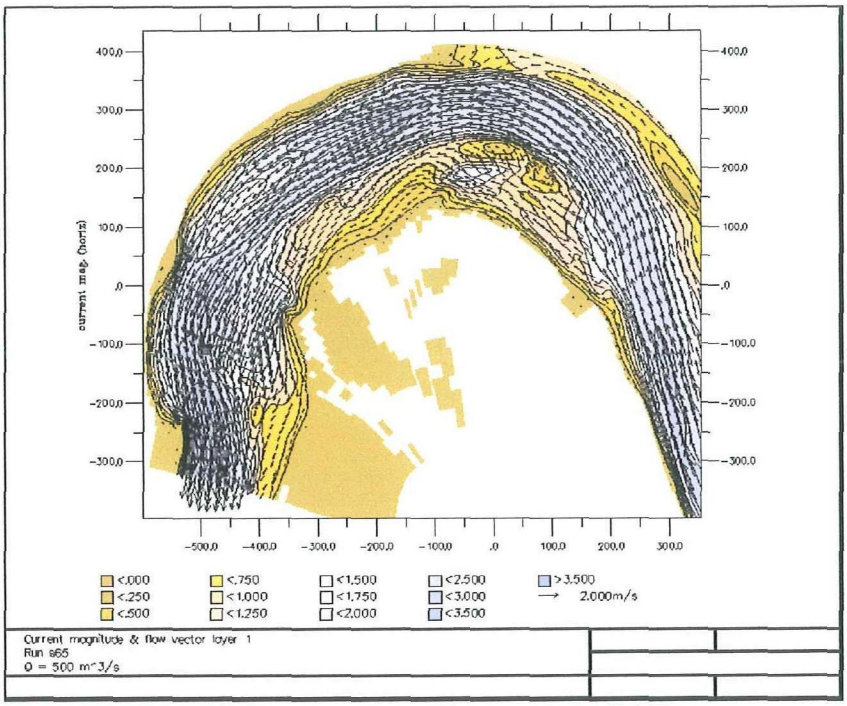

figure 61 : Flow velocity surface layer for a discharge of 500 m^3/s , steady state

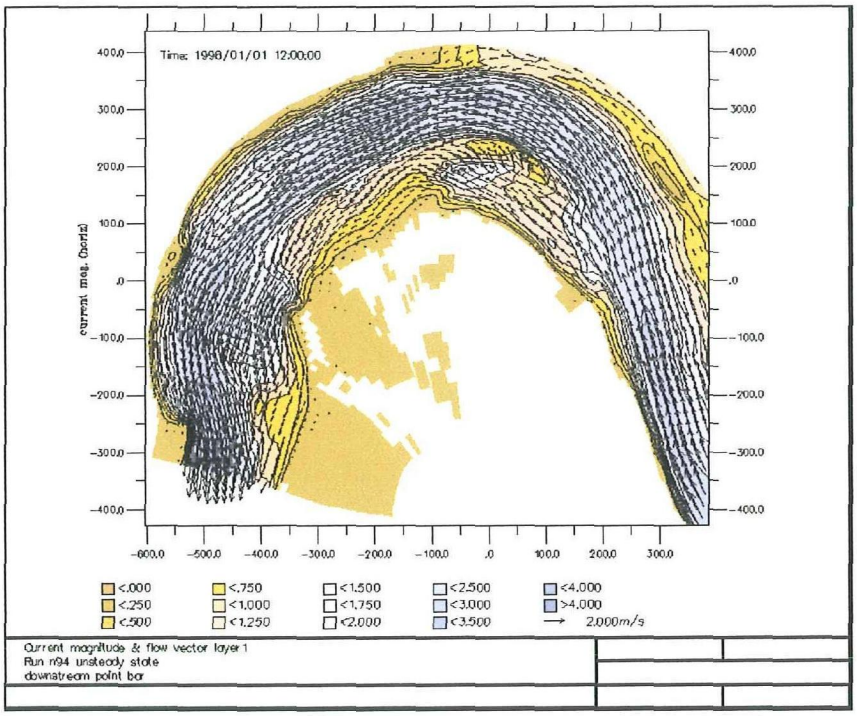

figure 62 : flow velocity surface layer for a discharge of 500 m^3/s , unsteady state

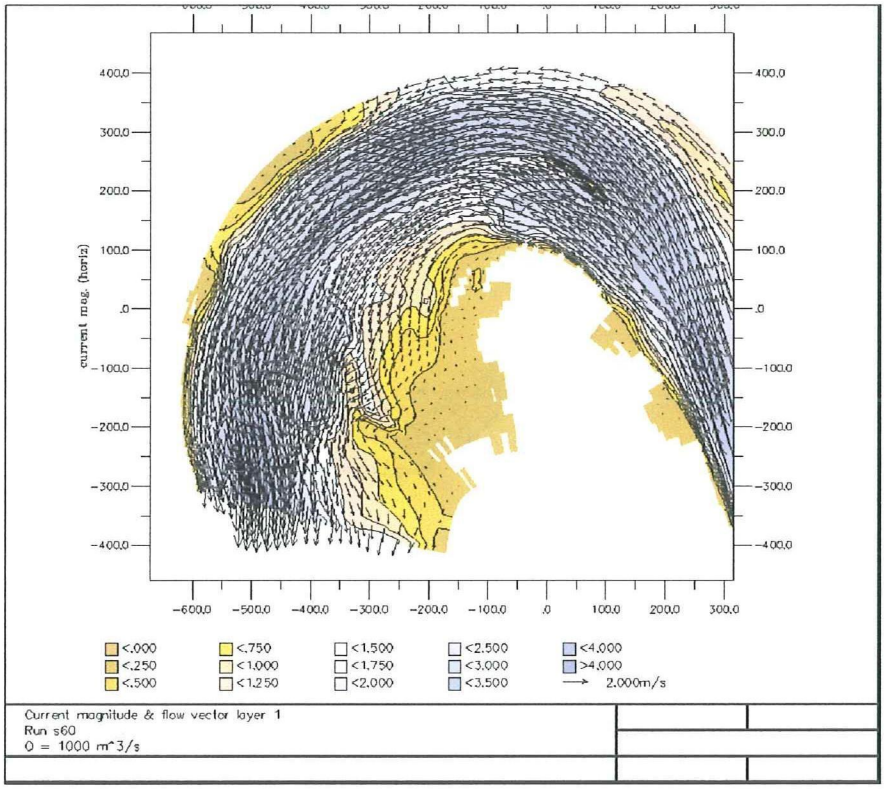

figure 63 : flow velocity surface layer for a discharge of 1000 m^3/s , steady state

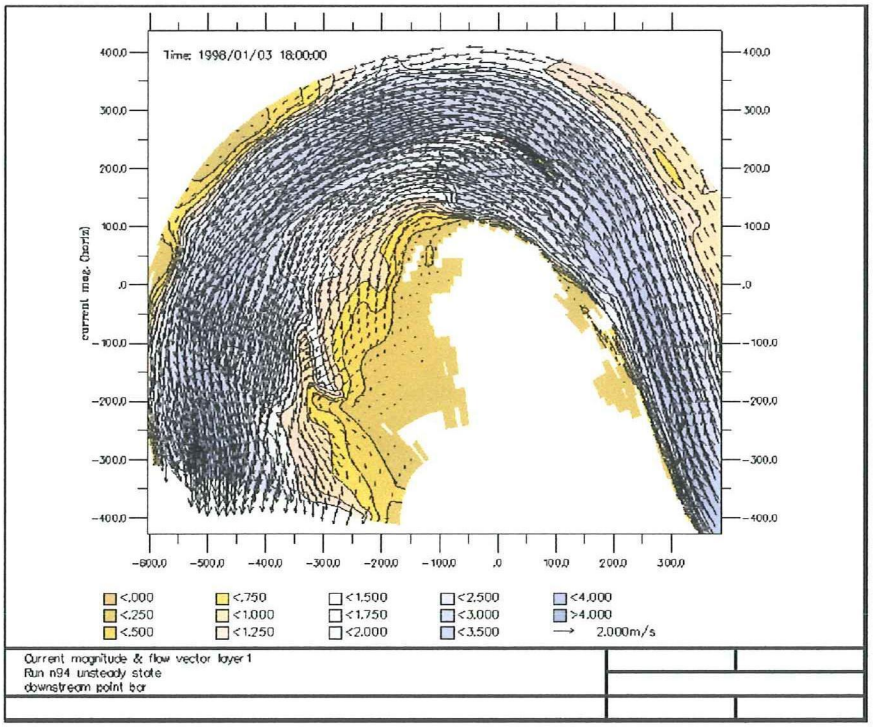

figure 64 : flow velocity surface layer for a discharge of 1000 m^3/s , unsteady state

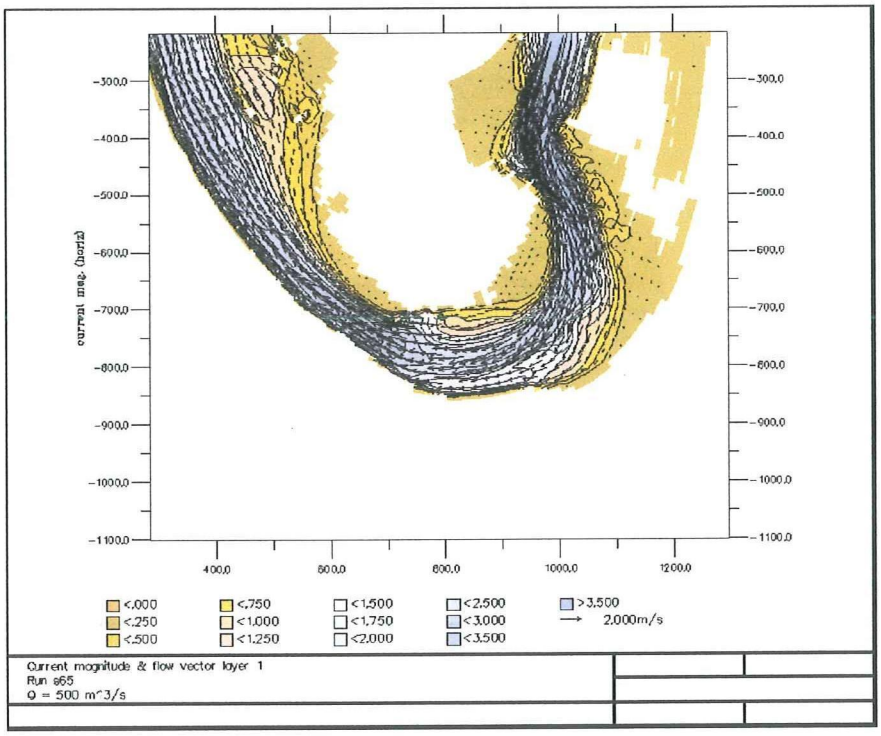

figure 65 : Flow velocity surface layer upstream bend for a discharge of 500 m^3/s ; steady state

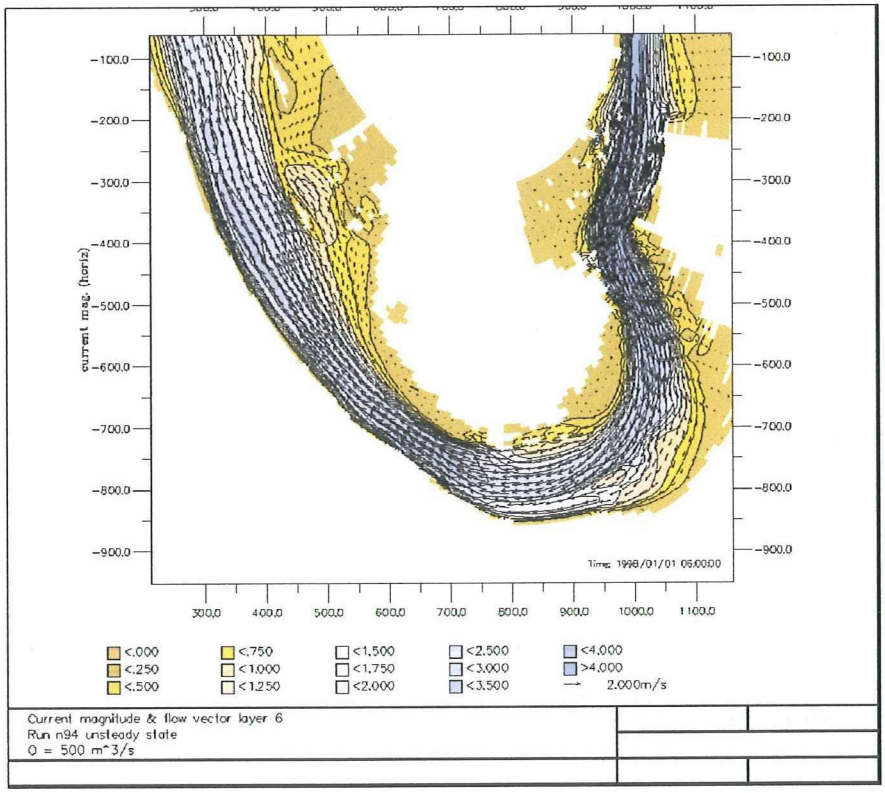

figure 66 : flow velocity surface layer upstream bend for a discharge of 500 m^3/s ; unsteady state

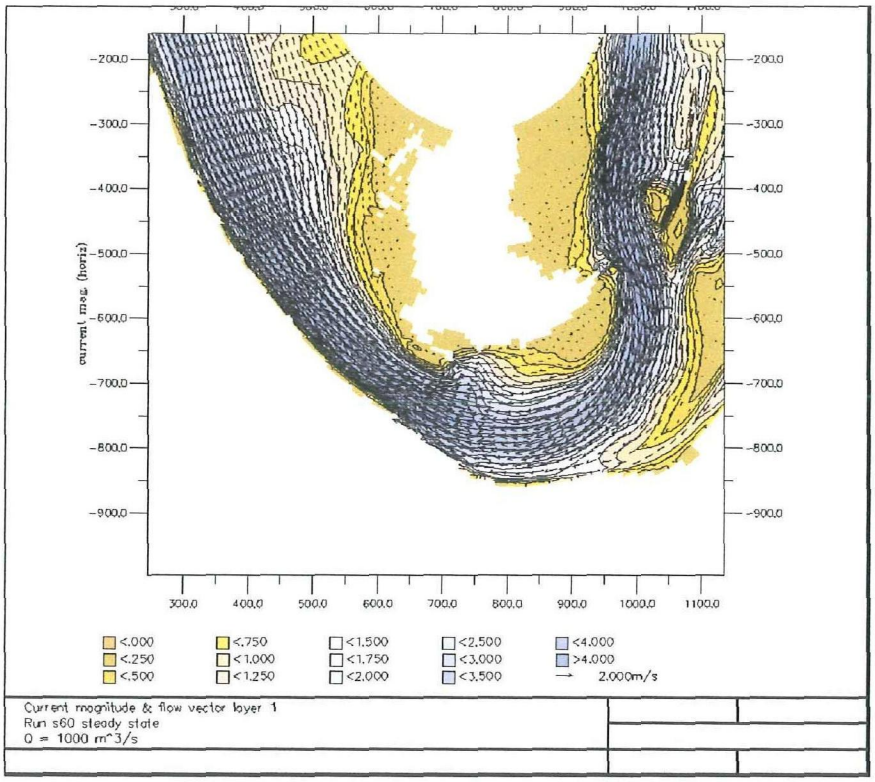

figure 67 : Flow velocity surface layer upstream bend for a discharge of 1000 m^3/s ; steady state

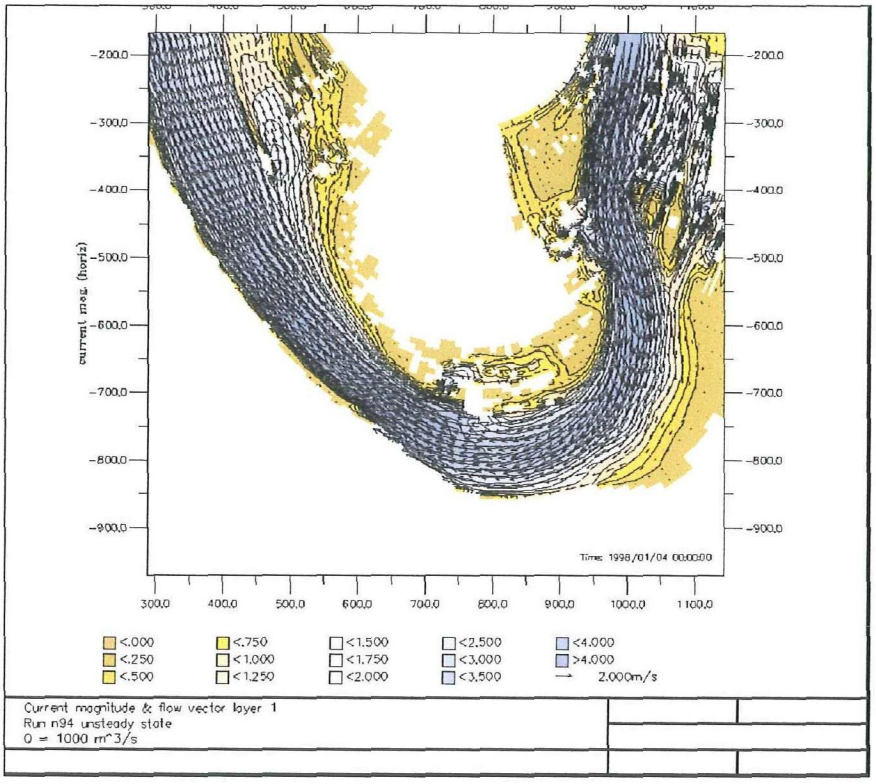

figure 68 : flow velocity surface layer upstream bend for a discharge of 1000 m^3/s ; unsteady state

6.7 Conclusion

Flow in the two bends just upstream of Chateau de Lys was simulated for discharges in the range of 100-1000 m^3/s. Both steady state simulations as well as an unsteady state simulation were made.
In chapter 5 it was shown that the downstream boundary condition was not generated well for discharges of approximately 20 m^3/s. Therefore, for the higher discharge ranges the influence of an error in the downstream water level on the flow was estimated. It was shown that an error in the downstream water level influences the flow for about 1000 m upstream of the boundary. However, the error in the downstream water level decreases rapidly and 300 m upstream of the boundary the error had already decreased to only $^1/_3$ of the boundary value.
The position of the secondary flow cells indicates an inbank flow pattern. Because the upstream point bar is not fully flooded at a discharge of 1000 m^3/s, the flow over the floodplain is directed approximately in main channel direction. Therefore no large interaction takes place between floodplain flow and main channel flow in the cross-over region.
As the discharge increases, parts of the point bars are gradually flooded. For a discharge of 500 m^3/s, near the end of the upstream bend and at the beginning of the downstream bend the flow is directed onto the point bars. For a discharge of 1000 m^3/s also the second half of the downstream point bar is flooded. In these areas sediment can be transported onto the point bars. The maximum grain size which can be transported onto the point bars is, according to the Shields-vRijn criterion, about 20 mm.
In the main channel flow velocities up to 4 m/s are calculated, leading to large bed shear stresses. At a discharge of 1000 m^3/s the Froude numbers in the main channel vary between 0.65-0.8.
The differences between the steady- and unsteady state simulations is not large. For a global impression of the flow pattern, the steady state simulations are sufficient. This saves a lot of computation time.

7 Armour layers in the river Allier

7.1 Introduction

In this chapter the surface based Oak Creek model by Parker (Parker, 1990) is used to estimate the threshold of motion for the different size fractions within a sample. This model is a transformation of the substrate-based model, which was developed solely on the basis of the Oak Creek field data by Milhous. Differences with the Shields relation will be discussed.

7.2 Samples

At several places in the area samples of the surface layer were obtained, see figure 69. The samples were obtained by placing a grid of 1 m^2 , with a spacing of 0.1 m, on the surface. The grain under each grid node was collected and for each grain the lenghts of the shortest, middle and longest axis were measured. So for each sample 100 grains were measured, the largest grain was classified as the D_{100} and the smallest grain as the D_1. In table 7 the results for the length of the middle axis are shown. For more information on the surface-grain size distribution and the sampling methods the reader is referred to van der Bruggen (??).

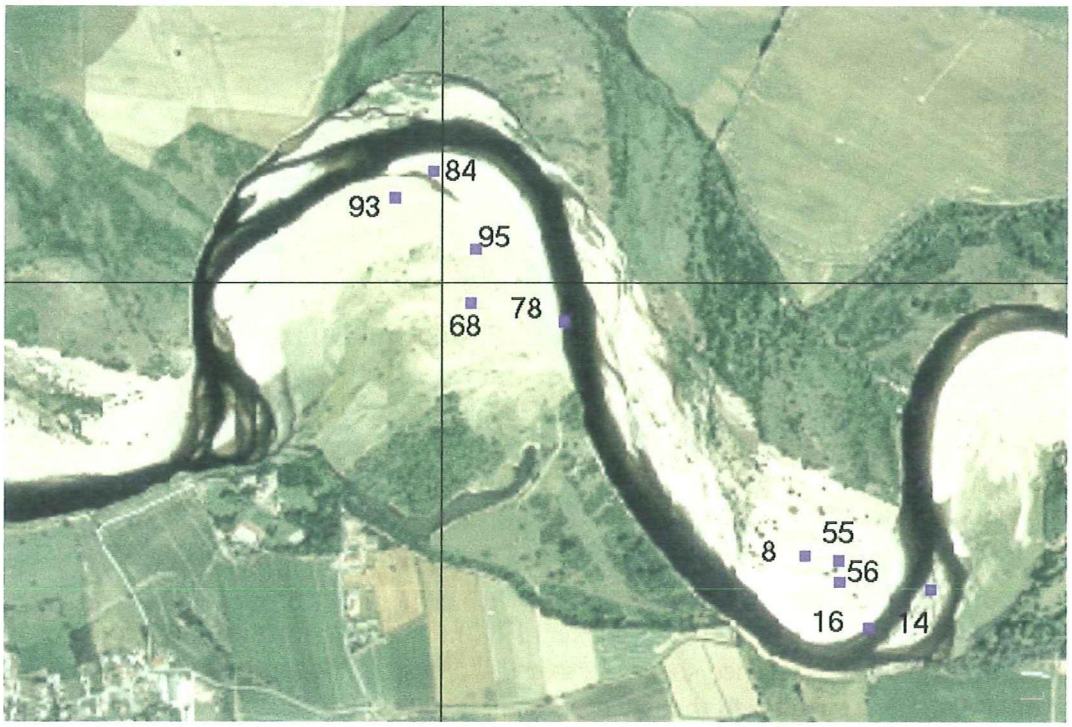

figure 69 : position of surface samples

Sample	Grading (mm)	D16 (mm)	D35 (mm)	D50 (mm)	D84 (mm)	$\sqrt{D_{84}/D_{16}}$
8-T-G	2 - 70	8	15	22	42	2.29
14-T-G	3 - 39	6	12	16	29	2.2
16-T-G	2 - 48	5	12	14	22	2.1
55-T-G	3 - 47	7	13	16	30	2.07
56-T-G	1 - 58	5	13	17	33	2.57
68-T-G	3 - 62	8	12	16	35	2.09
78-T-G	3 - 68	8	15	20	46	2.4
84-T-G	2 - 23	5	7	8	13	1.61
93-T-G	2 - 27	5	8	9	15	1.73
95-T-G	2 - 61	6	11	16	29	2.2

table 7 : grain sizes samples

7.3 Estimate of threshold of motion

In the surface based Oak Creek model the critical shear stress is calculated with the aid of a hiding factor. The hiding factor essentially scales the reference shear stress of the median grain size of the surface layer with the ratio between the diameter of an individual grain size with the median grain size.

$$\frac{\tau^*_{rsi}}{\tau^*_{rsg0}} = \left(\frac{D_i}{D_{sg}}\right)^{-0.9047} \qquad (7.1)$$

$$\tau^*_{rsi} = \frac{\tau_{rsi}}{(\rho_s - \rho_w)gD_i} \qquad (7.2)$$

In which τ_{rsi} is the reference bed shear stress for fraction i of the surface layer, τ^*_{rsg0} is the reference Shields stress for the median grain size of the surface layer, D_i is the grain size of fraction i of the surface layer, D_{sg} is the median grain size of the surface layer. For more information the reader is referred to Parker (1990).

The reference Shields stress is a substitute for the critical Shields stress. The reference Shields stress is defined as that Shields stress for which a small but measurable transport occurs. Transport rates are exceedingly small for $\tau^*_{si} < \tau^*_{rsi}$. For τ^*_{rsg0} the literature value of 0.0386 is taken (Parker, 1990).
For all samples the reference shear stress and the hiding factor are calculated and plotted below. According to the Oak Creek model the reference shear stress range within a mixture is limited, for the samples below within 4 N/m^2. Between the samples the differences in critical shear stress are larger. The reference shear stress for the same grain size varies between the samples. Especially between samples 84-t-g and 93-t-g

and the other samples the difference is large. This can be explained from the hiding factor. For samples 84-t-g and 93-t-g the D_{sg} is about 2 times smaller than for the rest of the samples, so the reference shear stress is also 2 times smaller.
If the reference shear stresses are compared with the critical shear stresses according to Shields-v Rijn (figure 52, chapter 6), the large difference in shear stress, especially for the larger grains, is the most striking feature. The explanation for this is twofold. First the reference Shields stress used in the Oak Creek model, 0.0386, is smaller than the one used for the Shield graph, 0.055. Second the hiding factor acts as a shear stress leveller, see figure 71.
Equation (7.1) can be rewritten with the aid of equation (7.2) to:

$$\tau_{rsi} = (\rho_s - \rho_w) g D_i^{(1-0.9047)} D_{sg}^{0.9047} \tau_{*rsgo} \qquad (7.3)$$

From equation (7.3) it follows that D_{sg} has a much larger influence on τ_{rsi} than D_i.
In fact equation (7.3) can be simplified to:

$$\tau_{rsi} = D_i^{(1-0.9047)} \times Const \qquad (7.4)$$

It can be shown that $D_i^{(1-0.9047)}$ varies from 0.5 for a grain size of 1mm to 0.75 for a grain size of 70 mm. So the reference shear stress of the largest particle in a mixture is approximately 1.5 times that of the smallest particle.

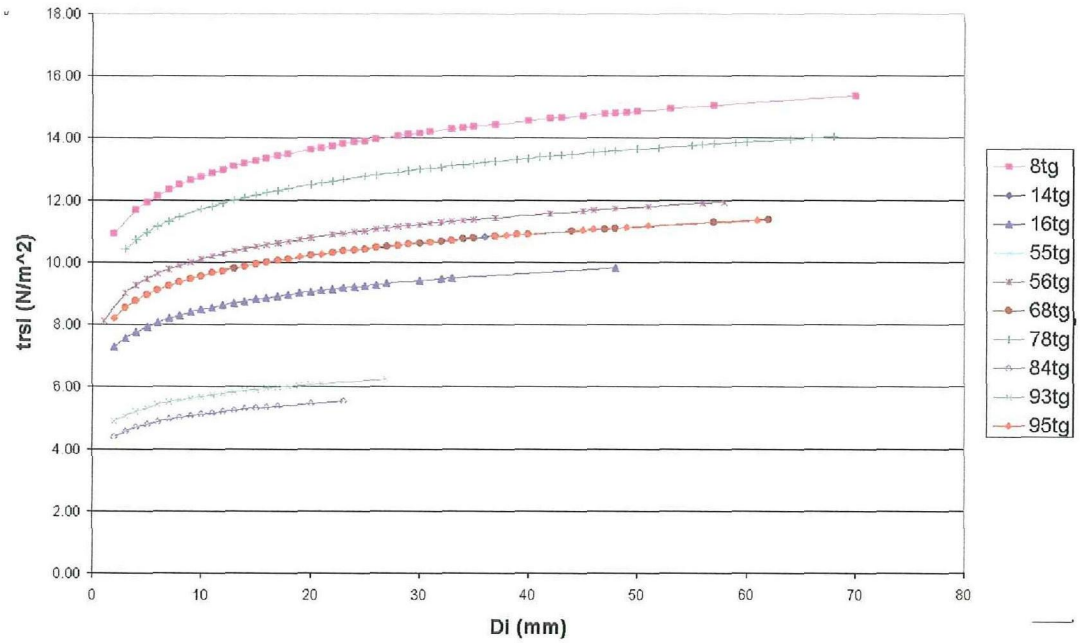

figure 70 : reference shear stress according to the Oak Creek model

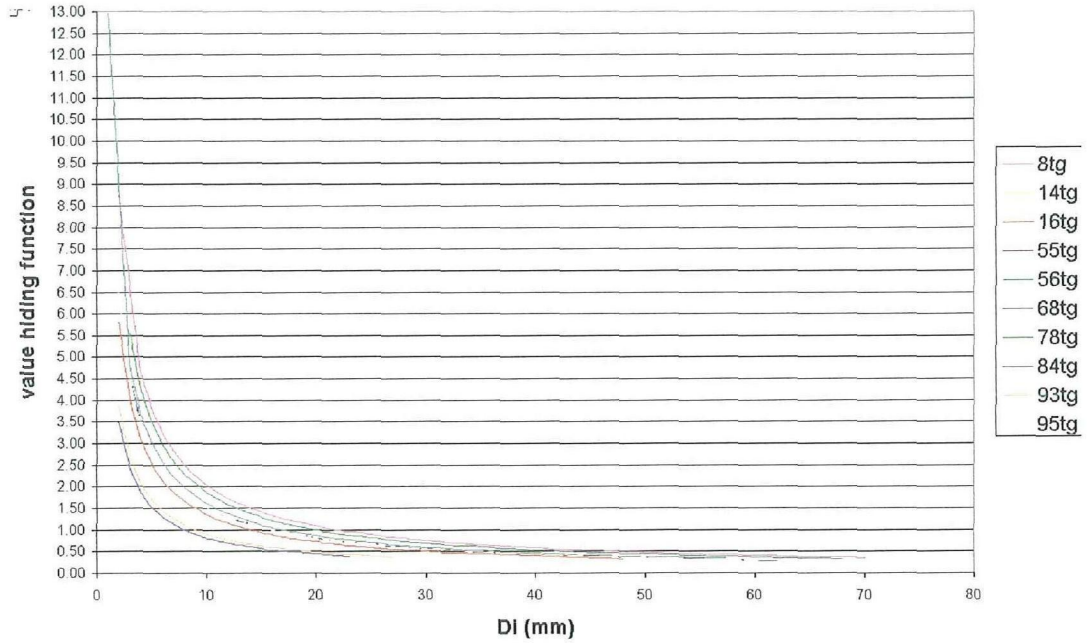

figure 71 : hiding factor as function of grain size

The reduction of the reference shear stress could explain the presence of the larger particles on top of the point bar. As discussed in chapter 6 the maximum grain size which could be transported onto the point bar according to the Shields criterion was about 20 mm. Due to the reduction of the critical shear stress by the hiding factor much larger particles could be transported onto the point bar. According to figure 71 the largest grains, with a diameter of about 70 mm, already start to move at a shear stress of 15 N/m^2. If the bed shear stresses of figure 72 are compared with the reference shear stresses calculated with the Oak Creek model, see figure 70, it appears that all grain sizes present in the samples could be transported onto the point bar.

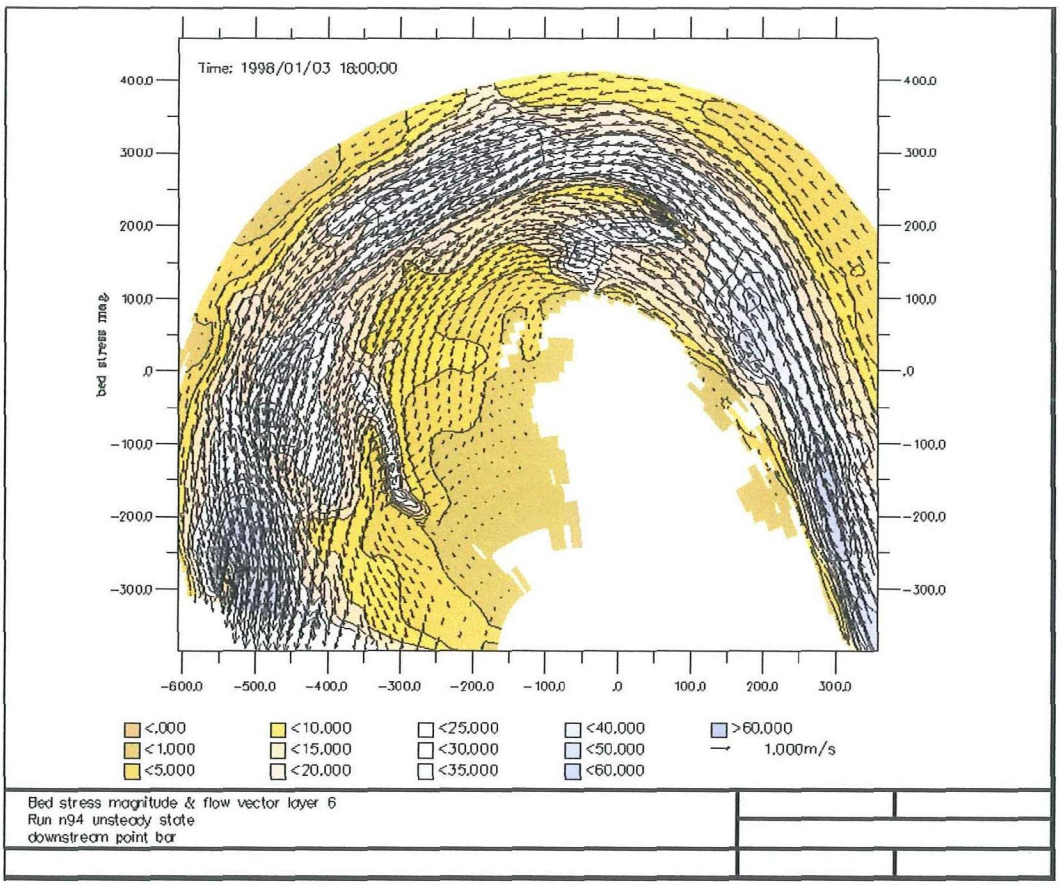

figure 72 : bed shear stress on downstream point bar for a discharge of 1000 m^3/s

The samples on the point bars can be explained combining figure 72 and figure 73 with the Oak Creek model. Sample 68 lies on a part of the downstream point bar which is not flooded at a discharge of 1000 m^3/s and is therefore excluded from the analysis. Sample 95 lies in an area which exhibits bed shear stresses between 10 and 15 N/m^2 for this discharge. From figure 70 it then follows that the grain sizes in the sample have exceeded of are near the threshold of motion. Sample 78 is situated in an area where the bed shear stresses well exceed the threshold of motion.
At the location of samples 84 and 93 the threshold of motion is exceeded. Bed stresses here vary between 10- and 15 N/m2.

On the upstream point bar samples 8, 55 and 56 lie on a part which is not flooded. Sample 16 lies near the main channel and sample 14 lies on the island. In both areas the threshold of movement for the mixtures is exceeded.

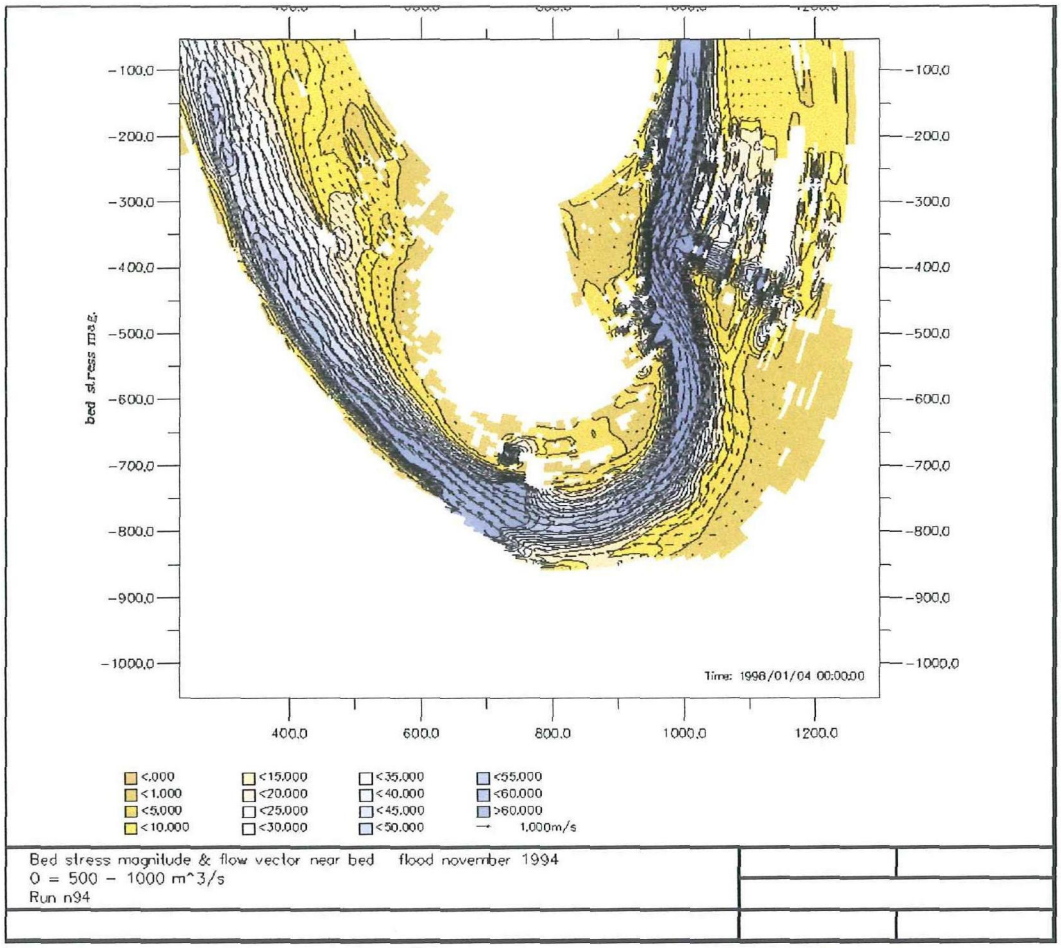

figure 73 : bed shears stress upstream point bar for a discharge of 1000 m^3/s

7.3.1 Indication of surface-grain size pattern

The data on the surface-grain size distribution is not yet worked out. But based on figure 70 and the plots of the bed shear stress in chapter 6, a rough indication of the surface-grain size distribution over the survey area can be given. It is assumed that the samples described in table 7 and their reference shear stresses from figure 70 are representative for the whole survey area.
In figure 74 the survey area is plotted with isolines of the bed shear stress magnitude at a discharge of 1000 m^3/s. These isolines also give an indication of the surface-grain size distribution. At location (1) a bar is present. This bar leads to a local acceleration of the flow and hence a local increase in the bed shear stress, see figure 72. Due to the increased bed shear stress smaller grain sizes will be eroded and a coarse surface layer is expected to develop here.
At location 2 the flow is directed onto the point bar and curves away from the main channel at discharges of 500 m^3/s and larger. Sediment from the main channel is transported onto the point bar. As the flow turns away from the main channel, flow velocities and bed shear stresses decrease (see figure 48 and figure 59, chapter 6). Therefore a coarse mixture will be found near the main channel and a finer mixture

further on the point bar. The bed shear stress near the main channel is large enough to move the largest grain found in the samples, D_{max} = 70 mm.

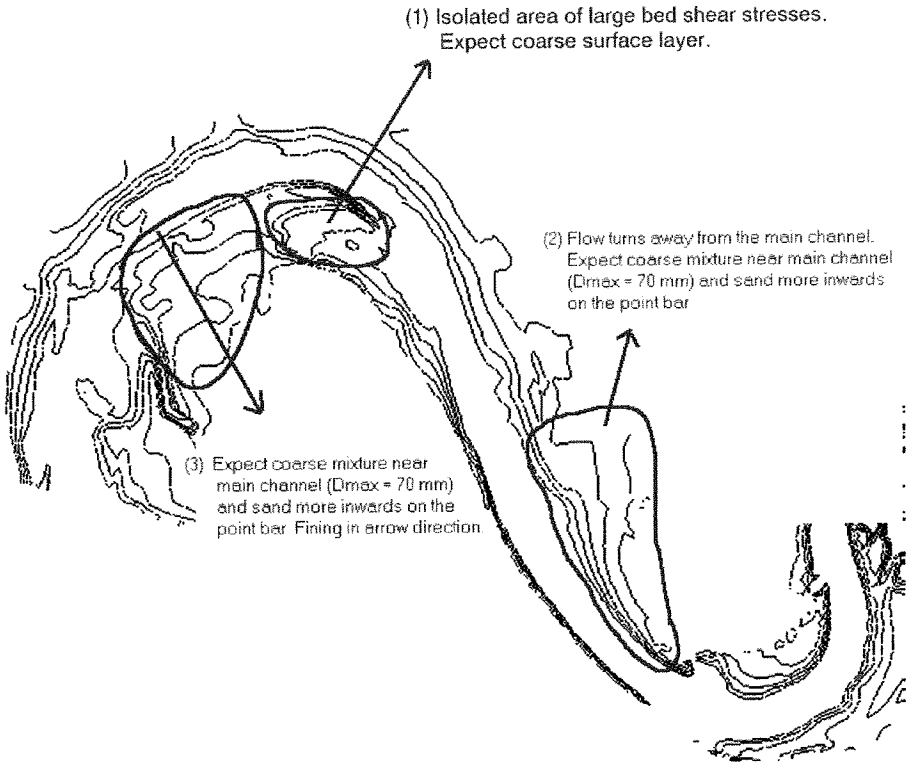

figure 74 : expected grain size distribution over the survey area

At location (3) a more or less identical situation is present. The flow is directed onto the point bar and the mixture becomes finer further on the point bar. Here also the flow is able to move the largest grain within the samples.

7.3.2 Validity of above approach

The above calculated reference shear stresses for the various samples are only indications. The surface based model is based on transport measurement in the Oak Creek. There are many differences between Oak Creek and the river Allier. Oak Creek is a small gravel stream and the sediment transport contains little sand, whereas the river Allier is much larger and transports large amounts of sand. Part of this sand is transported as bed forms. If these bed forms move over an armour layer the threshold of movement is disturbed. There are no sediment transport measurements of the river Allier to verify the Oak Creek model for this river, especially the value of the exponent in the hiding function, 0.9047.

7.4 Conclusion

By using the surface based Oak Creek model to estimate the threshold of motion for individual grain sizes within a sample, the reference shear stress is found to be much lower than the critical shear stress obtained from the Shields-v Rijn criterion.
There are two reasons for this. First the reference shear stress used in the Oak Creek model, 0.0386, is lower than the critical shear stress used by Shields-v Rijn, 0.055. Second the hiding factor increases the reference shear stress for the smaller-size fractions and decreases it for the larger-size fractions.
With these lower reference shear stresses a large part of the samples can be explained. The bed shear stress results from the flow model show that even the largest particles in the samples can be moved at discharges of 1000 m^3/s.
Also an indication of the surface-grain size distribution is given, see figure 74.
It is however stressed, that these results are just an indication. Oak Creek is quite a different river as the Allier and there are no sediment transport measurements to test the Oak Creek model for the river Allier.

8 Conclusions and recommendations

8.1 Conclusions

With the data obtained during a field survey in the summer of 1998, a flow model of the two bends just upstream of Chateau de Lys was made. This model was calibrated against velocity measurements made at a discharge of approximately 20 m^3/s. Steady- and unsteady flow simulations up to a discharge of 1000 m^3/s were made.

8.1.1 Flow velocity and bed shear stress

The simulations showed the flow mainly to follow the main channel. High velocities in the main channel lead to very large bed shear stresses. At several places the flow was directed onto the point bars. Here the bed shear stress magnitude indicates that large grains could be transported onto the point bar.
Secondary flow was found where the bend radius of curvature is smallest, indicating an inbank flow pattern.

8.1.2 Downstream boundary condition

As there was no information on the downstream boundary condition, it had to be estimated. During the calibration it became clear that the water level at the downstream boundary could not be estimated well. The influence of an error in the downstream water level was estimated. It proved to influence the flow for about 1000 m upstream of the downstream boundary. However, the magnitude of a water level error was shown to decrease rapidly in the upstream direction.

8.1.3 Inbank - overbank flow

Simulations up to 1000 m^3/s showed the flow to follow an inbank flow pattern. The upstream point bar is not fully flooded and most of the discharge is conveyed in the main channel. Therefore at the cross over region, upper- and lower layer flow have the same direction and no secondary flow develops due to the interaction between upper- and lower layer flow. This is confirmed by the position of the secondary flow cells.

8.1.4 Steady state – unsteady state

The differences between the steady state and the unsteady state simulations are small. Although there are some differences, the flow pattern and the magnitude of the velocity is largely the same, see paragraph 6.6.

For a global impression of the flow pattern at a certain discharge, the steady state simulations are sufficient. As the steady state simulations have a much shorter computation time, this saves a lot of computation time.

8.1.5 Armour layers

The presence of armour layers on the point bars could be explained with the aid of the Oak Creek model. Combining the bed shear stresses from the flow model with the reference shear stresses calculated with the Oak Creek model it was shown that the threshold of motion is exceeded for all grain sizes within the mixtures.
However, much uncertainty remains about the applicability of the Oak Creek model on the river Allier.

8.1.6 Surface-grain size pattern

A rough indication of the surface-grain size pattern over the survey area was given in chapter 7, see figure 74. This indication was based on the assumptions that the samples described in chapter 7 were representative for the whole survey area and that the Oak Creek model is valid for the Allier.

8.2 Recommendations

8.2.1 Boundary conditions

The downstream boundary could not be generated well. Measurements of the water level at the downstream boundary are very difficult. Boundary conditions could be obtained from a larger flow model with the downstream boundary situated in the city of Moulins. Here the stage-discharge relation is known.

8.2.2 Bed roughness

The influence of a different bed roughness coefficient at the point bars is not examined in the present study. With further data of the field survey a more realistic, space varying, bed roughness could be prescribed. The data necessary to construct such a bed roughness file is currently worked out.

8.2.3 The applicability of the Oak Creek model.

The applicability of the Oak Creek model should be tested. As there are no sediment transport measurements of the Allier, the validity of use of the Oak Creek model could

not be tested. The literature values of the reference Shields stress, 0.0386, and the coefficient in the hiding factor, -0.9047, should be verified for the river Allier.

8.2.4 Comparison of the sampled surface-grain size with the model results.

To check whether the model can predict the surface-grain size distribution, the bed shear stress results of the model should be compared to the results of the survey, when the data on the grain size distribution have been.

References

Andrews, E. D. and Parker, G. (1987)
Formation of a Coarse Surface Layer as a Response to Gravel Mobility.
Sediment Transport in Gravel-bed Rivers,
edited by Thorne, C. R., Bathurst, J. C. and Hey, R. D.
John Wiley & Sons, London U.K.

Bakke, P. D., Basdekas, P. O., Dawdy, D. R. and Klingeman, P. C. (1999)
Calibrated Parker-Klingeman Model for gravel transport.
Journal of Hydraulic Engineering, Vol. 125, No.6

Blanckaert, K. and Graf, W.H. (1999)
Outer-Bank Cell of Secondary Circulation and Boundary Shear stress in Open-Channel Bends
Proceedings coastal morphology conference, Genoa 1999

Blom, A. (1997)
Planform changes and overbank flow in meandering rivers – the river Allier.
Graduation Thesis, Delft University of Technology & Delft Hydraulics

Blom, A., Ribberink, J.S. and van der Scheer, P. (2000)
Sediment transport in flume experiments with tri-modal sediment mixtures.
CD-ROM contribution
Gravel-Bed Rivers Workshop (August 28 – September 2, 2000), New Zealand

Van der Bruggen, J. (??)
??? (in preperation)
Graduation thesis
Department of Physical Geography, University of Utrecht

Driesprong, A. (in preperation)
Boundary shear stress and hydraulic roughness in the Allier River.
Graduation thesis
Department of Physical Geography, University of Utrecht

Ervine, D.A.,Willets, B.B.,Sellin, R.H.J. and Lorena, M. (1993)
Factors affecting Conveyance in Meadering Compound Channels.
Journal of Hydraulic Engineering, Vol. 119, No.12

Ishigaki,T., Muto,Y. and Sawai, K. (1998)
Traction Process of Bed Materials by Three Dimensional Flow in a Compound Meandering Channel
Parallel Session: Basics of Sediment transport and Scouring [??]

Kruisinga, L. (??)
??? (in preperation)
Graduation thesis
Department of Physical Geography, University of Utrecht

Markham, A. J. and Thorne, C. R. (1992)
Geomorphology of Gravel-bed River bends.
Dynamics of Gravel-bed Rivers.
edited by Billi, P., Hey, R.D., Thorne, C.R. and Tacconi, P.
John Wiley & Sons, London, U.K.

Muto, Y., Imamoto, H. and Ishigaki, T. (1998)
Stage-Discharge Prediction for Overbank Flow in Meandering Channels
Parallel Session: Flow Experiments and Basics [??]

? (2000)
De Allier als morfologisch voorbeeld voor de Grensmaas, part I : Vergelijkbaarheid en rivierpatroon
Natuurhistorisch maandblad, July 2000

? (2000)
De Allier als morfologisch voorbeeld voor de Grensmaas, part II : Oevererosie en meandermigratie
Natuurhistorisch maandblad, August 2000

? (2000)
De Allier als morfologisch voorbeeld voor de Grensmaas, part III : Sedimenttransport en afpleistering
Natuurhistorisch maandblad, September 2000

Neessen, C. (in preperation)
3Dimensional flow patterns in the river Allier
Graduation thesis
Department of Physical Geography, University of Utrecht

Parker, G., Klingeman, P. C. and Mclean, D. G. (1982)
Bedload and size distribution in paved gravel-bed streams.
Journal of the Hydraulic Division, Vol. 108, No. 4

Parker, G. (1990)
Surface-based bedload transport relation for gravel rivers.
Journal of Hydraulic Research, Vol. 28, No. 4

Parker, G. and Sutherland, A. J. (1990)
Fluvial armor.
Journal of Hydraulic Research, Vol. 28, No. 5

Raudkivi, A. J. and Ettema, R. (1982)
Stability of Armour Layers in Rivers.
Journal of the Hydraulic Division, Vol. 108, No. HY9

Raudkivi, A. J. (1990)
Loose Boundary Hydraulics.
Pergammon Press

Ribberink, J. S. (1987)
Mathematical modelling of one dimensional morphological changes in rivers with non-uniform sediments.
Communications on Hydraulic and Geotechnical engineering, Report No. 87-2
Faculty of Civil Engineering, Delft University of Technology

Van Rijn, L.C. (1993)
Principles of sediment transport in rivers, estuaries and coastal seas

De Vriend, H.J. (1997)
Rivierwaterbouwkunde
Reader F8
Faculty of Civil Engineering, Delft University of Technology

White, W. R. and Day, T. J. (1982)
Transport of Graded Gravel Bed Material.
Sediment Transport in Gravel-bed Rivers,
edited by Thorne, C. R., Bathurst, J. C. and Hey, R. D.
John Wiley & Sons, London U.K.

Wilbers, A. (1997)
De Allier, een rivier met twee patronen
Graduation thesis
Department of Physical Geography, University of Utrecht

Wilbers, A. and de Kramer, J.
The Allier pages
http://globis.geog.uu.nl/wilbers/home.html

Wilcock, P. R. (1993).
Critical Shrear Stress of Natural Sediments.
Journal of Hydraulic Engineering, Vol. 119, No. 4

Overbank flow in the river Allier

Appendices

P-J Bart

Augustus 2000

Appendix A

Field data

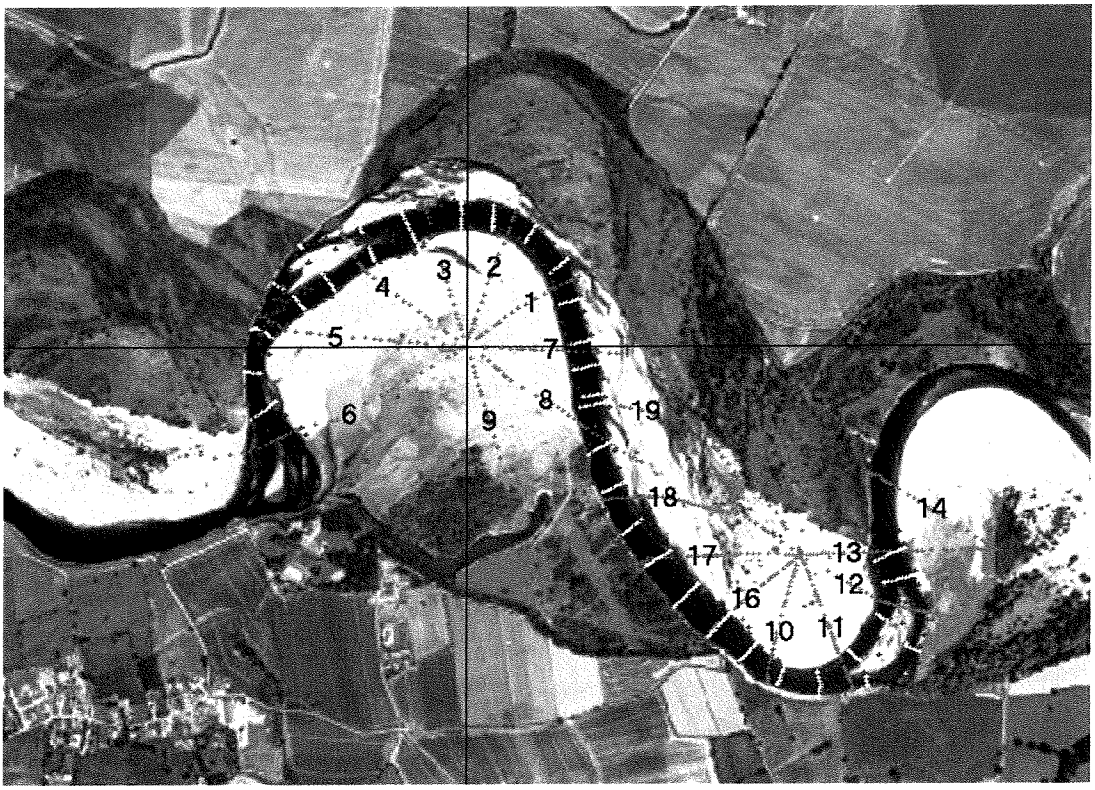
1
2
3
4
5
6
7
8
9
10
11
12
13
14
16
17
18
19

Appendix A1

Survey points

profiel	nr.	label	X	Y	Z
1	47		69	51	0.49
	48		26	18	-0.53
	49		32	24	0.1
	50		38	28	-0.48
	51		50	35	0.52
	52		79	58	-0.67
	53		76	56	0.16
	54		93	70	-0.94
	55		112	82	-1.48
	56		125	92	-0.68
	57		146	102	-0.86
	58		166	115	-0.93
	59		189	127	-1.3
	60		202	139	-1.92
	61	vp 1	214	142	-2.18
	62		229	150	-2.78
	63		242	156	-3.28
	64		250	160	-3.35
	65		257	162	-2.84
	66		269	167	-2.22
	67		274	169	-1.7
	68		293	177	-2.16
	69		297	181	-2.41
	70		301	184	-2.1
	71		305	188	-0.93
	71*		306	189	0.97
2	72	vp 2	30	86	0.13
	73		7	22	-0.5
	74		11	34	0.03
	75		14	43	-0.43
	76		19	56	0.13
	77		21	64	-0.18
	78		22	67	0.23
	79		37	106	-0.94
	80		44	125	-1.11
	81		52	151	-1.29
	82		58	166	-1.84
	83		62	179	-0.96
	84		67	195	-0.49
	85		71	206	-0.91
	86		77	223	-0.89
	87		90	248	-1.85
	88	vp 3	99	274	-2.24
	89		102	281	-2.92
	90		105	290	-3.3
	91		111	305	-3.16
	92		114	315	-2.8
	93		118	326	-2.25
	94		121	332	-1.3
	95		134	370	-1.46
	96		135	371	-2.07
	97		139	380	-3.24
	98		140	384	-2.06
	99		141	386	-1.3
	99*		141	387	-1.3

profiel	nr.	label	X	Y	Z
3	100		-30	101	-0.07
	101		-7	24	-0.34
	102		-13	43	0.27
	103		-16	54	-0.06
	104		-20	68	0.13
	105		-23	78	0.04
	106		-37	125	-0.46
	107		-40	137	-0.78
	108		-47	159	-0.74
	109		-55	182	-1.14
	110		-59	195	-0.92
	111		-71	233	-2.5
	112		-72	238	-1.79
	113	vp 4	-81	268	-2.27
	114		-82	272	-2.94
	115		-90	301	-2.94
	116		-92	315	-3.38
	117		-96	325	-3.53
	118		-103	333	-2.35
	119		-118	339	-1.07
	120		-126	357	-2.31
	121		-127	359	-1.09
	122		-134	371	-2.52
	123	niet aanwezig			
4	124	vp 5	-97	72	-0.37
	125		-23	18	-0.28
	126		-47	34	-0.28
	127		-53	38	-0.49
	128		-88	65	-0.13
	129		-113	84	-0.41
	130		-137	101	-0.51
	131		-149	110	-0.83
	132		-168	124	-1.11
	133		-199	148	-1.32
	134	vp 6	-238	179	-1.22
	135		-224	166	-1.58
	136		-243	183	-2.74
	137		-250	189	-3.19
	138		-251	191	-3.16
	139		-253	197	-3.94
	140		-259	203	-3.89
	141		-267	217	-2.7
	142		-270	223	-2.29
	143		-289	253	-2.12
	144		-291	256	-2.64
	145		-294	264	-3.2
	146		-296	270	-2.66
	147		-300	279	-1.66
	148		-305	290	-2.87
	149		-310	297	-2.53
	150		-319	309	-2.86
	151		-320	310	-2.25
	151*		-320	311	1.15

profiel	nr.	label	X	Y	Z
5	152		-138	11	-0.57
	153		-54	4	-0.06
	154		-96	8	-0.72
	155		-117	10	-0.54
	156		-163	12	-0.21
	157		-173	13	-0.55
	158		-185	16	-0.44
	159		-205	17	-0.78
	160		-221	18	-0.47
	161		-244	21	-0.75
	162		-273	23	-0.79
	163		-311	26	-1.04
	164	vp 7	-436	40	-1.78
	165		-316	26	-1.48
	166		-324	27	-1.48
	167		-332	28	-2.08
	168		-353	30	-2.11
	169		-376	32	-1.72
	170		-383	34	-1.84
	171		-412	37	-1.43
	172		-440	42	-2.88
	173		-448	47	-3.59
	174		-454	53	-3.21
	175		-465	61	-3.25
	176		-475	62	-3.48
	177		-486	73	-3.09
	178		-496	74	-5.04
	179		-503	83	-2.97
	180		-503	83	0.53
6	181		-142	-82	-0.66
	182		-28	-17	0.23
	183		-43	-27	-0.32
	184		-83	-49	-0.13
	185		-108	-63	-0.33
	186		-176	-102	-0.79
	187		-205	-117	-1.2
	188		-242	-138	-1.29
	189		-278	-158	-0.82
	190		-310	-176	-0.84
	191	vp 8	-399	-197	-1.64
	192		-325	-179	-1.85
	193		-363	-188	-1.56
	194		-403	-199	-3.03
	195		-412	-202	-3.73
	196		-422	-208	-3.78
	197		-435	-214	-3.47
	198		-443	-218	-3.66
	199		-448	-220	-3.02
	200		-453	-224	-2.65
	201		-465	-229	-3.03
	202		-470	-230	-3.47
	203		-481	-237	-3.53
	204		-497	-244	-3.04
	205		-522	-254	-3.08
	206		-538	-256	-2.89
	207		-569	-262	-1.39
	208		-606	-271	-0.56
	209		-638	-262	-0.24

profiel	nr.	label	X	Y	Z
7	210	vp 9	124	-6	-0.14
	211		46	-4	0.19
	212		86	-4	0.24
	213		107	-5	0.35
	214		134	-6	-0.44
	215		140	-7	-1.29
	216		155	-7	-1.25
	217		166	-8	-0.78
	218		183	-9	-0.54
	219		220	-11	-1.07
	220		234	-11	-1.48
	221		249	-11	-2.14
	222		266	-12	-2.57
	223		285	-13	-2.84
	224		307	-13	-3.06
	225		317	-14	-2.13
	226		322	-16	-0.79
	227		346	-17	-1.15
	228		363	-18	-0.93
	229		376	-19	-0.61
8	230		91	-69	-0.02
	231		42	-23	0.59
	232		54	-35	0.33
	233		70	-50	0.48
	234		74	-54	-0.07
	235		79	-58	0.28
	236		98	-74	0.17
	237		109	-83	0.38
	238		135	-101	0.49
	239		168	-120	0.47
	240		193	-134	0.41
	241		205	-138	0.12
	242	vp 10	248	-168	-0.65
	243		223	-148	-0.33
	244		235	-158	-0.47
	245		262	-178	-0.98
	246		276	-188	-1.58
	247		283	-193	-1.99
	248		292	-198	-2.39
	249		307	-211	-3.39
	250		313	-195	-3.41
	251		317	-218	-3.24
	252		330	-225	-2.48
	253		346	-236	-2.16
	254		351	-240	-1.95
	255		364	-247	-1.55
	256	vp 11	384	-259	-1.12
	257		405	-272	-1.63
	258		415	-278	-1.36
	259	vp 12	425	-283	-0.69

nr.	label	X	Y	Z	
9	260	vp 13	37	-116	0.45
	261		11	-28	0.38
	262		18	-50	-0.62
	263		21	-63	-0.54
	264		24	-75	0.33
	265		29	-95	0.41
	266		34	-108	0.43
	267		45	-144	0.41
	268		49	-156	0.09
	269		53	-169	0.29
	270		54	-177	-0.03
	271		57	-188	0.48
	272		68	-219	0.22
	273		76	-245	0.5
	274		84	-269	0.51
	275		95	-306	0.16
10	276		439	-391	-1.67
	277		484	-492	-1.71
	278		574	-594	-1.49
	279		669	-666	-0.21
	280	vp 14	744	-739	-0.23
	281		740	-751	-0.81
	282		739	-753	-1.79
	283		736	-760	-2.01
	284		734	-770	-2.38
	285		732	-785	-2.47
	286		729	-799	-2.9
	287	bestaat niet			
	288		728	-804	-3.24
	289		730	-809	-3.47
	290		729	-814	-2.95
	291		726	-818	-1.78
	292		724	-822	0.75
	293		746	-726	-0.02
	294		747	-719	-0.18
	295		750	-709	-0.12
	296		752	-701	0.38
	297		758	-676	0.58
	298		763	-657	0.85
	299		782	-584	1.17
	300		767	-633	1.37
	301		778	-599	0.99
	302		771	-624	1.31
	303		773	-618	1.17
	304		777	-606	1.12
	305		785	-574	1.4
	306		789	-564	1.38
	307		791	-560	1.52
	308		792	-555	1.29
	309		794	-549	1.6
	310		796	-545	1.24
	311		799	-535	1.31
	312		806	-519	1.57
	313	vp 15	807	-515	1.09
	314		809	-510	1.33
	315		843	-597	1.42

profiel	nr.	label	X	Y	Z
11	316		813	-521	1.42
	317		816	-528	1.38
	318		817	-532	1.47
	319		823	-546	1.33
	320		826	-553	1.28
	321		828	-560	1.59
	322		832	-570	1.4
	323		837	-583	1.38
	324		846	-606	1.2
	325		848	-610	1.45
	326		851	-618	1.37
	327		852	-622	1.5
	328		856	-631	1.21
	329		866	-657	0.75
	330		873	-674	0.34
	331		875	-681	0.16
	332		878	-688	0.67
	333		882	-699	-0.59
	334	vp 16	900	-747	-0.94
	335		885	-709	-0.72
	336		887	-714	-0.27
	337		889	-719	-0.1
	338		892	-727	-0.54
	339		895	-734	-0.68
	340		897	-738	-0.74
	341		905	-760	-1.66
	342		908	-767	-2.22
	343		913	-781	-2.33
	344		916	-787	-2.43
	345		919	-794	-2.13
	346		922	-800	-1.69
	347		922	-802	-1.51
	348		923	-804	-1.7
	349		924	-806	-2.06
	350		927	-813	-2.44
	351		930	-819	-2.46
	352		933	-829	-2.22
	353		935	-833	-1.66
	354		936	-836	-0.08
	355		937	-837	0.44

profiel	nr.	label	X	Y	Z
12	356	vp 17	923	-578	1.31
	357		824	-519	1.32
	358		873	-548	1.29
	359		897	-563	1.37
	360		902	-565	1.69
	361		930	-582	1.08
	362		941	-589	0.23
	363		953	-595	-0.49
	364		966	-603	-0.65
	365		980	-611	-0.95
	366		997	-622	-1.31
	367		1064	-640	-0.47
	368		1004	-624	-1.57
	369		1013	-626	-2.04
	370		1016	-626	-2.25
	371		1021	-628	-2.27
	372		1024	-629	-2.13
	373		1034	-631	-2.02
	374		1041	-633	-2.56
	375		1046	-634	-1.61
	376		1057	-638	-1.11
	377		1074	-642	-0.44
	378		1084	-644	-1.49
	379		1090	-645	-1.55
	380		1097	-647	-1.95
	381		1104	-648	-2.22
	382		1108	-649	-2.29
	383		1113	-650	-2.2
	384		1120	-651	-2.21
	385		1123	-652	-1.55
	386		1132	-654	-0.36
	387		1140	-655	-0.09
	388		1145	-656	0.15
	389		1151	-657	-0.16
	390		1167	-660	0.03
	391		1182	-663	-0.01
	392		1216	-669	-0.16
	393		1228	-672	-0.41
13	394		912	-505	1.78
	395		824	-509	1.52
	396		833	-509	1.39
	397		840	-509	1.72
	398		849	-508	1.59
	399		861	-507	1.73
	400		870	-507	1.3
	401		877	-506	1.71
	402		890	-506	1.66
	403		902	-506	1.75
	404		933	-504	1.82
	405		944	-503	1.88
	406		961	-502	1.95
	407		912	-505	1.91
	408		978	-502	-1.43
	409	vp 18	1091	-501	-0.59
	410		989	-502	-1.79
	411		982	-502	-2.01
	412		996	-501	-1.85
	413		1010	-502	-2.14
	414		1018	-501	-2.25
	415		1026	-501	-2.29
	416		1044	-502	-2.17
	417		1056	-501	-1.95
	418		1065	-501	-1.42
	419		1077	-501	-0.98

profiel	nr.	label	X	Y	Z
14	420		1102	-500	0.11
	421		1124	-499	0.27
	422		1155	-497	0.71
	423		1175	-497	0.75
	424		1283	-497	0.34
	425		1199	-496	0.77
	426		1211	-495	0.41
	427		1222	-496	0.54
	428		1238	-496	0.5
	429		1245	-496	0.05
	430		1263	-496	0.28
	431		1265	-486	0.24
	432		1255	-480	0.41
	433		1247	-475	-0.02
	434		1232	-466	0.65
	435		1211	-452	0.61
	436		1186	-437	0.86
	437		1092	-381	0.34
	438		1155	-418	0.7
	439		1141	-411	0.28
	440		1127	-402	0.67
	441		1119	-398	-0.1
	442		1110	-392	0.23
	443		1081	-374	0.1
	444		1068	-365	-0.41
	445		1044	-350	-0.94
	446		1040	-348	-1.33
	447		1027	-339	-1.5
	448		1023	-337	-1.68
	449		1015	-332	-2.02
	450		1010	-329	-1.93
	451		1006	-326	-2.26
	452		1002	-324	-2.12
	453		997	-317	-2.52
	454		998	-316	-2.74
	455		983	-315	-1.34
	456		989	-316	-3.12
	457		980	-313	0.25

profiel	nr.	label	X	Y	Z
16	458	vp 19	731	-571	1.11
	459		806	-512	1.16
	460		799	-518	1.54
	461		789	-525	1.35
	462		784	-529	1.24
	463		780	-533	1.34
	464		776	-536	1.21
	465		769	-542	1.41
	466		767	-544	1.21
	467		753	-554	1.46
	468		749	-557	1.23
	469		743	-561	1.44
	470		740	-563	1.13
	471		735	-567	1.18
	472		721	-579	1.16
	473		715	-584	1.3
	474		700	-596	1.2
	475		684	-610	0.56
	476		683	-612	0.94
	477		676	-617	0.92
	478	vp 20	650	-639	0.19
	479		667	-624	0.94
	480		656	-634	0.75
	481		640	-647	-1.09
	482		638	-649	-1.76
	483		632	-653	-2.34
	484		637	-649	-2.32
	485		621	-662	-2.51
	486		611	-671	-2.67
	487		605	-676	-2.98
	488		600	-681	-3.06
	489		597	-687	-2.6
	490		592	-693	-3.14
	491		582	-708	-2.7
	492		581	-710	-1.79
17	493		708	-506	1.26
	494		803	-510	1.16
	495		799	-511	1.45
	496		791	-510	1.5
	497		781	-509	1.6
	498		774	-508	1.42
	499		753	-507	1.36
	500		731	-507	1.26
	501		695	-507	0.89
	502		681	-507	1.23
	503		665	-507	1
	504		655	-508	0.49
	505		651	-509	0.15
	506		639	-509	0.39
	507		629	-510	-0.22
	508		619	-510	-0.65
	509		608	-511	-0.72
	510		606	-510	-0.3
	511		598	-511	-0.75
	512		591	-511	0.27
	513	vp 21	537	-513	-0.94
	514		585	-511	-0.2
	515		580	-511	0.07
	516		574	-512	-0.21
	517		563	-512	-0.35
	518		555	-513	-0.89
	519		547	-513	-0.85
	520	bestaat niet			

profiel	nr.	label	X	Y	Z
	521		498	-514	-1.82
	522		484	-514	-2.15
	523		466	-514	-2.41
	524		451	-515	-2.69
	525		440	-515	-3.01
	526		438	-520	-3.43
	527		437	-523	-3.59
	528		429	-523	-3.44
	529		428	-530	-3.24
	530		427	-531	-2.52
	531		425	-531	-1.86
	532		423	-532	-0.58
18	533		745	-465	1.3
	534		787	-494	1.2
	535		763	-478	1.27
	536		731	-455	1.07
	537		722	-448	1.1
	538		717	-445	0.91
	539		701	-434	1.07
	540		687	-424	1.21
	541		675	-415	0.95
	542		615	-402	0.15
	543		654	-410	0.68
	544		638	-407	0.42
	545		633	-405	0.58
	546		629	-405	0.01
	547		622	-403	0.17
	548		608	-400	-0.09
	549		601	-399	0.07
	550		590	-396	0.47
	551		585	-395	0.05
	552		578	-393	-0.23
	553		573	-392	-0.87
	554		562	-389	-0.78
	555		555	-387	-0.52
	556		547	-384	-0.33
	557		537	-382	-0.49
	558		529	-380	-0.09
	559		526	-379	-0.06
	560		516	-377	-0.89
	561		503	-374	-0.58
	562		495	-371	-0.48
	563		487	-369	-1.22
	564		477	-367	-0.07
	565		441	-368	-1.24
	566		461	-368	-0.17
	567		454	-368	-0.55
	568		446	-368	-0.96
	569		432	-368	-1.51
	570		429	-368	-1.67
	571		422	-368	-1.49
	572		409	-368	-1.44
	573		402	-368	-1.66
	574		392	-370	-1.82
	575		378	-370	-2.04
	576		366	-369	-2.44
	577		354	-370	-2.75
	578		346	-373	-3.02
	579		338	-373	-2.96
	580		335	-374	-2.42
	581		334	-374	-1.84
	582		331	-374	-0.71
	583		329	-374	0.1

profiel	nr.	label	X	Y	Z
19	584		751	-407	0.89
	585		804	-499	1.76
	586		773	-445	1.04
	587		768	-438	0.43
	588		764	-430	0.7
	589		734	-390	1.15
	590		710	-369	0.9
	591		696	-355	0.49
	592		671	-331	0.49
	593		655	-319	0.67
	594		650	-315	0.46
	595		607	-254	0.24
	596		649	-307	0.5
	597		633	-287	0.22
	598		620	-270	0.01
	599		561	-206	-0.03
	600		602	-249	-0.22
	601		597	-244	-0.93
	602		550	-183	-0.49
	603		532	-179	-0.5
	604		462	-163	-0.69
	605		536	-180	-1.67
	606		521	-175	-1.26
	607		510	-173	-1.08
	608		483	-168	-1.36
	609		443	-159	-0.35
	610		424	-156	-0.07
	611		418	-155	-1.13
	612		398	-150	-1.33
	613		382	-147	-1.67
	614		375	-145	-2.11

cross section 1

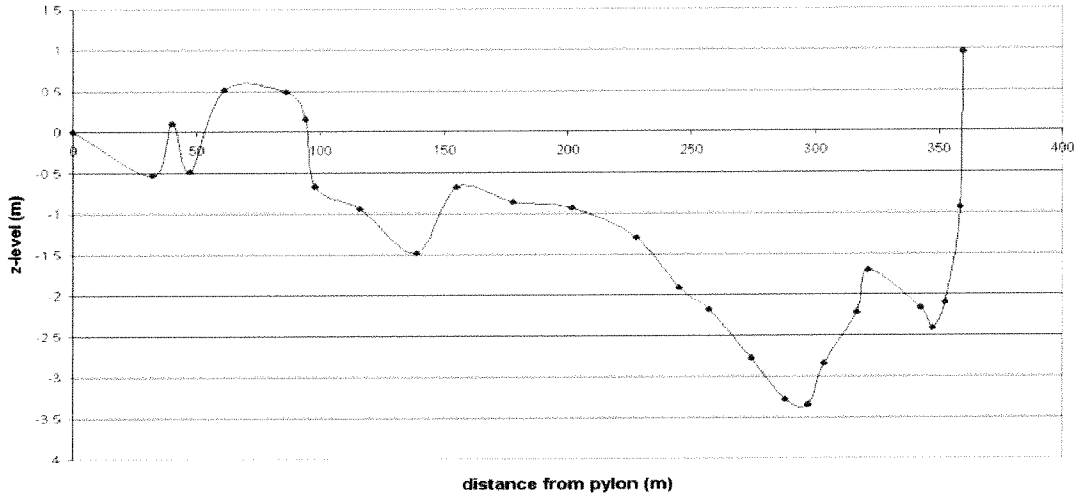

cross section 2

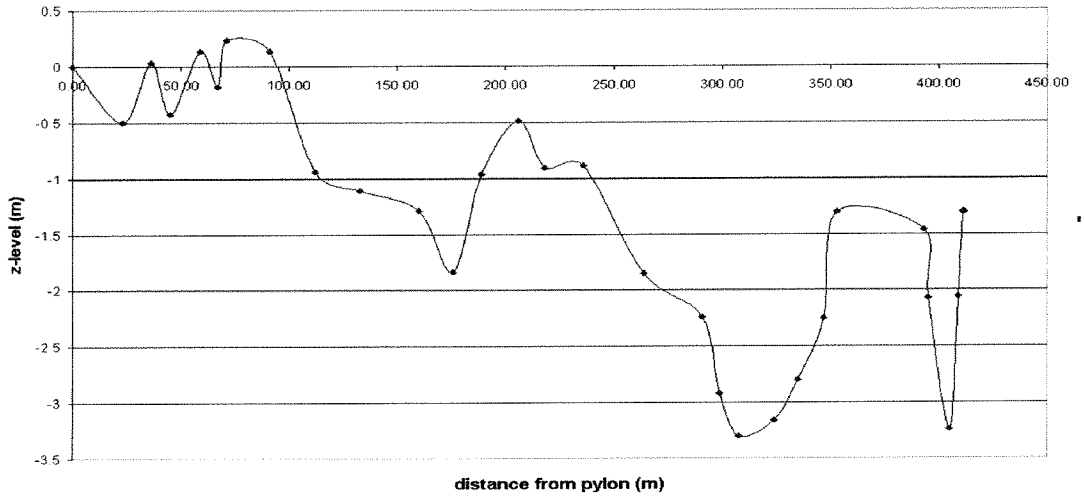

cross section 3

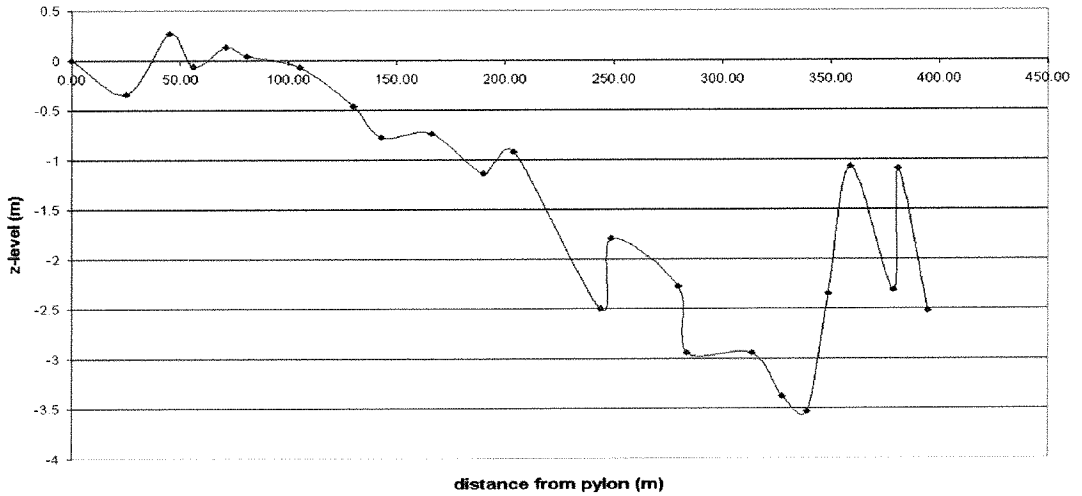

cross section 4

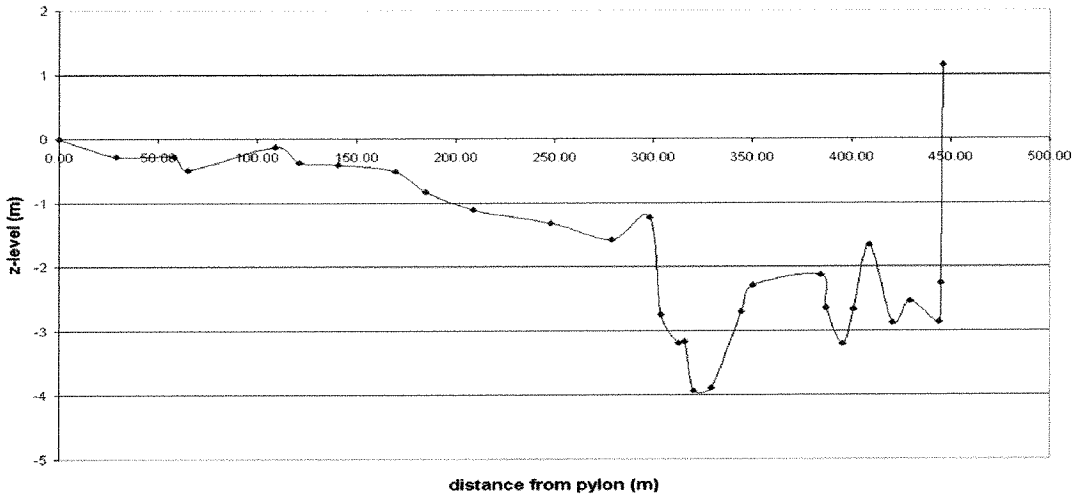

cross section 5

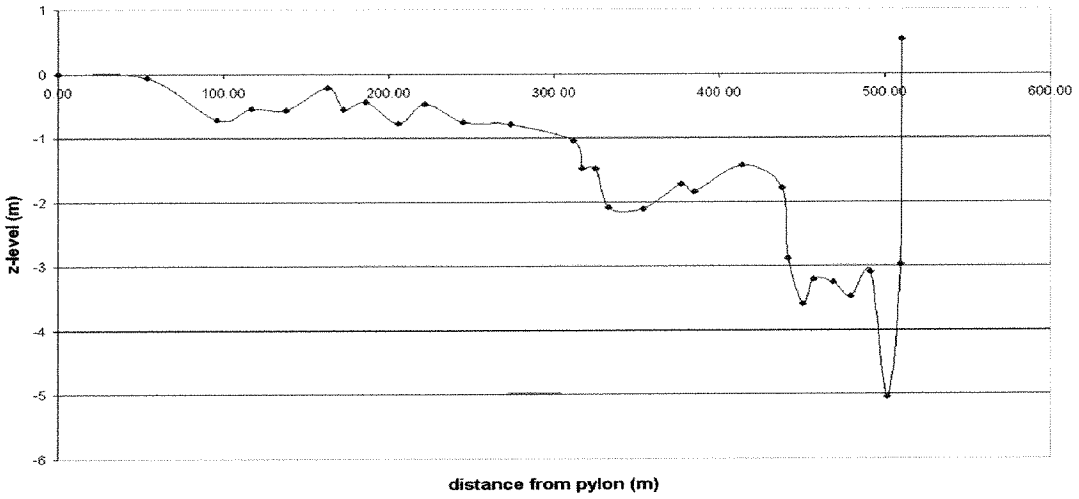

cross section 6

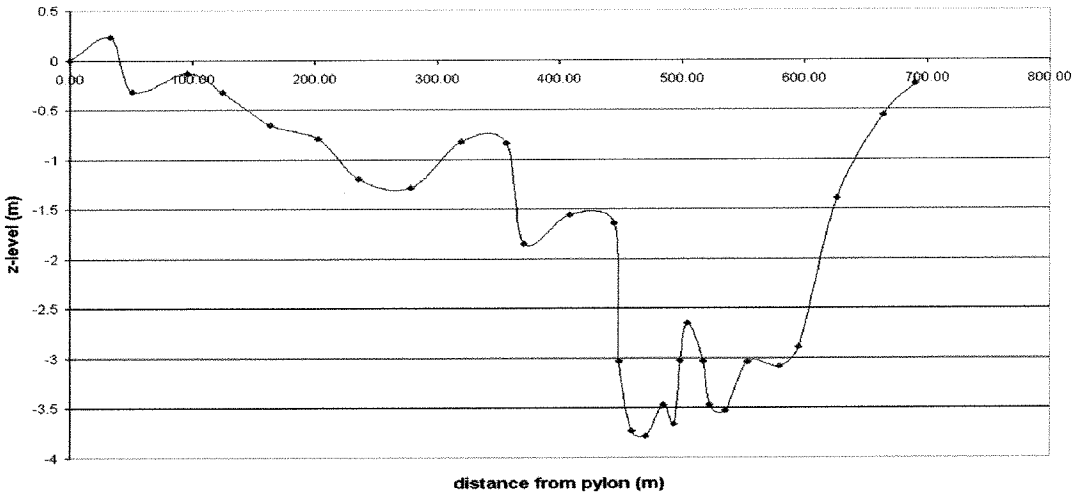

cross section 7

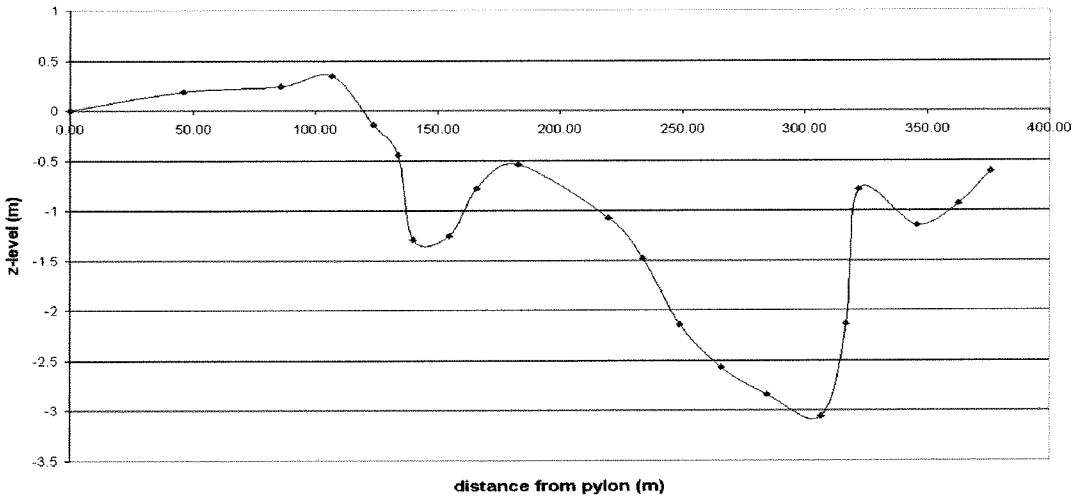

cross section 8

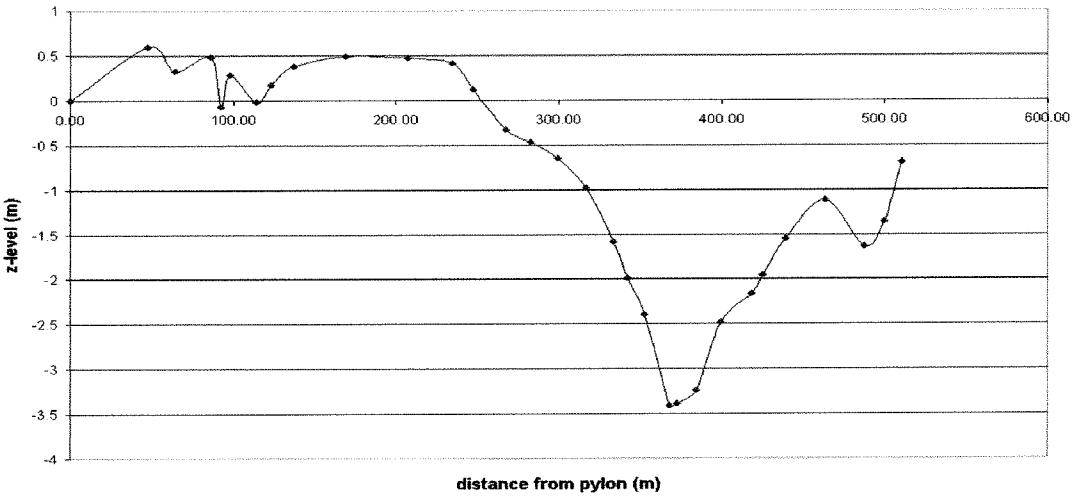

cross section 9

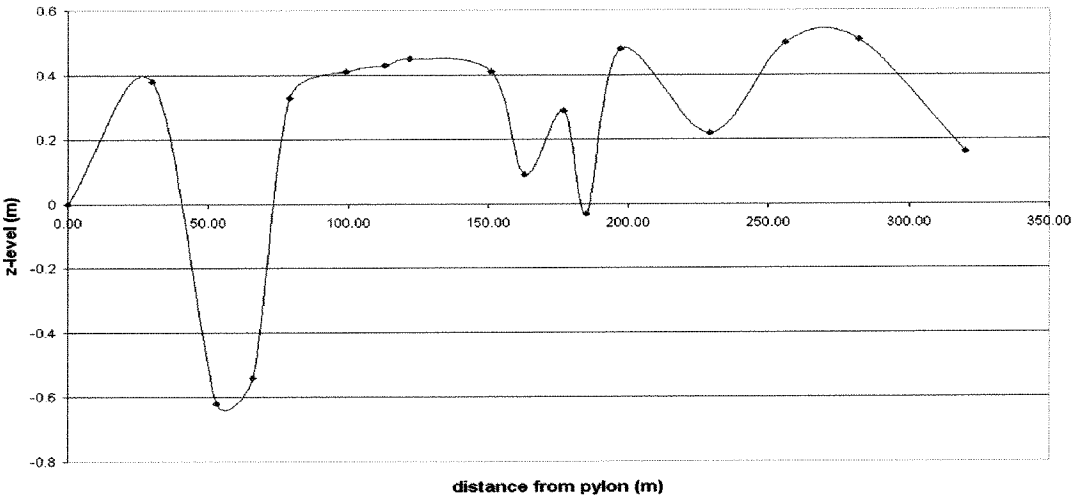

cross section 10

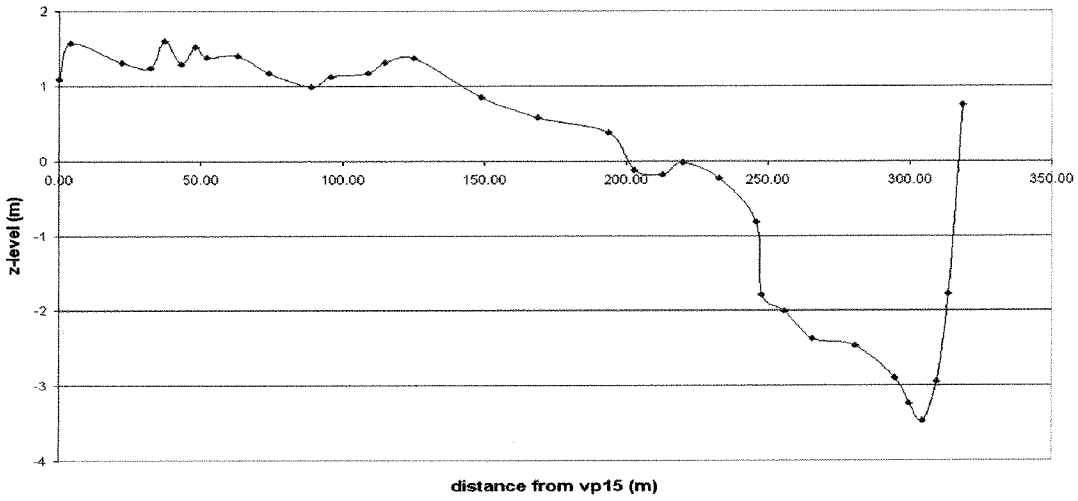

cross section 11

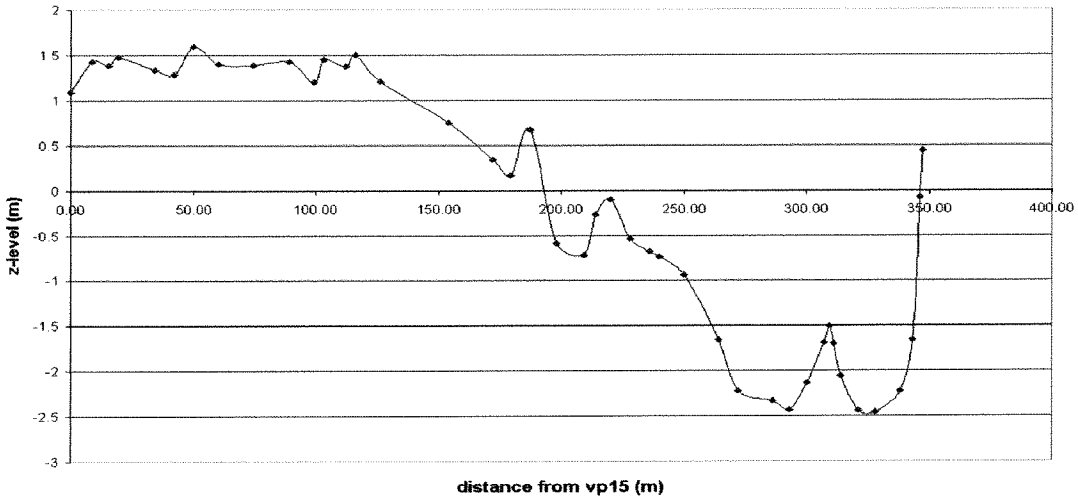

cross section 12

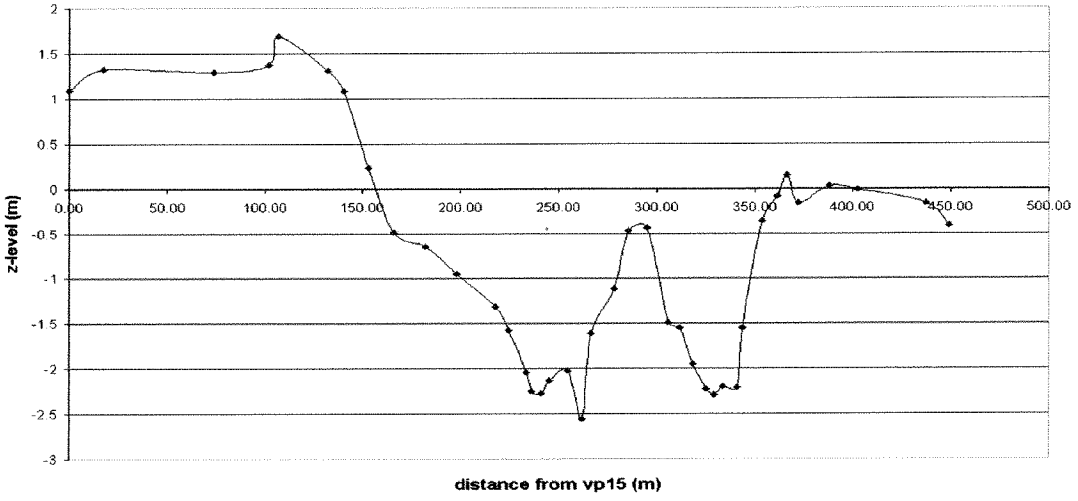

cross section 13

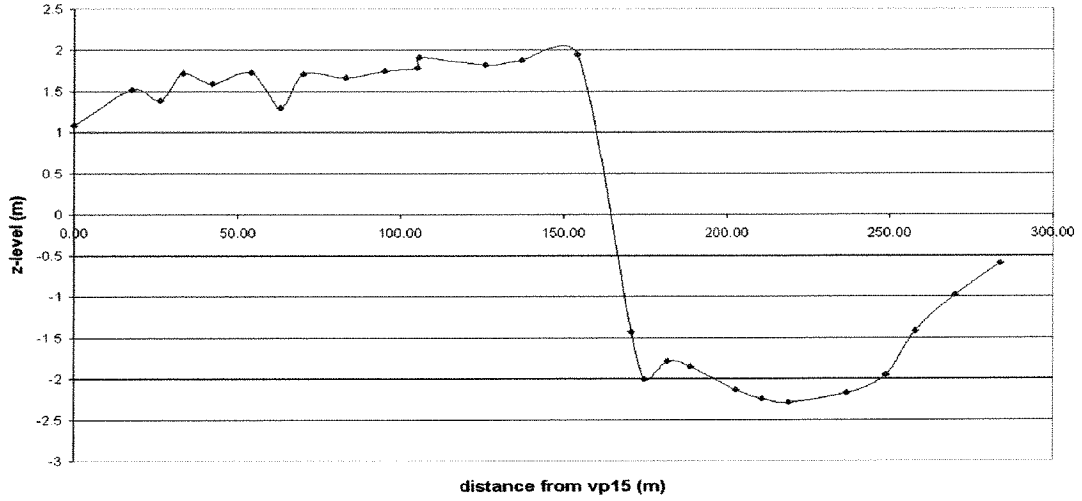

cross section 16

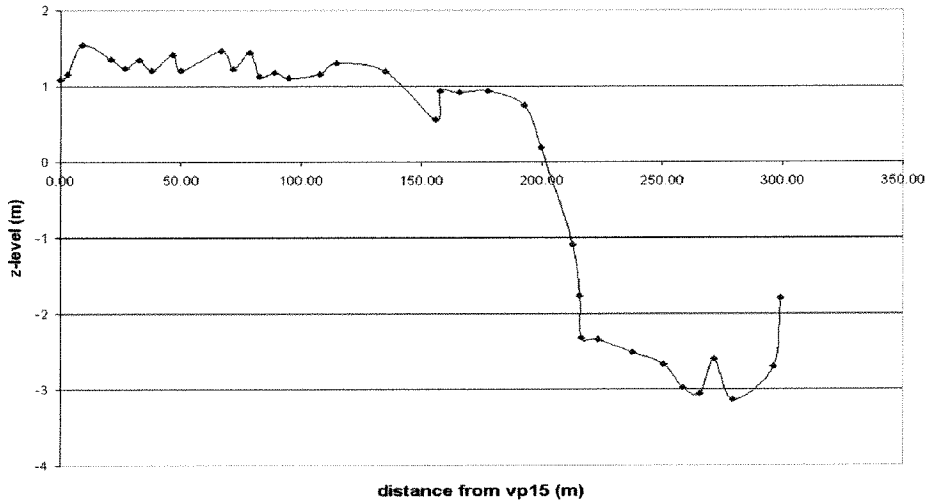

cross section 17

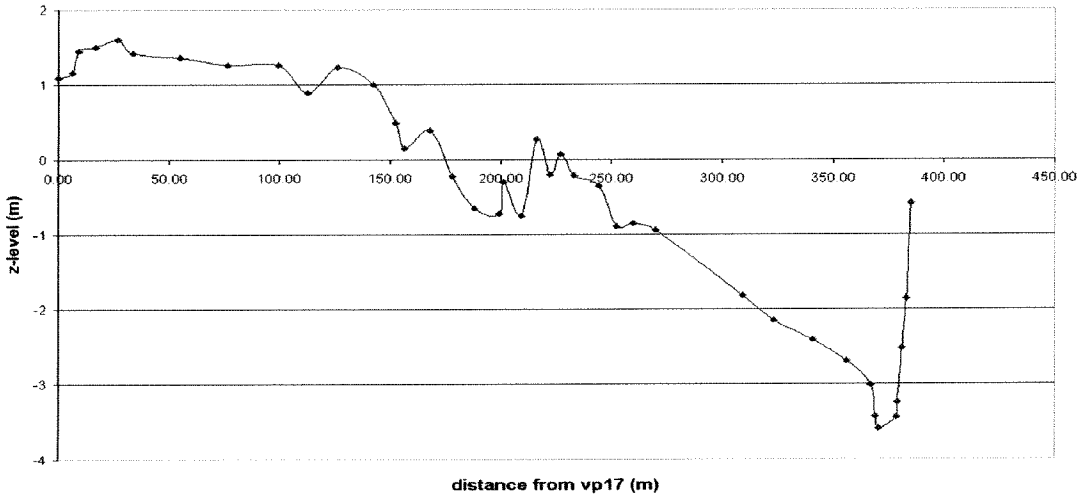

cross section 18

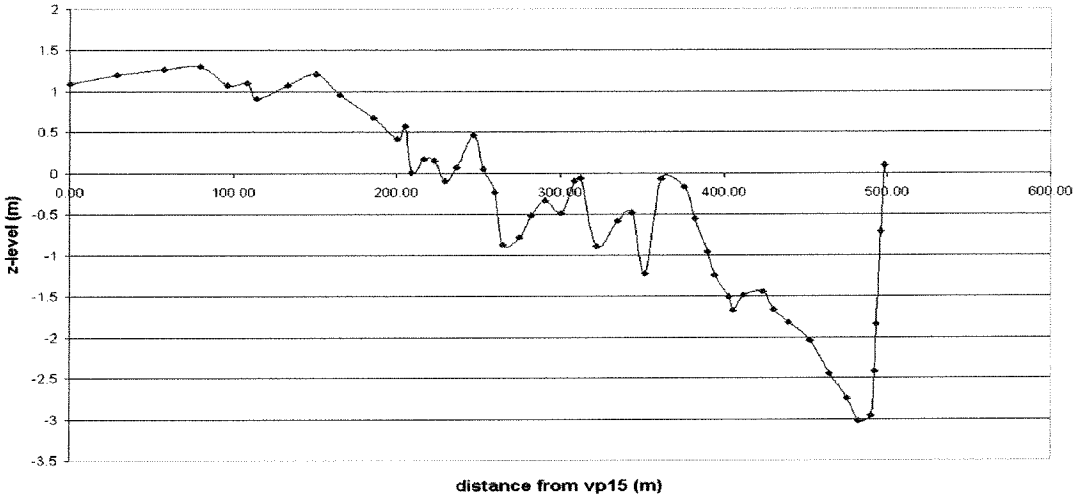

cross section 19

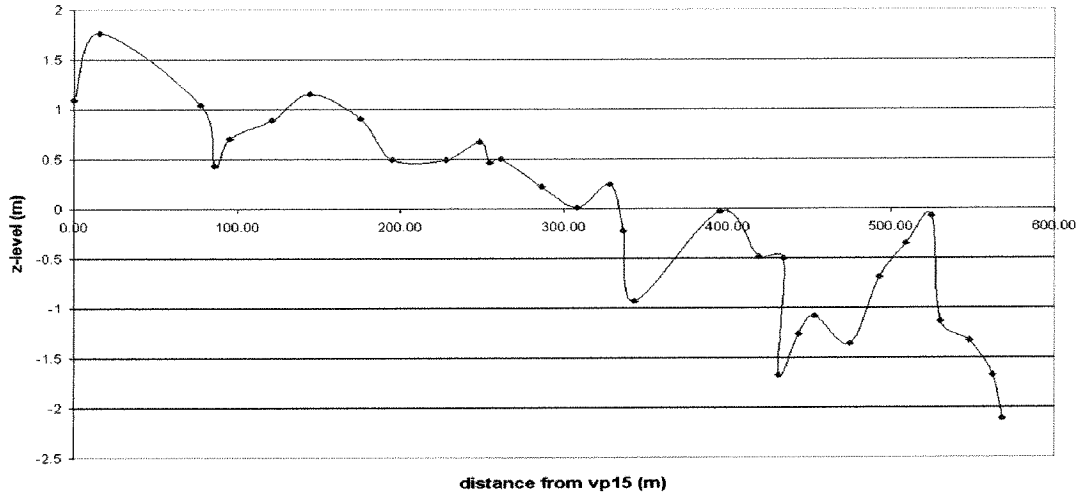

Appendix A2

Survey points velocity measurements

nr.	label	X	Y	Z
900	1.R	331.11	-115.77	-2.11
901	1.6	320.25	-117.51	-2.67
902	1.5	315.31	-118.30	-2.86
903	1.4	306.44	-119.84	-2.40
904	1.3	298.55	-121.16	-2.98
905	1.2	288.69	-122.83	-2.83
906	1.1	281.74	-123.67	-2.49
907	wpi 2	987.51	-525.04	-1.42
908	2.R	988.42	-524.62	-1.44
909	2.1	998.40	-520.00	-1.71
910	2.2	1006.66	-516.43	-1.92
911	2.3	1013.98	-513.19	-2.10
912	2.4	1020.34	-510.28	-2.18
913	2.5	1026.13	-507.31	-2.28
914	2.6	1034.77	-503.34	-2.28
915	2.7	1042.04	-500.00	-2.20
916	2.8	1049.31	-496.67	-2.03
917	2.9	1056.58	-493.33	-1.69
918	2.L	1060.21	-491.66	-1.45
919	wpi 3	1009.68	-577.56	-1.40
920	3.R	1010.65	-577.32	-1.42
921	3.1	1019.87	-575.05	-1.71
922	3.2	1028.10	-572.92	-1.89
923	3.3	1038.81	-570.38	-2.02
924	3.4	1046.52	-568.23	-2.06
925	3.5	1054.77	-566.21	-1.81
926	3.6	1062.07	-564.46	-1.87
927	3.7	1069.83	-562.52	-1.93
928	3.8	1077.53	-560.37	-1.75
929	3.9	1083.35	-558.89	-1.67
930	3.L	1085.26	-558.28	-1.45
931	4.R	991.07	-654.45	-1.53
932	4.4	996.64	-657.79	-2.12
933	4.3	1003.95	-662.14	-2.29
934	4.2	1010.48	-665.83	-2.45
935	4.1	1017.09	-669.38	-2.21
936	4.R eiland	1020.65	-671.62	-1.52
937		1025.54	-691.23	-0.75
938		1065.91	-723.82	-1.05
939	5.L eiland	1063.03	-730.71	-1.53
940	5.1	1066.30	-731.96	-1.71
941	5.2	1074.25	-734.97	-1.95
942	5.3	1081.76	-737.72	-2.23
943	5.4	1088.69	-740.60	-1.98
944	5.L	1096.24	-743.26	-1.52
945		1062.04	-797.53	-1.57
946	6.L eiland	966.37	-804.96	-1.58
947	6.1	966.88	-807.91	-2.08
948	6.2	968.31	-816.29	-1.94
949	6.3	968.51	-824.34	-2.77
950	6.L	969.33	-828.27	-1.57

nr.	label		X	Y	Z
951	7.R		849.46	-794.16	-1.53
952		7.1	850.20	-797.07	-1.65
953		7.2	852.91	-808.25	-2.18
954		7.3	854.57	-815.05	-2.22
955		7.4	856.78	-823.26	-2.17
956	ingemeten voor diepste punt		856.50	-829.98	-2.58
957	diepte 1.5m		856.06	-836.15	-3.03
958	diepte 1.7m		855.10	-842.34	-3.23
959	diepte 1.9m		853.65	-848.51	-3.43
960	ingemeten bij oever L		851.41	-853.64	-2.78
961	7.L		853.42	-858.55	-1.51
962	8.R		925.12	-741.40	-1.54
963		8.1	928.00	-744.18	-1.83
964		8.2	934.05	-750.15	-2.32
965		8.3	939.10	-755.00	-2.40
966		8.4	945.35	-760.76	-2.23
967		8.5	950.56	-765.44	-1.98
968	8.R eiland		954.05	-768.30	-1.55
969	Wpi 9		773.04	-775.78	-1.60
970		9.1	771.19	-779.89	-2.04
971		9.2	768.07	-787.25	-2.08
972		9.3	765.12	-794.15	-2.26
973		9.4	762.16	-801.58	-2.55
974		9.5	759.59	-808.10	-2.84
975			757.92	-812.28	-3.25
976			756.20	-816.43	-3.25
977			754.47	-820.59	-3.45
978	9.L		752.91	-824.81	-1.61
979	Wpi 10		705.66	-721.63	-1.55
980	10.R		705.30	-721.99	-1.72
981		10.1	701.41	-725.87	-2.33
982		10.2	696.48	-730.84	-2.38
983		10.3	690.08	-737.17	-2.58
984		10.4	685.18	-742.17	-2.66
985		10.5	679.41	-747.72	-2.65
986		10.6	673.79	-753.40	-2.71
987	Ingemeten begin helling geul		671.58	-756.14	-2.81
988	Diepste punt (veel rotsblokken)		666.77	-760.53	-3.15
989	10.L		662.02	-765.68	-1.69
990	Wpi 11		637.45	-648.60	-1.45
991	11.R		643.52	-644.89	-1.54
992		11.1	640.99	-647.45	-2.07
993		11.2	635.37	-653.15	-2.35
994		11.3	630.23	-658.61	-2.42
995		11.4	625.20	-664.18	-2.57
996		11.5	619.48	-669.78	-2.43
997	Geul		614.22	-675.82	-3.02
998			609.29	-680.79	-2.72
999	Begin nieuwe geul		601.08	-689.54	-2.86
1000			597.94	-693.45	-5.34
1001			594.51	-697.10	-4.94
1002			591.09	-700.74	-4.54
1003			587.67	-704.39	-4.14
1004	11.L		585.42	-707.76	-1.54

nr.	label	X	Y	Z
1005	Wpi 12	560.97	-578.12	-1.51
1006	12.R	560.28	-578.85	-1.53
1007	12.1	556.83	-582.47	-1.84
1008	12.2	551.29	-587.53	-2.14
1009	12.3	545.84	-592.69	-2.43
1010	12.4	539.89	-598.04	-2.53
1011	12.5	533.64	-604.53	-2.50
1012	12.6	528.19	-610.39	-2.62
1013	Ingemeten helling geul	522.79	-616.31	-2.95
1014		517.84	-621.26	-3.73
1015		512.89	-626.21	-3.93
1016		507.94	-631.16	-3.63
1017	12.L	502.74	-637.27	-1.58
1018	Wpi 13	496.46	-496.55	-1.55
1019	13.R	496.03	-496.82	-1.58
1020	13.1	489.65	-500.76	-1.96
1021	13.2	483.04	-505.27	-2.07
1022	13.3	476.29	-509.57	-2.14
1023	13.4	469.29	-514.40	-2.38
1024	13.5	462.55	-517.77	-2.57
1025	13.6	456.46	-521.24	-2.71
1026	Ingemeten begin diepe geul	451.71	-524.95	-2.99
1027		446.64	-528.17	-3.18
1028		441.57	-531.38	-3.68
1029		436.51	-534.60	-3.58
1030	13.L	432.48	-537.58	-1.65
1031	(1) Wpi 14, naar Wpi 13 geschatte hoogte 0.8m	425.56	-420.34	-1.57
1032	14.R	424.00	-421.60	-1.71
1033	14.1	415.70	-428.81	-1.94
1034	14.2	410.23	-433.18	-2.34
1035	14.3	403.84	-438.01	-2.65
1036	14.4	396.05	-444.28	-2.87
1037	Extra	390.13	-448.08	-3.05
1038	Diepste punt is 1.6m sterke stroming	384.97	-452.85	-3.31
1039	14.L	380.40	-456.74	-1.74
1040	(1) Wpi 15, naar vast punt 12 (1.5 m van R)	385.01	-330.64	-1.87
1042	15.R	383.66	-331.29	-1.92
1043	15.1	374.20	-335.85	-2.13
1044	15.2	366.92	-339.18	-2.13
1045	15.3	360.25	-342.62	-2.32
1046	15.4	353.48	-345.84	-2.56
1047	15.5	345.28	-349.56	-2.87
1048	15.6	340.64	-351.43	-3.09
1049	Diepste punt 1.42 m	334.26	-354.32	-3.34
1050	15.L	328.83	-356.86	-1.92
1051	(1) Wpi 16, naar vast punt 12	350.54	-232.48	-1.90
1053	16.R	348.35	-233.67	-1.96
1054	16.1	342.12	-236.87	-2.14
1055	16.2	334.62	-240.87	-2.27
1056	16.3	327.49	-244.50	-2.69
1057	16.4	321.31	-247.78	-3.12
1058	diepte 1.6m	315.19	-251.19	-3.58
1059	diepte 1.8m	309.01	-254.47	-3.78
1060	diepte 1.6m	301.94	-258.21	-3.58
1061	16.L	296.12	-264.20	-2.00

nr.	label	X	Y	Z
1062	(1) Wpi 17, naar Wpi 16 = +/- R	335.97	-137.59	-2.06
1063	17.R	335.48	-137.66	-2.11
1064	17.1	331.52	-138.26	-2.35
1065	17.2	323.61	-139.45	-2.85
1066	17.3	316.19	-140.53	-3.04
1067	Positie 20 min. Meting	310.80	-141.66	-3.07
1068	17.4	308.77	-141.59	-3.08
1069	17.5	300.37	-142.88	-2.91
1070	17.6	292.05	-144.76	-2.49
1071	17.7	286.53	-145.02	-2.25
1072	17.L	277.79	-147.37	-2.10
1073	(1) Wpi 18, naar vast punt 1 =+/- waterlijn L	253.32	4.30	-2.22
1074	18.R	309.90	17.04	-2.27
1075	18.7	306.89	16.72	-2.74
1076	18.6	300.09	15.06	-3.44
1077	18.5	292.47	12.47	-3.05
1078	18.4	284.58	11.13	-2.89
1079	18.3	276.66	9.86	-2.83
1080	18.2	268.87	8.03	-2.51
1081	18.1	261.12	6.04	-2.39
1082	18.L	253.80	4.41	-2.27
1083	19.R	280.99	116.34	-2.275
1084	19.6	272.21	114.37	-3.060
1085	19.5	265.44	112.58	-3.275
1086	19.4	257.47	109.26	-3.340
1087	19.3	250.53	108.26	-3.060
1088	19.2	243.13	106.96	-2.770
1089	19.1	235.33	105.22	-2.500
1090	19.L	224.62	102.70	-2.290
1091	(1) Wpi 20, naar vast punt 1 (1.55m van R)	244.41	212.88	-1.96
1092	20.R	243.26	211.92	-2.31
1093	20.1	240.57	209.67	-2.84
1094	20.2	234.88	204.79	-3.18
1095	20.3	229.08	200.03	-3.54
1096	20.4	224.56	194.58	-3.38
1097	20.5	217.59	190.40	-3.10
1098	20.6	210.85	185.20	-2.70
1099	20.L	203.90	178.71	-2.32
1100	(1) Wpi 21, naar vast punt 3? (2m van R)	169.13	294.97	-1.95
1101	top steilrand (Hoogte steilrand is 0.9m)	168.21	293.54	-1.95
1102	21.R	168.05	293.28	-2.85
1103	21.6	166.17	290.33	-3.11
1104	21.5	162.38	284.45	-3.13
1105	21.4	157.46	277.51	-3.38
1106	21.3	152.58	270.54	-3.37
1107	21.2	147.87	263.47	-3.21
1108	21.1	143.93	256.48	-2.60
1109	21.L	141.87	253.05	-2.34

nr.	label	X	Y	Z
1110	(1) Wpi 22, naar vast punt 3?(+/- 0.7m van R)	66.47	343.68	-2.30
1111	22.R	66.40	342.98	-2.33
1112	22.1	65.52	333.72	-2.58
1113	22.2	64.99	327.25	-2.79
1114	22.3	65.15	319.72	-3.04
1115	22.4	64.03	310.77	-3.16
1116	Positie 20 min. Meting	65.75	308.69	-3.21
1117	22.5	63.70	302.77	-3.20
1118	22.6	62.54	294.84	-3.10
1119	Begin steile helling	62.59	291.32	-2.97
1120	Einde helling	62.33	287.83	-2.45
1121	22.L	61.76	283.86	-2.34
1122	(1) Wpi 23, naar vast punt 3?(2.6m van R)	-13.10	351.75	-0.02
1123	top steilrand(Oeverhoogte 2.30m)	-13.15	349.75	-0.02
1124	23.R	-13.17	349.15	-2.32
1125	23.1	-13.25	345.75	-2.99
1126	23.2	-12.95	337.75	-3.38
1127	23.3	-13.24	330.75	-3.56
1128	23.4	-11.22	321.81	-2.96
1129	23.5	-12.55	312.75	-2.92
1130	23.6	-12.22	304.76	-2.92
1131	23.7	-12.33	296.76	-2.93
1132	23.8	-12.41	288.75	-2.56
1133	23.L	-12.11	281.76	-2.28
1134	top steilrand (Oeverhoogte 1.2m)	-155.45	327.31	-1.15
1135	24.R	-155.30	326.94	-2.35
1136	24.1	-152.48	319.89	-2.76
1137	24.2	-149.38	312.51	-2.77
1138	24.3	-145.93	304.20	-2.78
1139	24.4	-142.43	296.99	-2.76
1140	24.5	-139.04	289.74	-2.67
1141	24.6	-135.72	281.91	-2.74
1142	24.7	-131.97	273.73	-2.73
1143	24.8	-128.17	265.57	-2.85
1144	24.9	-125.13	259.26	-2.98
1145	24.10	-121.27	254.42	-2.92
1146	24.11	-117.76	247.24	-3.23
1147	24.L	-115.03	235.30	-2.49
1148	25.R	-257.06	289.24	-2.45
1149	25.7	-256.06	287.49	-2.97
1150	25.6	-253.42	281.00	-2.77
1151	25.R eiland	-251.17	276.53	-2.45
1152	25.L eiland	-234.74	240.08	-2.62
1153	25.1	-231.51	232.75	-3.15
1154	25.2	-228.27	225.43	-3.56
1155	Diepte geul 1.15m	-226.94	220.55	-3.77
1156	25.3	-225.74	215.63	-3.30
1157	Positie 20 min. Meting	-222.84	216.40	-3.20
1158	25.4	-222.44	208.34	-2.88
1159	25.L	-216.02	201.36	-2.66

nr.	label	X	Y	Z
1160	(1) Wpi 26, naar 25.Leiland (was 24.L)	-346.03	178.90	-2.27
1162	26.L eiland	-340.02	169.09	-2.67
1163	26.1	-334.45	162.59	-3.40
1164	26.2	-330.47	155.62	-3.48
1165	26.5 (testmeting, frame 90grad gedraaid)	-328.69	155.03	-3.49
1166	26.3	-324.80	148.59	-3.38
1167	26.4	-321.18	142.59	-3.52
1168	26.L	-316.31	135.62	-2.66
1169	27.R	-403.65	249.98	-2.740
1170	27.2	-402.07	247.39	-3.680
1171	27.1	-398.92	242.83	-3.080
1172	27.R eiland	-396.91	239.94	-2.750
1173	(1) Wpi 28, naar Wpi 26	-417.57	124.30	-2.18
1174	28.R	-465.75	154.76	-2.83
1175	28.6	-461.21	152.57	-3.48
1176	28.5	-454.54	148.17	-3.18
1177	28.R eiland	-443.51	141.28	-2.85
1178	28.L eiland	-412.76	117.91	-2.71
1179	28.1	-407.65	111.75	-3.09
1180	28.2	-402.59	105.54	-3.52
1181	28.3	-398.85	100.86	-3.70
1182	28.4	-395.02	95.60	-3.41
1183	28.L	-391.31	91.52	-2.70
1184	(1) Wpi 29, naar Wpi 28 (hoogte .95m?)	-484.96	34.84	-2.63
1185	29.R	-518.39	41.05	-2.79
1186	diepte 1.7m	-515.34	43.15	-4.47
1187	diepte 2.1m	-512.32	44.45	-4.87
1188	diepte 1.7m	-509.28	45.36	-4.47
1189	Extra punt	-506.33	45.77	-3.96
1190	29.3	-502.93	43.61	-3.56
1191	29.R eiland	-497.24	41.56	-2.77
1192	29.L eiland	-482.33	33.39	-2.75
1193	29.1	-478.51	30.11	-3.43
1194	29.2	-471.97	25.50	-3.21
1195	29.L	-465.24	21.16	-2.74
1196	(1) Wpi 30, naar Wpi 29	-496.32	-62.50	-2.79
1197	30.R	-534.18	-59.16	-2.88
1198	diepte 1.3m	-532.23	-59.96	-4.12
1199	diepte 1.7m	-526.28	-60.85	-4.52
1200	diepte 1.9m	-521.31	-61.52	-4.72
1201	Extra (1.3m diep)	-516.32	-62.28	-4.09
1202	30.2	-513.28	-63.70	-3.92
1203	30.1	-504.32	-62.57	-3.00
1204	30.L	-501.32	-62.50	-2.82
1205	(1) Wpi 31, naar Wpi 30	-458.81	-132.02	-2.43
1206	31.R	-517.93	-178.18	-2.93
1207	31.7	-505.60	-168.79	-3.39
1208	31.6	-498.67	-163.04	-3.49
1209	31.5	-491.84	-157.97	-3.58
1210	31.4	-485.28	-153.37	-3.73
1211	31.3	-479.05	-148.34	-3.51
1212	31.2	-472.47	-142.97	-3.50
1213	31.1	-466.23	-137.96	-3.35
1214	31.L	-461.12	-133.94	-2.93

Appendix A3

Survey points water line

Water line left bank

In downstream direction

point	label	X	Y	Z
613	l	1046.56	-451.46	-1.37
615	l	1058.20	-483.73	-1.38
617	l	1070.52	-517.17	-1.36
619	l	1083.70	-549.62	-1.42
621	l	1093.59	-582.99	-1.48
626	l	1109.79	-613.92	-1.46
628	l	1122.66	-637.55	-1.48
629	l	1114.31	-669.25	-1.44
630	l	1106.16	-703.71	-1.39
646	l	1094.91	-732.27	-1.51
650	l	1091.07	-771.75	-1.51
651	l	1056.51	-804.16	-1.57
652	l	1021.69	-822.50	-1.57
653	l	985.35	-825.38	-1.55
654	l	943.41	-831.64	-1.61
655	l	904.47	-839.72	-1.64
656	l	866.94	-844.43	-1.66
658	l	827.55	-845.17	-1.66
661	l	784.42	-835.74	-1.69
662	l	754.70	-827.59	-1.67
664	l	720.57	-816.20	-1.7
666	l	687.79	-794.17	-1.69
668	l	661.56	-769.34	-1.7
670	l	631.68	-741.87	-1.73
672	l	598.80	-725.27	-1.75
676	l	571.65	-705.37	-1.76
677	l	547.87	-686.95	-1.75
678	l	525.42	-662.95	-1.73
679	l	494.16	-628.51	-1.76
681	l	466.25	-593.90	-1.73
684	l	441.49	-559.12	-1.77
686	l	422.93	-533.86	-1.74
689	l	394.40	-490.64	-1.71
693	l	368.00	-449.32	-1.74
694	l	338.58	-397.45	-1.78
695	l	309.82	-332.59	-1.83
697	l	297.60	-238.08	-1.92
699	l	289.77	-197.75	-1.91
701	l	275.12	-142.58	-1.94
703	l	270.84	-103.47	-1.96

point	label	X	Y	Z
705	l	256.02	-45.19	-2.02
707	l	245.92	6.12	-2.06
709	l	239.42	31.56	-2.07
714	l	231.71	58.34	-2.07
716	l	220.64	93.71	-2.07
718	l	215.43	135.52	-2.1
721	l	208.28	158.36	-2.11
723	l	185.81	198.66	-2.12
725	l	160.17	231.70	-2.14
727	l	126.64	263.78	-2.15
731	l	84.37	282.53	-2.18
733	l			
734	l	60.34	285.64	-2.2
738	l	16.59	287.28	-2.21
740	l	-22.95	285.13	-2.22
742	l	-71.01	274.00	-2.26
745	l	-89.69	264.41	-2.31
747	l	-101.28	251.38	-2.42
749	l	-106.58	242.45	-2.44
751	l	-126.14	225.24	-2.45
753	l	-161.26	216.60	-2.6
755	l	-209.71	202.61	-2.57
758	l	-254.67	182.93	-2.62
760	l	-276.90	169.27	-2.63
762	l	-308.62	143.98	-2.63
764	l	-344.47	113.23	-2.68
807	l	-367.39	98.59	-2.65
808	l	-400.34	79.65	-2.69
809	l	-429.98	55.13	-2.75
818	l	-456.67	30.18	-2.83
819	l	-491.48	-18.32	-2.9
821	l	-501.30	-65.91	-2.91
823	l	-486.90	-113.23	-2.94
825	l	-461.75	-141.91	-2.92
826	l	-436.63	-165.52	-2.97
828		-384.90	-212.37	-2.98

Water line right bank

In downstream direction

point	label	X	Y	Z
614	r	983.24	-462.29	-1.34
616	r	982.55	-488.28	-1.36
618	r	977.87	-514.47	-1.34
620	r	994.60	-547.51	-1.35
622	r	1011.72	-585.84	-1.4
623	r	1002.17	-622.15	-1.48
625	r	985.63	-663.23	-1.48
627	r	954.98	-702.23	-1.54
647	r	927.43	-737.38	-1.58
648	r	907.98	-763.54	-1.61
649	r	889.05	-780.05	-1.61
657	r	844.09	-792.43	-1.65
660	r	796.45	-790.31	-1.68
663	r	752.51	-763.36	-1.71
667	r	712.82	-733.17	-1.7
669	r	682.68	-698.19	-1.72
671	r	652.93	-668.87	-1.72
673	r	610.40	-638.63	-1.75
674	r	569.50	-599.38	-1.74
675	r	536.69	-561.93	-1.74
682	r	509.69	-526.92	-1.74
683	r	474.57	-487.21	-1.74
685	r	443.93	-458.13	-1.74
687	r	447.77	-432.67	-1.74
688	r	442.84	-396.22	-1.76
690	r	393.20	-380.75	-1.78
691	r	382.73	-337.76	-1.82
692	r	370.33	-296.84	-1.86
698	r	362.02	-253.60	-1.88
700	r	344.69	-212.63	-1.9
702	r	333.90	-165.38	-1.92
704	r	334.49	-123.71	-1.95
706	r	330.49	-79.63	-2.01
708	r	329.55	-40.06	-2.02
710	r	313.75	-5.49	-2.04
711	r	300.53	26.25	-2.08
713	r	299.59	22.39	-2.07
715	r	288.57	55.98	-2.07
717	r	283.53	83.99	-2.09
719	r	274.52	123.05	-2.09

point	label	X	Y	Z
720	r	266.29	158.05	-2.1
722	r	255.22	189.97	-2.11
724	r	233.70	218.32	-2.1
726	r	209.39	249.37	-2.12
728	r	180.50	280.44	-2.13
730	r	151.40	306.47	-2.14
732	r	120.75	325.01	-2.17
735	r	83.83	337.39	-2.19
737	r	82.41	337.53	-2.2
739	r	44.20	351.88	-2.2
741	r	9.24	345.24	-2.2
743	r	-30.02	352.88	-2.2
744	r	-59.90	342.26	-2.22
746	r	-92.05	330.51	-2.22
748	r	-115.10	332.12	-2.27
750	r	-151.32	325.32	-2.28
752	r	-188.07	314.45	-2.28
754	r	-223.84	301.35	-2.28
756	r	-262.83	285.23	-2.47
757	r	-301.58	272.19	-2.51
759	r	-337.56	263.16	-2.55
763	r	-382.12	250.03	-2.77
765	r	-412.54	240.72	-2.8
768	r	-447.06	192.87	-2.9
771	r	-464.64	162.91	-2.87
774	r	-479.24	135.20	-2.89
777	r	-492.20	105.26	-2.87
779	r	-502.94	88.10	-2.9
820	r	-523.23	29.88	-2.9
822	r	-531.07	-9.47	-2.92
824	r	-533.12	-48.81	-2.89
827	r	-532.01	-95.16	-2.92
829	r	-524.40	-138.74	-2.91
831	r	-515.92	-184.22	-2.92
832	r	-511.70	-196.38	-2.91
833	r	-509.78	-189.23	-2.94
834	r	-506.38	-213.19	-2.95

Appendix B

Oak Creek model

Substrate based Oak creek model

Based on the measurements of Milhous at Oak Creek, Parker and Klingeman developed a model to predict sediment transport in gravel bed rivers.

$$W_i^* = 0.0025G(\phi_{50})$$

$$W_i^* = \frac{Rgq_i}{\left(\tau/\rho\right)^{3/2} f_i}$$

$$\phi_{50} = \frac{\tau_{50}^*}{\tau_{r50}^*}$$

$$\tau_{50}^* = \frac{\tau}{\rho RgD_{50}}$$

$$\tau_{r50} = 0.0876$$

$$G(\phi_{50}) = \begin{cases} 5474\left(1 - \dfrac{0.853}{\phi_{50}}\right)^{4.5} & \phi_{50} \geq 1.59 \\ \exp\left[14.2(\phi_{50} - 1) - 9.28(\phi_{50} - 1)^2\right] & 1 \leq \phi_{50} \leq 1.59 \\ \phi_{50}^{M_0} & \phi_{50} \leq 1 \end{cases}$$

$$W_T^* = \frac{Rgq_T}{\left(\tau/\rho\right)^{3/2}}; \qquad \text{met } q_T = \sum q_i$$

The critical Shields stress in this formula is replaced by a reference stress τ_{r50}^* below which transport rates are very small.

Surface based Oak Creek model

Assumption:
Because the transport relation of Parker deals with bed load and at flow conditions which can move significant amounts of gravel the sand fraction is often found to be transported in suspension. The sand fraction was removed from the analysis.

$$W_{si}^* = 0.00218 \sum G\left[\omega \phi_{sg0} g(\delta_i)\right]$$

$$\omega_0 = 1.048\left(\frac{D_{sg}}{D_{50}}\right)^{1-\beta} \frac{\tau_{rsg0}^*}{\tau_{r50}^*}$$

$$\phi_{sg0} = \frac{\tau_{sg}^*}{\tau_{rsg0}^*}$$

$$\tau^*_{sg} = \frac{\tau}{(\rho_s - \rho_w)gD_{sg}}$$

$$\tau^*_{rsg0} = 0.0386$$

$$\delta_i = \frac{D_i}{D_{sg}}$$

G is the same function as in the substrate based model
D_{sg} is the surface mean grain size.